



















**STRUCTURAL STUDIES AND GABBRO MYLONITIZATION**

**WITHIN THE BARTON BAY DEFORMATION ZONE,**

**GERALDTON, ONTARIO**

by

**SHANE BUCK**

A thesis submitted to the Department of Geological Sciences

**Brock University**

In partial fulfillment of the requirements for the degree of

**Master of Science**

© Shane Buck 1986

Dr. H.R. Williams

Supervisor



## ABSTRACT

Structures related to ductile simple shear parallel to the Bankfield-Tombill Fault, define a 5km wide zone, the Barton Bay Deformation Zone. Structures present within this zone include; simple shear fabrics S, C and C', asymmetric Z shaped folds with rotated axes, boudinage and pinch and swell structures and a subhorizontal extension lineation.

The most highly deformed rock is a gabbro mylonite which occurs in the fault zone. The deformation of this gabbro has been traced in stages from a protomylonite to an ultramylonite in which feldspar and chlorite grainsize has been reduced from over 100 microns to as little as 5 microns.

Evidence from the mylonite and the surrounding structure indicates that deformation within the Barton Bay Deformation Zone is related to a regional simple shear zone, the Bankfield-Tombill Fault. Movement along this shear zone was in a south over north oblique strike slip fashion with a dextral sense of displacement.

## ABSTRACT

Structures related to ductile simple shear parallel to the Bankfield-Tomball Fault, define a 3 km wide zone, the Barton Bay Deformation Zone, structure present within the zone includes simple shear fabrics S, C and N, asymmetric Z shaped folds with rotated axes, boudinage and pinch and swell structures and a subhorizontal extension lineation.

The most highly deformed rock is a gabbro dyke which occurs in the fault zone. The deformation of this gabbro has been traced in stages from a protomylonite to an ultramylonite in which feldspar and chlorite grains have been reduced from over 100 microns to as little as 5 microns.

Evidence from the mylonite and the surrounding structure indicates that deformation within the Barton Bay Deformation Zone is related to a regional simple shear zone, the Bankfield-Tomball Fault. Movement along this shear zone was in a south over north oblique strike slip fashion with a dextral sense of displacement.



## ACKNOWLEDGEMENTS

The author would like to thank the faculty and staff of the Brock University Geology Department for their help and support in the writing of this thesis. Special thanks go to Greg and Dr. Peach for their help and advice and the Reillys for room, board and moral support and especially to Howard who supervised and proofread the thesis. As always thanks go to my wife Beth.

1941-1942

2010年10月10日 星期六

1130

## TABLE OF CONTENTS

	PAGE
Abstract .....	1
Acknowledgements .....	11
Introduction .....	7
Regional Geology .....	9
Volcanics .....	9
Sedimentary Rocks .....	13
Gabbro-Diorite .....	23
Porphyry .....	27
Diabase Dykes .....	28
Metamorphism .....	30
Structural Geology .....	31
The Bankfield-Tombill Fault .....	31
Foliations .....	33
Lineations .....	42
Shear Fabrics in the Gabbro Mylonite .....	44
Folding .....	53
Minor Shears .....	75
Veins .....	75
Stages of Gabbro Mylonitization .....	80
Statistical Analysis and Mineralogical Description .....	97
Detailed Feldspar Microstructures .....	112
Discussion .....	127
Conclusions .....	131
References .....	133
Appendix I .....	136



## LIST OF FIGURES

	PAGE
Map 1 .....	in pocket
1. Location of Study Area .....	8
2. Agglomerate-Tuff .....	11
3. Thin Section of Tuff .....	11
4. C' in Tuff .....	12
5. Graded Bedding Folded .....	12
6. Pelitic Layer .....	15
7. Thin Section of Psammitic Rock .....	15
8. Pressure Solution Cleavage .....	17
9. Thin Section of Deformed Psammitic Rock .....	17
10. Undeformed Conglomerate .....	18
11. Deformed Conglomerate .....	18
12. Deformed Conglomerate .....	20
13. Macroscopic Fold .....	22
14. Thin Section of Iron Formation .....	22
15. Gabbro Intruding Sediments .....	25
16. C' Fabric in Gabbro .....	25
17. Thin Section of Gabbro .....	26
18. Porphyry Intruding Sediments .....	29
19. Thin Section of Porphyry .....	29
20. Simple Shear Fabrics .....	34
21. Layering-Stereoplot .....	37
22. Bedding-Stereoplot .....	37
23. Foliation Trend Maps .....	38
24. C-Stereoplot .....	39



25.	Displaced Veins .....	39
26.	S-Stereoplot .....	41
27.	S Fabric .....	41
28.	C'-Stereoplot .....	43
29.	Crinkle Lineation .....	45
30.	Stretching Lineation-Stereoplot .....	45
31.	Displaced S Fabric .....	47
32.	Plots of C and C' Orientations .....	49
33.	Plots of C and C' Orientations at Location 2 .....	51
34.	Histograms of the Angle Between C and C' .....	54
35.	Spaced Cleavage Folded .....	57
36.	Z Folds-Stereoplot .....	57
37.	Folded Veins .....	58
38.	Folded Agglomerate .....	59
39.	Wide Zone of Z Folds .....	59
40.	Rotated Axial Trace of Fold .....	60
41.	Fractured Fold .....	60
42.	Fold with Opposite Plunging Hinges .....	63
43.	Shear Planes in Fold .....	63
44.	Close up of Shear Planes .....	63
45.	Separation of Fold Hinges .....	66
46.	Modified Z Fold .....	66
47.	Refolded Fold .....	69
48.	Unfolded Fold .....	69
49.	Sinistral Kinks-Stereoplot .....	71
50.	Dextral Kinks-Stereoplot .....	71
51.	Simple Shear Rotation .....	73



1	...
2	...
3	...
4	...
5	...
6	...
7	...
8	...
9	...
10	...
11	...
12	...
13	...
14	...
15	...
16	...
17	...
18	...
19	...
20	...
21	...
22	...
23	...
24	...
25	...
26	...
27	...
28	...
29	...
30	...
31	...
32	...
33	...
34	...
35	...
36	...
37	...
38	...
39	...
40	...
41	...
42	...
43	...
44	...
45	...
46	...
47	...
48	...
49	...
50	...
51	...
52	...
53	...
54	...
55	...
56	...
57	...
58	...
59	...
60	...
61	...
62	...
63	...
64	...
65	...
66	...
67	...
68	...
69	...
70	...
71	...
72	...
73	...
74	...
75	...
76	...
77	...
78	...
79	...
80	...
81	...
82	...
83	...
84	...
85	...
86	...
87	...
88	...
89	...
90	...
91	...
92	...
93	...
94	...
95	...
96	...
97	...
98	...
99	...
100	...



52.	Displaced Vein .....	76
53.	Minor Shears-Stereoplot .....	77
54.	Veins-Stereoplot .....	78
55.	Location of Gabbro Mylonites .....	81
56.	Gabbro Mylonite at Location 2 .....	82
57.	Gabbro Mylonite at Location 1 .....	83
58.	Anastomosing Shears .....	86
59.	Thin Section of S Fabric .....	86
60.	Elongated Mineral Fabric .....	88
61.	Thin Section of C Fabric .....	88
62.	Sigmoidal Feldspar .....	90
63.	Stage III Layering .....	90
64.	Stage V Layering .....	92
65.	Folded Layering .....	92
66.	Carbonate Infilled C' Fabric .....	96
67.	Histograms for Leucoxene .....	100
68.	Thin Section of Stage I .....	103
69.	Epidote at Stage V .....	103
70.	Thin Section of Actinolite Aggregates .....	105
71.	Separation of Actinolite at Stage V .....	107
72.	Two Generations of Chlorite .....	107
73.	Stage V Layering .....	109
74.	Crenulated Leucoxene .....	109
75.	Grain Boundary Bulging .....	117
76.	Subgrains in Feldspar .....	117
77.	Polygonal Texture in Feldspar Aggregate .....	119
78.	Grain Boundary Bulging .....	119



79.	First and Second Order Feldspar Grains .....	121
80.	Stage IV layering .....	121
81.	Isolated Feldspar Grains .....	122
82.	Thin Chlorite and Feldspar .....	122
83.	Histograms for Feldspar .....	125
84.	Formation of Z Folds .....	129



## LIST OF TABLES

	PAGE
Table 1. Stages of Gabbro Mylonitization .....	85
Table 2. R, L, and W Values .....	99
Table 3. Feldspar Microstructures .....	113



## INTRODUCTION

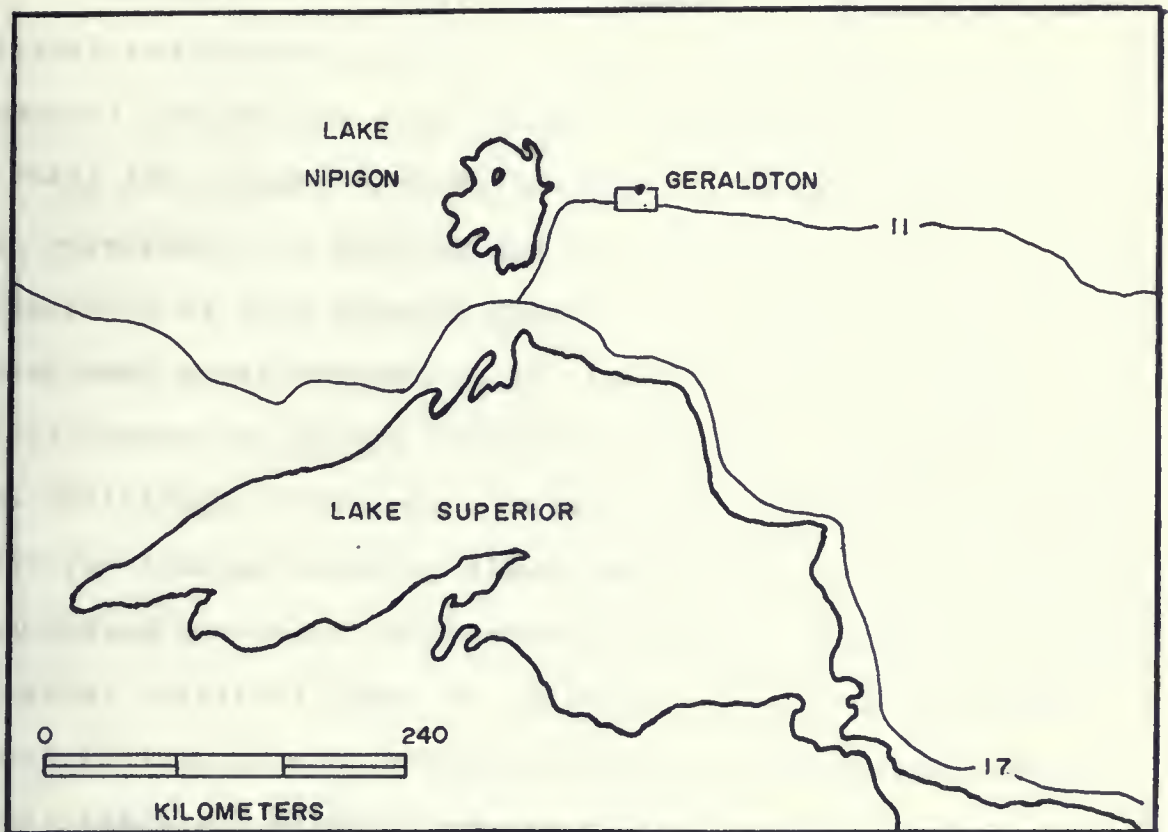
The area described by this study lies within the Beardmore-Geraldton metasedimentary-metavolcanic belt of Northwestern Ontario (Fig. 1). Specifically the area studied in detail, is near the town of Geraldton and within the townships of Ashmore and Errington. This region has a history of gold production since 1934 and was geologically mapped by Horwood and Pye in 1951 (Map 1 in pocket). During this mapping, these authors described rocks within the Bankfield-Tombill Fault which had undergone deformation through shearing, producing what they called a volcanic breccia. Outcrops of this breccia were studied by Lavigne (1983) who re-interpreted the rock as a gabbro intrusive deformed by ductile shear. Together, Lavigne (1983) and Macdonald (1983) observed in the Geraldton area, an association of diverse rock types and deformation. Described as a "lithotectonic" package, this area has been informally termed the "Barton Bay Deformation Zone".

The purpose of the present study has been to study, in detail the deformed gabbro, and also to describe in detail, structural styles found within the Barton Bay Deformation Zone.

# INTRODUCTION

The main object of this study is to provide a comprehensive survey of the history of the English language from its earliest beginnings to the present day. The study is divided into three main parts: the first part deals with the prehistoric period, the second with the historical period, and the third with the modern period. The prehistoric period covers the time from the arrival of the first settlers in Britain to the beginning of the historical period. The historical period covers the time from the beginning of the historical period to the present day. The modern period covers the time from the present day to the future. The study is based on a wide range of sources, including ancient and modern writers, and is intended to provide a clear and concise account of the history of the English language.





**Fig. 1. Location of the study area.**



## REGIONAL GEOLOGY

The regional geology of the study area was mapped by Pye (1952) and Horwood and Pye (1955), who produced excellent maps (Map 1), which were used extensively during the present study.

These two authors worked together on these reports and will be referred to as Horwood and Pye from this point. With the exception of late diabase dykes, all of the rocks in the area have been metamorphosed to the lower greenschist facies. For this reason the prefix "meta" has not been used when referring to individual lithologies. Lithologies outlined by Horwood and Pye include volcanic flows and tuffs, sedimentary rocks including greywacke, conglomerate and iron formation and also several different types of intrusive rocks. As detailed descriptions of each rock type are provided in the reports of Pye (1952) and Horwood and Pye (1955), only brief descriptions have been included in this study. Outcrops exposed since the original mapping and detailed structural study of the original outcrop has led to re-interpretation of the original progenitors of some of the lithologies.

## VOLCANICS

Volcanic rocks represented in the study area include mafic to intermediate lavas, tuffs, agglomerates and volcanic breccias. Horwood and Pye mapped these lavas as packages of basalts with subordinate andesites and rare flows of dacitic composition. The flow rocks are restricted to the northern part of the Geraldton area and have not been studied in detail

THE JOURNAL OF THE AMERICAN MEDICAL ASSOCIATION

(1900) PUBLISHED WEEKLY  
535 N. Dearborn Ave. CHICAGO, ILL.  
Subscription price, \$5.00 per annum in advance.  
Single copies, 15 cents.  
Entered as Second-Class Matter, May 2, 1892.  
Postage paid at Chicago, Ill., May 2, 1892.  
Acceptance for mailing at special rate of postage provided for in Act of October 3, 1917.  
Copyright, 1900, by American Medical Association.  
Published by American Medical Association, 535 N. Dearborn Ave., Chicago, Ill.  
Entered as Second-Class Matter, May 2, 1892.  
Postage paid at Chicago, Ill., May 2, 1892.  
Acceptance for mailing at special rate of postage provided for in Act of October 3, 1917.  
Copyright, 1900, by American Medical Association.  
Published by American Medical Association, 535 N. Dearborn Ave., Chicago, Ill.

1900

Published by American Medical Association, 535 N. Dearborn Ave., Chicago, Ill.  
Entered as Second-Class Matter, May 2, 1892.  
Postage paid at Chicago, Ill., May 2, 1892.  
Acceptance for mailing at special rate of postage provided for in Act of October 3, 1917.  
Copyright, 1900, by American Medical Association.  
Published by American Medical Association, 535 N. Dearborn Ave., Chicago, Ill.

during the present study.

Outcrops of tuff, agglomerate and breccia are shown on Map 1, as a narrow east-west trending zone in the central part of the study area. The least deformed examples of these rock types were observed on the peninsula at the eastern end of Lake Kenogamisis. Exposures of agglomerate consist of large (5-15cm), pale green clasts in a matrix of dark green fine grained tuff (Fig. 2). These rock types are commonly well foliated and often folded. More intensely deformed examples are increasingly schistose with elongated and folded clasts (Fig. 38). At most locations an irregular, discontinuous layering was observed and appeared to be related to deformation.

In thin section the tuff is seen to consist of a matrix of extremely fine grained (5-15 micron) quartz, plagioclase and chlorite surrounding larger (50-100 micron) fragments of sericitized feldspar (Fig. 3). The layered appearance is due to alternating chlorite rich-chlorite poor zones. Opaque minerals, especially sulphides, are common at all grain sizes.

Typical pyroclastic textures were not observed, suggesting that the fine grained masses of quartz and plagioclase may represent recrystallization of an original ash-bomb tuff.

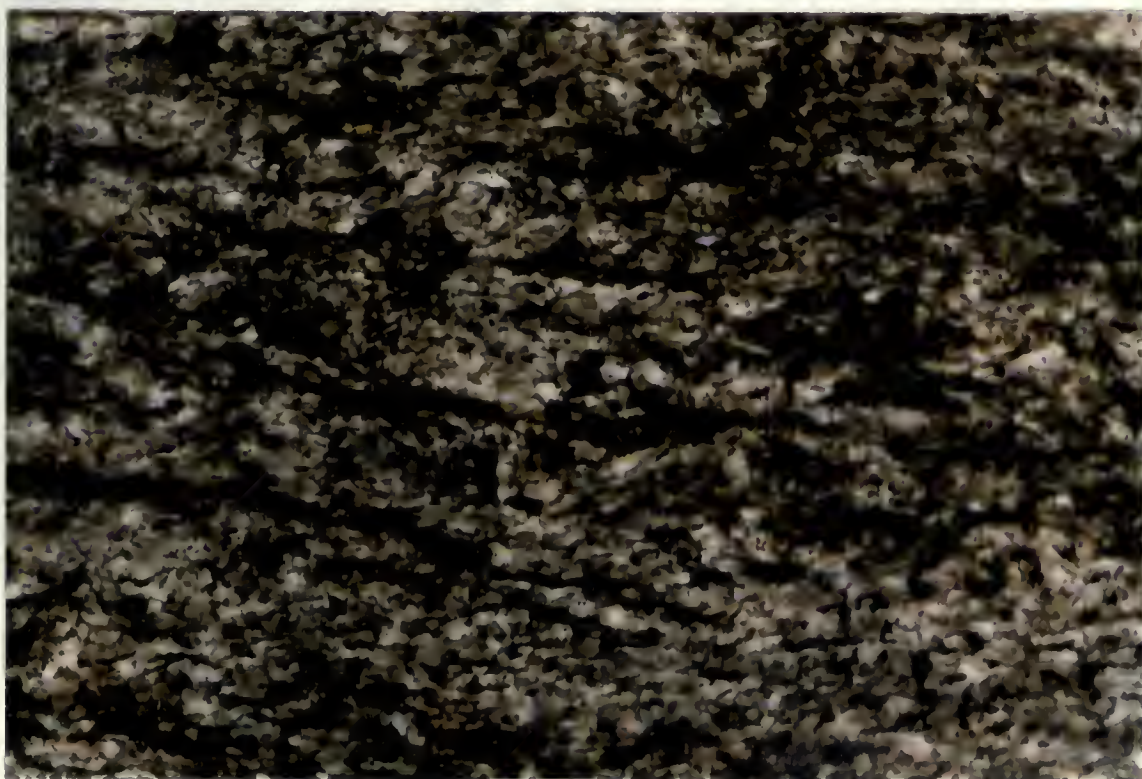
At several locations the tuff has a rough irregular pitted surface (Fig. 4) which led Horwood and Pye to an interpretation of the material as a volcanic breccia. However close examination during the present study revealed that the pitted appearance is caused by erosion of carbonate which has







**Fig. 2. Agglomerate - tuff outcrop.**



50  $\mu$ m

**Fig. 3. Thin section of tuff.**







**Fig. 4. Closely spaced C' in tuff.**



**Fig. 5. Z folds in graded greywacke.**

Fig. 4. Closely spaced C, in tuft.

Fig. 5. Z folds in graded greywacke.

infilled a closely spaced shear fabric oblique to the foliation in the tuff. The presence of this fabric is related to deformation by simple shearing and will be discussed in a later section.

Outcrops with this pitted appearance along with an irregular layering were observed at several locations west of the eastern peninsula. These were interpreted as tuff and breccia units by Horwood and Pye and mapped as the narrow zone shown on Map 1. Outcrops exposed since the original mapping, provide evidence that in many cases this unit may in fact be a sheared gabbro instead of a tuff.

## SEDIMENTARY ROCKS

The sedimentary rocks of the study area were divided by Horwood and Pye into two groups based on lithological and structural differences. Those sediments in the north, group A, include units of greywacke, conglomerate, arkose and iron formation. Structurally this group has been extensively deformed by folding and shearing. The southern most unit of conglomerate marks the boundary between groups A and B. The southern, group B sediments are dominantly greywacke and show less evidence of deformation.

### Group B

The sediments of this group occur mainly as massive layers of buff coloured, coarse clastic sediments alternating with thin layers of dark green to black fine grained



... ..

... ..

... ..

... ..

... ..

... ..

... ..

... ..

... ..

... ..

... ..

... ..

... ..

sediments. The strike of these is east-west with dips of vertical to steep south. At several locations well developed graded bedding (Fig. 5), was observed which usually indicated younging to the north. The slate layers vary in thickness from a few centimeters up to 1 meter. In the exposures studied during the present study it appeared that the slate layers became less numerous and the psammitic layers more massive towards the south. Dewatering structures and layers of post sedimentary hydrofracturing breccia (Williams pers. comm.) were observed in the southern part of group B. These breccia layers consisted of angular fragments of graded greywacke in a dark fine grained matrix. This rock type was confined to a single layer and were observed at only two locations in the study area.

Evidence of deformation within the group B sediments includes folding (Fig. 5) in the northern part of the group, close to the Bankfield-Tombill fault and also a well developed fabric subparallel to the layering. This fabric is best developed in the pelitic layers where it often causes displacement of veins (Fig. 6). At several locations layering becomes lensoid, pinching out along strike, indicating local extension parallel to the layering.

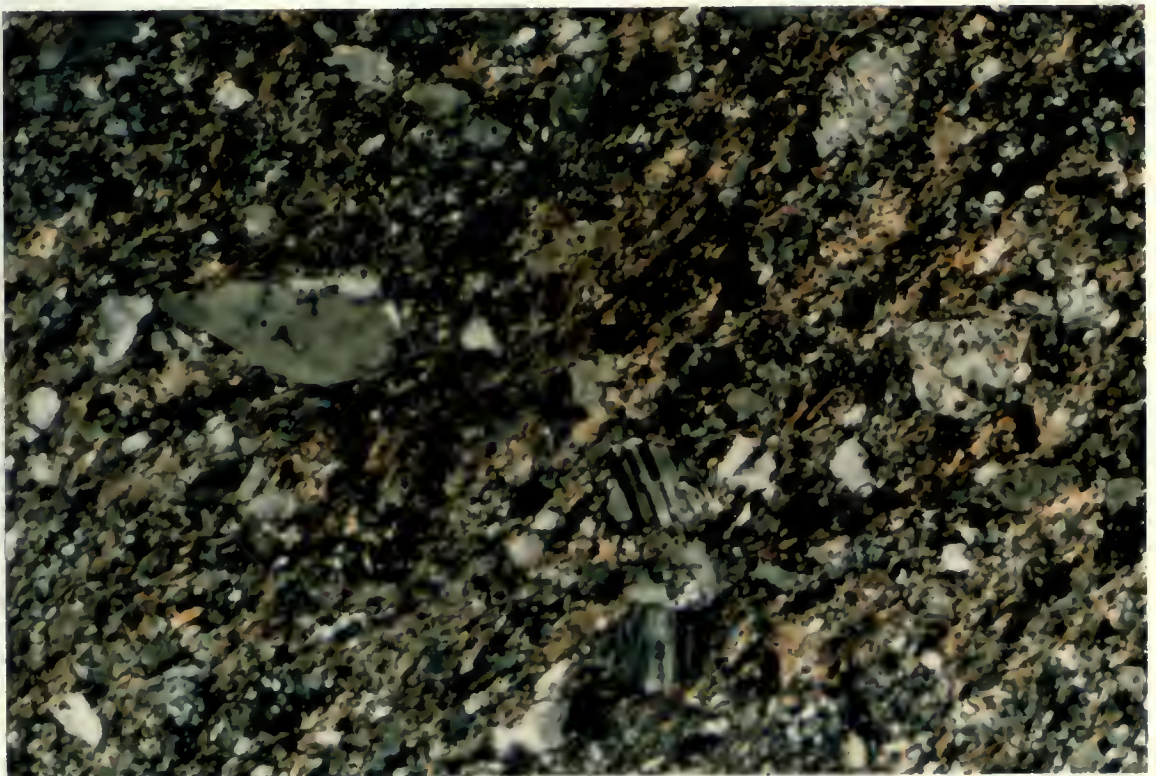
In thin section (Fig. 7), the psammitic layers are seen to consist of coarse, angular to subangular fragments of albite and quartz with lesser amounts of fine grained white mica, chlorite and opaques. The pelitic layers have a similar mineralogy but display a finer grain size and increased







**Fig. 6. Intense deformation in pelitic layers creates boudinage and pinch and swell structures.**



**Fig. 7. Thin section of psammitic layer. The fabric is defined by parallel chlorite and white mica.**





amounts of chlorite and white mica. The well developed fabric seen in outcrop is due to parallel aggregates of chlorite and white mica (Fig. 7).

#### Group A

The greywackes of the northern group A sediments are essentially the same as those to the south. However the group A sediments have been more extensively folded and often have a well developed spaced and/or pressure solution cleavage (Fig. 8). Thin sections of strongly deformed psammitic rocks show that minor recrystallization of the quartz and feldspar has taken place and also that chlorite is more common than in undeformed examples (Fig. 9).

#### Conglomerate

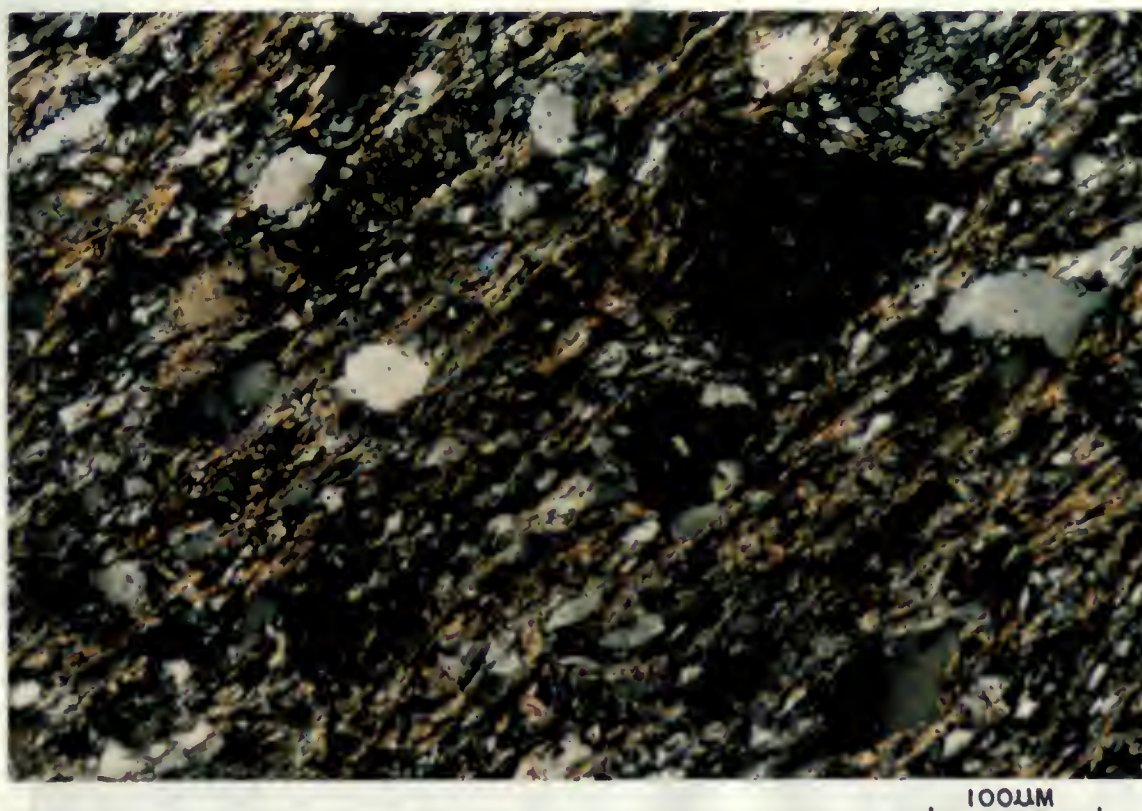
Thin discontinuous units of conglomerate are present both in the northern and southern parts of the group A sediments (Map 1). The only undeformed outcrop of these conglomerates was observed north of Magnet Lake (Fig. 10). The best exposures of the conglomerate were observed in the central part of the study area, adjacent to the Bankfield-Tombill fault. At these locations the conglomerate is extremely deformed with elongated and even folded pebbles (Fig. 11). Pebble lithologies include; mafic and felsic volcanics, granites, quartz and feldspar porphyries, red chert and quartz. The volcanic pebbles are often so elongated as to become barely distinguishable from the fine grained wacke







**Fig. 8. Pressure solution cleavage in greywacke.**



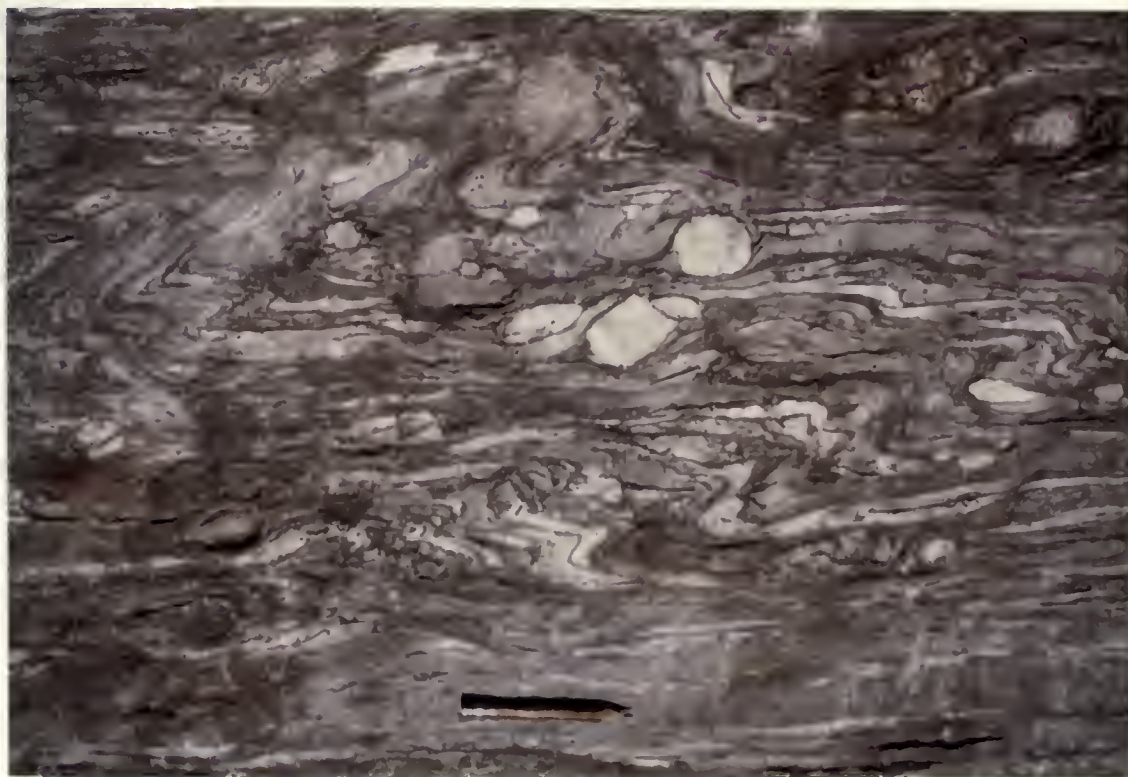
**Fig. 9. Thin section of deformed psammitic rock showing increased chlorite and rotated clasts.**







**Fig. 10. Undeformed conglomerate. Note the easily recognized mafic pebbles.**



**Fig. 11. Deformed conglomerate.**



matrix. Granitic and porphyry pebbles are more commonly rounded with diameters up to 15cm. Often these rounded pebbles appear to have rolled within the fine grained matrix producing asymmetric "tails" (Fig. 12). In several cases pebbles have fractured and pieces have become separated from one another (Fig. 11). The Z shape of the folded pebbles, asymmetric tails and displaced sections of pebbles all indicate a dextral sense of simple shear deformation.

### Arkose

This unit shown on Map 1, south of the northern contact between sediments and volcanics, was first defined by Bruce in 1935. As pointed out by Horwood and Pye, this term is not used in its normal sense, but has been retained on the map due to its common use by local mine geologists and earlier mappers. The rock could more aptly be called a quartz rich greywacke, as a larger percentage of quartz is the main difference between the arkose and the typical greywackes. In the few outcrops observed during the present study the arkose appeared as a pale buff coloured, medium to coarse grained clastic sediment. The arkose was distinguishable from the greywacke only by its lighter colour and the absence of slate layers.

### Iron Formation

The units of iron formation in the area have been studied by several workers (Macdonald 1982, Fralick and Barrett 1983).







**Fig. 12. Asymmetric tails around pebbles in deformed conglomerate.**

Fig. 12. Asymmetric tails around pebbles in detrital conglomerate.

During detailed mapping of the Hardrock mine's "gloryhole", Macdonald (1982) divided the iron formation into three subunits; 1. lean iron formation: discrete beds of magnetite (typically up to 1cm thick) in wacke and siltstone, 2. magnetite iron formation: alternating beds (typically 1cm) of magnetite (with minor hematite) and silicified mudstone or dark chert, 3. magnetite/jasper iron formation: alternating 1cm beds of magnetite and jasperitic quartz or red chert. Examples of each of these subunits were observed at several locations during the present study. Regionally the jasper iron formation is relatively uncommon whereas the magnetite iron formation was often seen as beds up to 1 meter in thickness.

The iron formation is commonly deformed by both large (Fig. 13) and small scale folds and usually have a well developed fabric subparallel to the layering, similar to that seen in the greywackes. In thin section the iron formation is seen to consist of thinly laminated magnetite and greywacke with local concentrations of chlorite (Fig. 14).

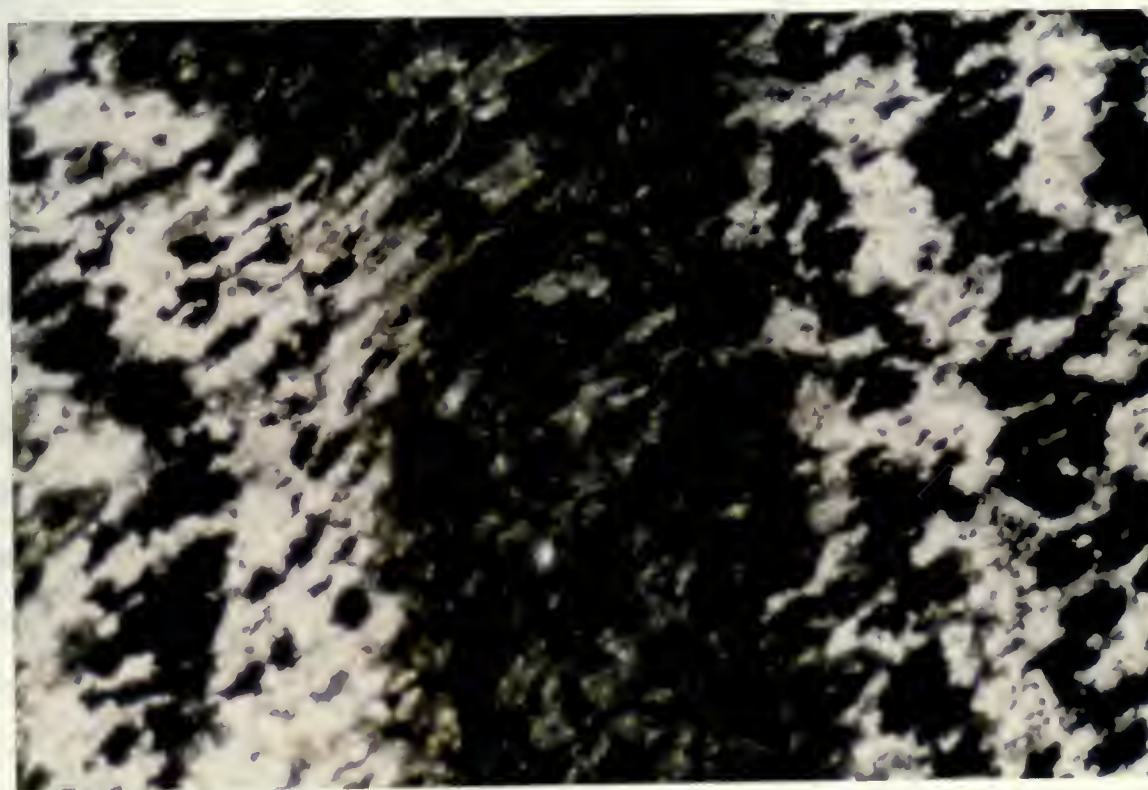
Preliminary studies by Fralick and Barrett (1983) have suggested that while the iron formation of the area seems to be interbedded with the turbiditic sediments, evidence for both deep and shallow water origins have been observed. These writers also point out that the fine grained iron formation should deform in a more ductile fashion than the surrounding greywackes.







Fig. 13. Macroscopic fold in iron formation.



100UM

Fig. 14. Thin section of folded iron formation with local chlorite.





## GABBRO-DIORITE

Mafic intrusions into the sediments are common throughout the study area north of the Bankfield-Tombill fault. Similar intrusives were not seen south of the fault in the study area but were observed to the south in areas to the east and west of the study area. Although the composition of these intrusives is heterogeneous regionally and even at a single outcrop, they can be generally subdivided into darker mafic gabbros and lighter more felsic, diorites. These intrusives can be further subdivided into, those within or closely adjacent to the Bankfield-Tombill Fault, which are strongly deformed and those away from the fault which are generally undeformed. The major focus of the present study has been on those intrusives associated with the fault. Those observed away from the fault have essentially the same mineralogy but have not been affected to the same degree by deformation and associated alteration.

Within the Bankfield-Tombill Fault zone, the most common mafic intrusive has a gabbroic composition of; altered pyroxene, actinolite, chlorite, plagioclase (albite), epidote, leucoxene and +/- quartz and opaques. The intrusive nature of the gabbro is often difficult to discern as the contact with sediments is usually conformable with the local and regional strike. In many cases the gabbro has been deformed to a fine grained, layered mylonite. This layering is parallel with the sedimentary layering, sometimes making it difficult to distinguish contacts. However the cross cutting relationship



of the gabbro to the sediments has been observed in many underground workings by Horwood and Pye and also on the surface (Fig. 15) at the Bankfield Mine site (Lavigne 1983).

At many locations the deformed gabbro has been disrupted by an oblique shear fabric C' (Berthe et al., 1979b) (Fig. 16). At most locations this fabric has been infilled by carbonate which has weathered out leaving a very rough, pitted surface. This appearance led to the interpretation of these rocks by Horwood and Pye as volcanic breccia and tuff.

Thin section analysis of the gabbro reveals its compositional heterogeneity. For instance at a single outcrop three separate phases of the gabbro were observed. The most common phase (at this outcrop) was a relatively undeformed, coarse grained (3-5mm) rock with a composition common to most of the gabbros in the study area; pyroxene replaced by actinolite, chlorite, albite, epidote, leucoxene +/- quartz and opaques (Fig. 17). A second phase consisted of pale green, fine grained patches or vugs within the coarse gabbro. This situation was observed at only a few locations and is believed to represent two separate phases of the same magma. The pale green patches consist of long (2-3mm) prisms of actinolite and rare hornblende in a fine matrix of plagioclase, quartz and epidote. The presence of primary hornblende in this rock may be related to a higher activity of volatiles (H<sub>2</sub>O) in the crystallizing melt. Hornblende was not observed in any other samples looked at during the present study.

The third sample from this same outcrop appeared similar







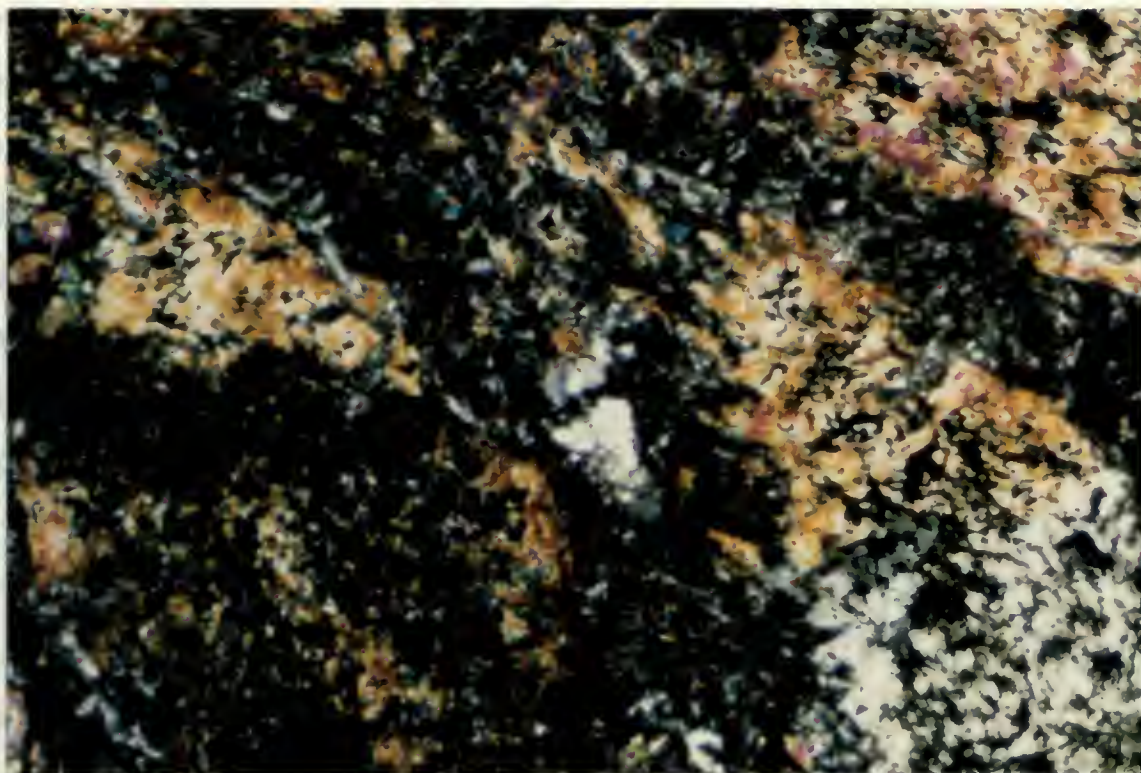
**Fig. 15. Gabbro intruding sediments. Dark green rock at bottom is gabbro.**



**Fig. 16. C fabric in gabbro.**

Fig. 15. Gabbro intruding sediments. Dark green rock at bottom is gabbro.

Fig. 16. C fabric in gabbro.



100μm

**Fig. 17. Thin section of undeformed gabbro.**





to the first gabbro but had a weak schistosity. In thin section it was seen to consist almost entirely of chlorite, carbonate and small amounts of plagioclase and epidote. The carbonate is a secondary mineral and appears to be introduced through alteration by CO<sub>2</sub> bearing fluids which combined with the calcium from altered pyroxenes and original plagioclase. This same situation was observed at many locations where the gabbro has been deformed.

## PORPHYRY

Felsic intrusions in the form of porphyries are also common throughout the study area. These intrusions were subdivided by Horwood and Pye into two units; a less common plagioclase diorite porphyry and the more common albite or quartz-albite porphyry. For the purpose of the present study these were combined and referred to as a felsic porphyry. Like the gabbro, porphyries are common near the Bankfield-Tombill fault and often deformed.

In general the porphyry is a grey to green rock which weathers to a pale grey or brown in which large (>5mm) phenocrysts of plagioclase are visible. As with the gabbro, the intrusive nature of the porphyry is difficult to determine at surface exposures due to concordance with the regional strike of the sediments. The problem becomes more difficult when the porphyry is deformed to a chloritic schist similar in appearance to both the deformed gabbro and sediments. The cross cutting relationship of the porphyry has been observed

1997-1998

in underground workings (Pye 1952) and also at the surface near the Bankfield mine site by Lavigne (1983), where it cuts layered sediments (Fig. 18). At this same location xenoliths of the deformed gabbro were observed (Lavigne 1983) within the porphyry, suggesting that felsic intrusions occurred after the intrusion and deformation of the gabbro. The porphyry too, is often deformed and so it seems that deformation continued or was reactivated during or after intrusion of the porphyry.

In thin section the porphyry is seen to consist of large (2 - 3 mm) grains of albite +/- quartz in a finer matrix of albite, quartz, chlorite and white mica. Many of the albite phenocrysts are altered to white mica (Fig. 19).

#### DIABASE DYKES

Two sets of diabase dykes are shown on Map 1. A north-south set has been displaced dextrally by the Bankfield-Tombill fault, while an east-west set has intruded parallel to that fault and another east-west break to the south. Outcrops of the north-south set, observed during the present study showed a typical diabasic texture and appeared to be undeformed. The displacement of these dykes, appears to have occurred during a late brittle stage of deformation along the Bankfield-Tombill fault.

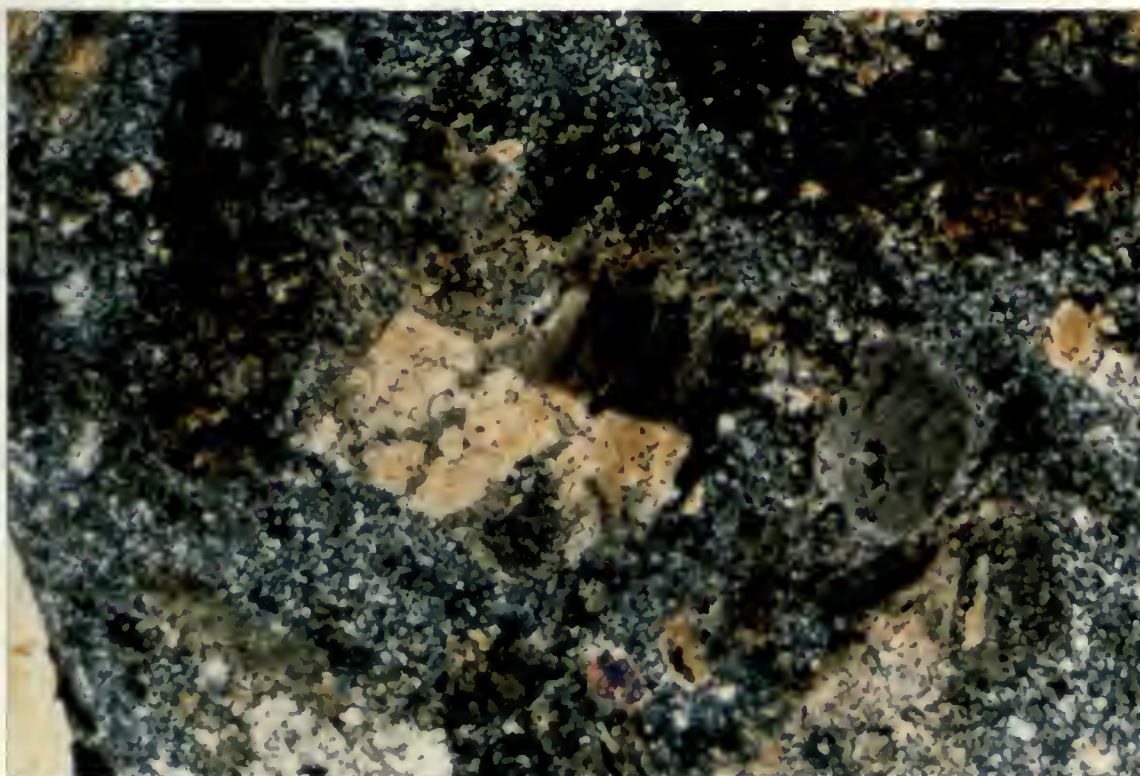
Pye (1952) found that the east-west set of dykes were essentially of the same composition as the north-south set. They consist mainly of labradorite and clinopyroxene with smaller amounts of quartz, hornblende, biotite and chlorite

PLEASE PRINT





**Fig. 18. Intrusive contact of porphyry and layered sediments.**



100µm

**Fig. 19. Thin section of porphyry showing large phenocrysts of feldspar and quartz.**



with +/- uralitic amphibole, sericite, magnetite and apatite.

## METAMORPHISM

The equilibrium mineral assemblages recorded in the metamorphosed gabbro and pelitic lithologies of the study area are; actinolite-chlorite-albite-epidote +/- quartz and albite-quartz-chlorite-white mica respectively. The observed assemblages suggest that lithologies of the area have been regionally metamorphosed to greenschist facies, in agreement with previous studies in the Beardmore-Geraldton belt (Mackasey 1976). The peak of metamorphism appears to pre-date deformation as highly deformed lithologies are characterized by late stage retrograde metamorphism, indicated by the presence of white mica in pelites and replacement of actinolite by chlorite in gabbros. The sheared rocks have also been subjected to a late carbonate alteration producing in most cases a chlorite-carbonate rich rock.

Biotite was not observed in rocks of suitable bulk composition, confining the area to the chlorite zone of the greenschist facies (Turner 1968). The observed assemblages within the chlorite zone suggest pressures between 2-10kb and temperatures between 250-450 degrees C (Turner 1968).





## STRUCTURAL GEOLOGY

Evidence of simple shear deformation within the Bankfield-Tombill Fault zone is provided by the presence of the gabbro mylonite. Structures outlined in the following section were mapped in detail in an attempt to determine the extent of deformation in rocks outside the shear zone.

Outcrops in the study area were almost always exposed only as a horizontal surface. Rare vertical exposure is usually parallel with both bedding or foliation. Where measurable, the dip of bedding and foliation was most often vertical or steep to the south. For these reasons, foliation measurements without dips were assumed to be vertical. For the same reasons, plunges of fold axes were usually difficult to determine and therefore at many locations axial traces only, could be measured. Statistically the orientation of folds with a measured plunge and those where the axial trace was measured is almost identical. For instance, the stereo plot maximum for "Z" fold axes is 257/24 (Fig. 41). The mean orientation of "Z" folds where only the axial trace was measured is 078, equivalent to 258 degrees.

## THE BANKFIELD-TOMBILL FAULT

The most intensely deformed rocks of the study area, mylonites, are found within the Bankfield-Tombill Fault (Map 1). The trace of this fault was mapped on surface and in drill core by the presence of a "tuff breccia" unit (Horwood and Pye), which has been reinterpreted by Lavigne (1983), as a



Evidence of simple shear is shown in Fig. 10. The  
Banded-Tourmaline Foliation (BTF) is composed of alternating  
the gabbro gneiss. At various points in the  
section were mapped in detail in an effort to determine the  
extent of deformation in these rocks. The shear is  
obvious in the study area where it is well exposed.  
Only a horizontal section. Both vertical sections in  
exactly horizontal with both bedding in foliation. However,  
whereas, the two sections and foliation are not often  
vertical or steep to the north. For example, the  
assessments within the area are as follows: (1)  
The same region, though it is not very different  
to determine and therefore it may be that the  
only could be measured. Characteristically, the  
foliation with a westward trend and where the  
are measured is almost identical. For example, the  
place maximum is 17° and is total (i.e., the  
orientation of the fold axis is only the angle  
measured is 0.9, equivalent to 208 degrees.

THE Banded-Tourmaline Foliation

The most intensely deformed zone of the area  
is foliated, and lying within the Banded-Tourmaline  
1). The (line of) fold axis is approximately  
parallel to the foliation. The fold axis is  
and eyes, which are approximately vertical.

gabbro mylonite. According to Horwood and Pye the fault trends east-west, dipping steeply southwards-100-110/65-70/s. However in outcrop, the well developed foliation defining the fault undulates through various orientations. Dips of vertical to steep south were most common but northerly dips were also measured suggesting that the foliation-fault system may also be undulating in a vertical plane.

Horwood and Pye noted that the fault zone was 40 to 200 feet in width. During the present study exposures of the fault 40 to 60 meters in width were mapped (Fig. 56). However, as observed on a small scale (Fig. 58), shear zones often form in an anastomosing pattern around large lithons of less deformed rock. A larger scale reflection of this pattern can be seen south of Mosher lake (Map 1), where a tuff-breccia unit, re-interpreted as gabbro mylonite, surrounds elongate lithons of less deformed gabbro. A more reasonable estimate of the width of the fault-shear zone is the 400-500 meter width of tuff-breccia shown on Map 1. Although displacement of north-south trending diabase dykes suggests a brittle component of deformation, the presence of mylonites and regional shear fabrics indicates that the dominant style of deformation was ductile shearing. Therefore the Bankfield-Tombill Fault can be interpreted as a regional scale ductile shear zone in which there has been a late period of brittle behavior.



## FOLIATIONS

The development of planar fabrics related to ductile shear has been well documented for both discrete centimeter wide shear zones (Ramsay and Graham 1970) and also for kilometer wide regional shear zone-ductile faults (Escher et al., 1975, Berthe et al., 1979a, Berthe et al., 1979b, Ponce de Leon and Choukroune 1980, Vernon et al., 1982, Simpson 1984). Three separate fabrics may form in a shear zone and accompanying mylonites, and each has been observed in the Geraldton area. These fabrics have been most clearly described by Berthe et al., (1979) and Simpson (1984), and it is their descriptions that were used to recognize the shear fabrics in the present study.

The S fabric is defined by a preferred mineral orientation which often produces a distinct schistosity (Berthe et al., 1979). When associated with small discrete shear zones (Fig. 20A), S is considered to represent the XY plane of the finite strain ellipsoid (Ramsay and Graham 1970).

In large regional shear zones the S fabric forms oblique to the shear direction and is often displaced by a second fabric defined by discrete millimeter-wide shear planes (Fig. 20B), which are oriented parallel with the shear zone boundaries. This second fabric has been defined by Berthe et al., as a C (cisaillement, shear) fabric and represents zones of higher strain concentration on which slip has taken place (Simpson 1984). Displacement along the C surfaces is in the same direction as that in the shear zone overall. The S fabric



The development of a new type of...  
 which has been well demonstrated...  
 when these zones began to...  
 characterized with various...  
 at 1970...  
 de Leon and...  
 1964). These...  
 accompanying...  
 described by...  
 in their...  
 fabric in the...

The 2...  
 orientation...  
 (Barton et al., 1970)...  
 shear zones...  
 plane of the...  
 in large...  
 the shear...  
 defined by...  
 which are...  
 This second...  
 crystalline...  
 repeat...  
 1964...  
 directed...



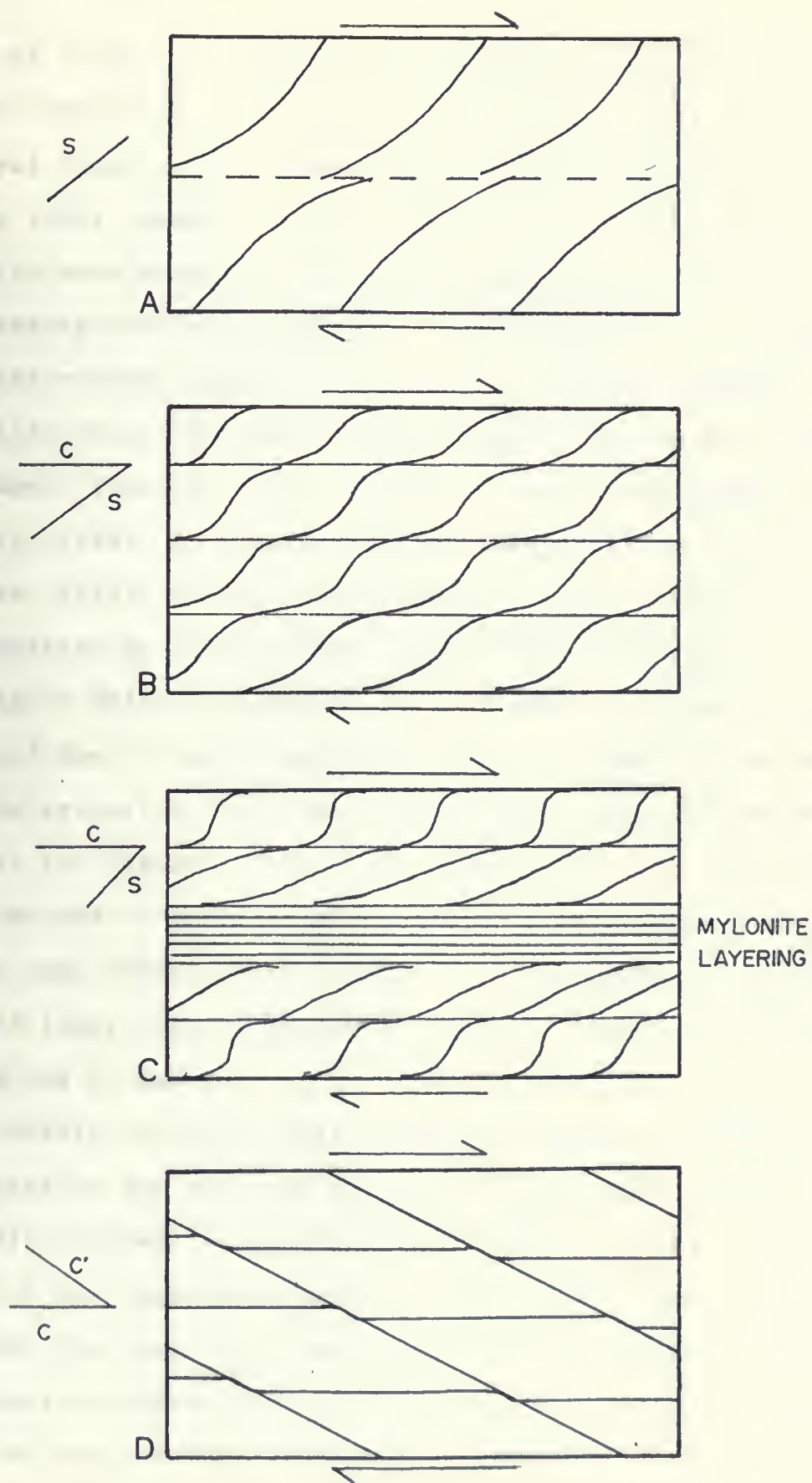


Fig. 20. Simple shear fabrics.



acts as a passive marker and the angle between it and the C fabric decreases with increased strain (Fig. 20C). At the highest strains they become parallel and are indistinguishable (Fig. 20C), producing a very strong mylonitic foliation.

In many mylonites and sheared pelitic rocks (Platt 1979, Weijermars and Rondeel 1984), a third fabric forms oblique to the shear zone boundary and often cuts and displaces the mylonite foliation (Fig. 20D). This fabric has been termed a C' fabric (Berthe et al., 1979), a "shear band" fabric (White et al., 1980), or an extensional "crenulation cleavage" (Platt, 1979), and is considered to develop during the same deformation episode as that which produces the mylonitic C fabric it deforms, but at a later stage. In some cases two sets of the C' fabric have been observed, both at low angles to the mylonitic foliation, with one set usually dominating (Platt and Vissars 1980). When only one set is observed it can be used to indicate the sense of displacement within the shear zone (White et al., 1980). In the present study only one of these late stage fabrics was observed and is referred to as the C' fabric.

Within the study area, fabrics related to ductile deformation are observed most clearly in rocks within or closely adjacent to the Bankfield-Tombill fault. However several well developed fabrics exist in rocks up to 2 km outside the fault zone and appear to be related to the same deformation mechanism.

The most obvious foliation in the study area is seen as

with a positive effect on the rate of growth.

Public investment with increasing rates of growth.

higher rates they become positive and the rate of growth.

(Fig. 200), producing a very strong positive effect.

in many cases and the effect is very strong.

Wallerstein and Mandel (1963) in their study of the

the same time, however, and often only in a few cases.

economic situation (Fig. 100). This fact is very

of fact (Gordon et al. 1963), a "strong" effect.

et al. 1963, or to a significant "strong" effect.

(Fig. 100), and it is considered as a "strong" effect.

deformation of the rate of growth is very strong.

change in the rate of growth is very strong.

rate of the rate of growth is very strong.

to the rate of growth is very strong.

(Fig. 100) when the rate of growth is very strong.

can be used to indicate the rate of growth is very strong.

where the rate of growth is very strong.

rate of growth is very strong.

rate of growth is very strong.

rate of growth is very strong.

rate of growth is very strong.

rate of growth is very strong.

rate of growth is very strong.

rate of growth is very strong.

rate of growth is very strong.

rate of growth is very strong.

rate of growth is very strong.

rate of growth is very strong.



the well graded layering of the sediments. In several locations, especially in the southern portion of the map area, grading and dewatering structures were so well formed that the layering is considered to represent unmodified original bedding. However in most cases, evidence of deformation within the layers, especially the pelitic layers suggests that original bedding has been subjected to a great deal of transposition. In some cases layering becomes discontinuous and original bedding is destroyed. The average regional strike of the layering is 096-099/V-65/s (Fig. 21). Where well developed bedding is obvious, the strike is 100/V-65/s (Fig. 22). In both cases these strikes are very close to the average orientation of the Bankfield-Tombill Fault 100/65/s. The trend of the layering varies both at outcrop scale and also regionally (Fig. 23A), often producing an undulating pattern.

The best evidence of deformation within the layered sediments is the presence of a strong, usually layer parallel fabric. This fabric is defined by elongated pebbles and clasts in conglomerates and coarser psammitic layers (Fig. 11) and a weak slaty cleavage to well developed spaced cleavage in the pelitic sediments (Fig. 35). Although this cleavage is usually subparallel with the layering, differences of up to 10 degrees were observed in the field. The orientation, 097-099/V-65/s (Fig. 24) of this fabric is approximately parallel with the Bankfield-Tombill Fault and the C fabric in the gabbro mylonite, and is considered to represent a regional



Keywords: *workplace spirituality, organizational commitment, turnover intentions, organizational citizenship behaviors, organizational trust*

ALL INFORMATION CONTAINED HEREIN IS UNCLASSIFIED

1993, 1994, 1995, 1996, 1997, 1998, 1999, 2000, 2001, 2002, 2003, 2004, 2005, 2006, 2007, 2008, 2009, 2010, 2011, 2012, 2013, 2014, 2015, 2016, 2017, 2018, 2019, 2020, 2021, 2022, 2023, 2024, 2025, 2026, 2027, 2028, 2029, 2030, 2031, 2032, 2033, 2034, 2035, 2036, 2037, 2038, 2039, 2040, 2041, 2042, 2043, 2044, 2045, 2046, 2047, 2048, 2049, 2050, 2051, 2052, 2053, 2054, 2055, 2056, 2057, 2058, 2059, 2060, 2061, 2062, 2063, 2064, 2065, 2066, 2067, 2068, 2069, 2070, 2071, 2072, 2073, 2074, 2075, 2076, 2077, 2078, 2079, 2080, 2081, 2082, 2083, 2084, 2085, 2086, 2087, 2088, 2089, 2090, 2091, 2092, 2093, 2094, 2095, 2096, 2097, 2098, 2099, 2100, 2101, 2102, 2103, 2104, 2105, 2106, 2107, 2108, 2109, 2110, 2111, 2112, 2113, 2114, 2115, 2116, 2117, 2118, 2119, 2120, 2121, 2122, 2123, 2124, 2125, 2126, 2127, 2128, 2129, 2130, 2131, 2132, 2133, 2134, 2135, 2136, 2137, 2138, 2139, 2140, 2141, 2142, 2143, 2144, 2145, 2146, 2147, 2148, 2149, 2150, 2151, 2152, 2153, 2154, 2155, 2156, 2157, 2158, 2159, 2160, 2161, 2162, 2163, 2164, 2165, 2166, 2167, 2168, 2169, 2170, 2171, 2172, 2173, 2174, 2175, 2176, 2177, 2178, 2179, 2180, 2181, 2182, 2183, 2184, 2185, 2186, 2187, 2188, 2189, 2190, 2191, 2192, 2193, 2194, 2195, 2196, 2197, 2198, 2199, 2200, 2201, 2202, 2203, 2204, 2205, 2206, 2207, 2208, 2209, 2210, 2211, 2212, 2213, 2214, 2215, 2216, 2217, 2218, 2219, 2220, 2221, 2222, 2223, 2224, 2225, 2226, 2227, 2228, 2229, 2230, 2231, 2232, 2233, 2234, 2235, 2236, 2237, 2238, 2239, 2240, 2241, 2242, 2243, 2244, 2245, 2246, 2247, 2248, 2249, 2250, 2251, 2252, 2253, 2254, 2255, 2256, 2257, 2258, 2259, 2260, 2261, 2262, 2263, 2264, 2265, 2266, 2267, 2268, 2269, 2270, 2271, 2272, 2273, 2274, 2275, 2276, 2277, 2278, 2279, 2280, 2281, 2282, 2283, 2284, 2285, 2286, 2287, 2288, 2289, 2290, 2291, 2292, 2293, 2294, 2295, 2296, 2297, 2298, 2299, 2300, 2301, 2302, 2303, 2304, 2305, 2306, 2307, 2308, 2309, 2310, 2311, 2312, 2313, 2314, 2315, 2316, 2317, 2318, 2319, 2320, 2321, 2322, 2323, 2324, 2325, 2326, 2327, 2328, 2329, 2330, 2331, 2332, 2333, 2334, 2335, 2336, 2337, 2338, 2339, 2340, 2341, 2342, 2343, 2344, 2345, 2346, 2347, 2348, 2349, 2350, 2351, 2352, 2353, 2354, 2355, 2356, 2357, 2358, 2359, 2360, 2361, 2362, 2363, 2364, 2365, 2366, 2367, 2368, 2369, 2370, 2371, 2372, 2373, 2374, 2375, 2376, 2377, 2378, 2379, 2380, 2381, 2382, 2383, 2384, 2385, 2386, 2387, 2388, 2389, 2390, 2391, 2392, 2393, 2394, 2395, 2396, 2397, 2398, 2399, 2400, 2401, 2402, 2403, 2404, 2405, 2406, 2407, 2408, 2409, 2410, 2411, 2412, 2413, 2414, 2415, 2416, 2417, 2418, 2419, 2420, 2421, 2422, 2423, 2424, 2425, 2426, 2427, 2428, 2429, 2430, 2431, 2432, 2433, 2434, 2435, 2436, 2437, 2438, 2439, 2440, 2441, 2442, 2443, 2444, 2445, 2446, 2447, 2448, 2449, 2450, 2451, 2452, 2453, 2454, 2455, 2456, 2457, 2458, 2459, 2460, 2461, 2462, 2463, 2464, 2465, 2466, 2467, 2468, 2469, 2470, 2471, 2472, 2473, 2474, 2475, 2476, 2477, 2478, 2479, 2480, 2481, 2482, 2483, 2484, 2485, 2486, 2487, 2488, 2489, 2490, 2491, 2492, 2493, 2494, 2495, 2496, 2497, 2498, 2499, 2500, 2501, 2502, 2503, 2504, 2505, 2506, 2507, 2508, 2509, 2510, 2511, 2512, 2513, 2514, 2515, 2516, 2517, 2518, 2519, 2520, 2521, 2522, 2523, 2524, 2525, 2526, 2527, 2528, 2529, 2530, 2531, 2532, 2533, 2534, 2535, 2536, 2537, 2538, 2539, 2540, 2541, 2542, 2543, 2544, 2545, 2546, 2547, 2548, 2549, 2550, 2551, 2552, 2553, 2554, 2555, 2556, 2557, 2558, 2559, 2560, 2561, 2562, 2563, 2564, 2565, 2566, 2567, 2568, 2569, 2570, 2571, 2572, 2573, 2574, 2575, 2576, 2577, 2578, 2579, 2580, 2581, 2582, 2583, 2584, 2585, 2586, 2587, 2588, 2589, 2590, 2591, 2592, 2593, 2594, 2595, 2596, 2597, 2598, 2599, 2600, 2601, 2602, 2603, 2604, 2605, 2606, 2607, 2608, 2609, 2610, 2611, 2612, 2613, 2614, 2615, 2616, 2617, 2618, 2619, 2620, 2621, 2622, 2623, 2624, 2625, 2626, 2627, 2628, 2629, 2630, 2631, 2632, 2633, 2634, 2635, 2636, 2637, 2638, 2639, 2640, 2641, 2642, 2643, 2644, 2645, 2646, 2647, 2648, 2649, 2650, 2651, 2652, 2653, 2654, 2655, 2656, 2657, 2658, 2659, 2660, 2661, 2662, 2663, 2664, 2665, 2666, 2667, 2668, 2669, 2670, 2671, 2672, 2673, 2674, 26

Labeling is considered to represent

Published by the American Psychological Association or one of its allied publishers. This article is intended solely for the personal use of the individual user and is not to be disseminated broadly.

With the above, we can now state the following theorem:

and related building is destroyed. The owner is liable

ALL INFORMATION CONTAINED HEREIN IS UNCLASSIFIED DATE 01-25-2001 BY 60322 UCBAW/STP

[illegible]

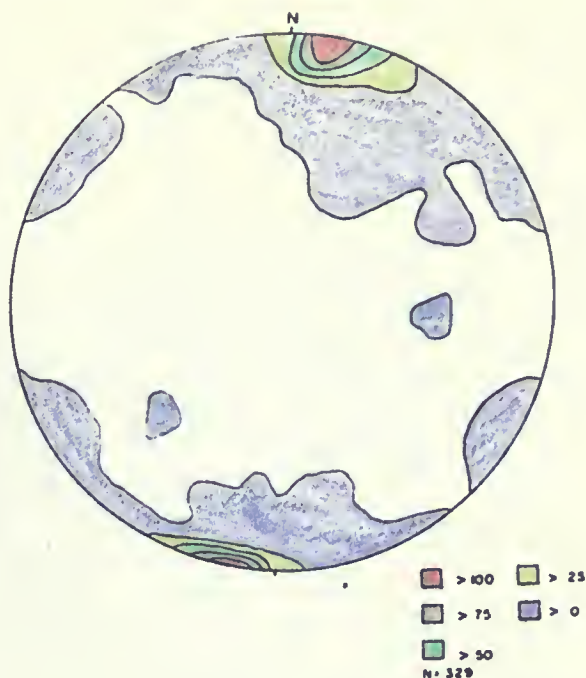
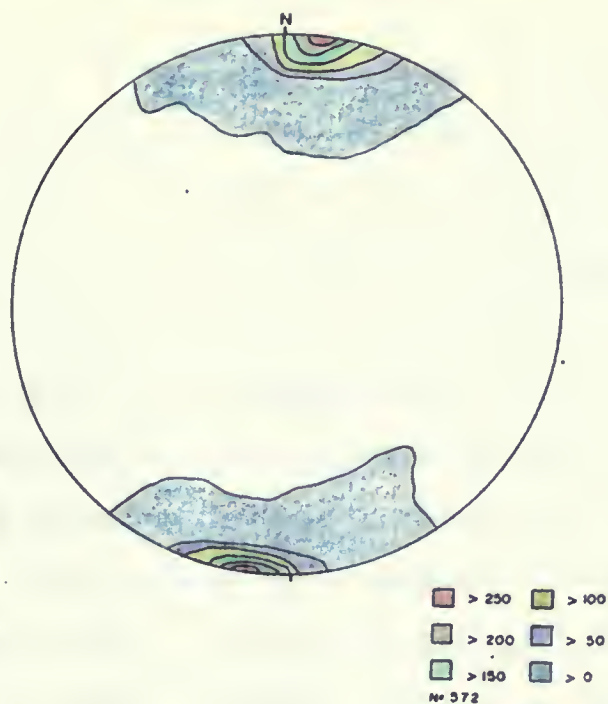


Fig. 21 Layering plotted as poles to a plane.  
Maximum=096-099/V-65/s.



Fig. 22 Bedding plotted as poles to a plane.  
Maximum=100/V-65s.





**Fig. 24 "C" fabric plotted as poles to a plane.  
Maximum=097-099/V-65/s.**



**Fig. 25 Vein displaced and folded by "C" fabric.**





reflection of a C fabric. Quartz veins oblique to this fabric are commonly displaced dextrally or tightly folded with their axial traces parallel with the cleavage (Fig. 25). Veins parallel to the cleavage often exhibit boudinage and pinch and swell structures (Fig. 6). At most locations the cleavage along with the layering is asymmetrically folded. In some cases the folded layering and cleavage are disrupted by discrete shear planes parallel with the axial trace of the fold (Fig. 42). The similarities between the orientation of the layering and this C fabric and their parallelism with the Bankfield-Tombill fault is shown in Figures 23A and 23B. Within the, sediments deformation seems to be concentrated in the pelitic layers. The alternating psammitic layers often appear totally undeformed and exhibit well developed grading which is considered a reliable indicator of younging direction (Hobbs et al., 1976). In most cases this method suggests a northwards younging direction and in some locations indicates slightly overturned bedding.

At several locations a secondary fabric is observed in the psammitic layers. This fabric is usually weakly defined by a preferred mineral and clast orientation. It is discordant to the C fabric by 15-25 degrees with an average orientation of 084/V-80/s (Fig. 26). A similar fabric with the same orientation is often defined by elongated minerals in some outcrops of gabbro and tuff. At other places in the sediments this fabric is defined by irregular spaced cleavage planes which at one location were seen to be displaced by a

reflection of a C fabric. Quartz veins within the fold are commonly oriented vertically or slightly inclined with their axial traces parallel with the cleavage (Fig. 2). Within parallel to the cleavage some (small) bedding was found with well structures (Fig. 3). At one location the cleavage along with the folding is asymmetrically folded. The same cases the folded bedding and cleavage are not necessarily discrete shear planes (small) with the axial trace of the fold (Fig. 4). The relationships between the axial trace of the layering and the C fabric and their horizontal distance from Bankfield Tombill are shown in Figure 2. Within the sedimentary deformation zone the cleavage is the pelitic layers. The siliceous (quartzite) layers appear locally undisturbed and locally well deformed in places which is considered a reliable indicator of relative position (Hobbs et al., 1970). In some cases this relation suggests that the younging direction and is from left to right. Xlightly deformed bedding.

At several locations a secondary C fabric is observed in the pelitic layers. This fabric is usually well developed by a preferred mineral and cleavage pattern. It is discordant to the C fabric by the disagreement with orientation of cleavage (Fig. 5). A similar pattern in the same orientation is then defined by elongated mineral in some outcrops of gneiss and quartz. A similar pattern is defined in the fold. It is not clear if this is a secondary fabric or if it is a remnant of the primary C fabric.



Fig. 26 "S" fabric plotted as poles to a plane.  
Maximum=084/V-80/s.



Fig. 27 "S" fabric here defined by a cleavage which bends  
into the "C" fabric.





strong C fabric (Fig. 27). When plotted on a regional map (Fig. 23C), this fabric appears to be displaced dextrally by the Bankfield-Tombill fault, producing a sigmoidal pattern. This suggests that this fabric may represent a regional reflection of an S fabric.

A third fabric with an orientation approximately 110-120/V, discordant to all other fabrics was also seen in a few outcrops, mainly in the southwestern part of the map area.

The sediments in this area are for the most part relatively undeformed. This discordant fabric is usually defined by an irregularly spaced cleavage which often exhibited refraction from one layer to another. Displacement along this fabric was not observed.

A well developed C' fabric was not clearly observed in rocks other than the mylonites within the fault zone. However at some locations where pelitic sediments or tuff have been strongly deformed, planes of displacement with a similar orientation as the C' in the mylonite were observed (Fig. 6). The average regional attitude of the C' fabric 130/V as shown in Figure 28, is derived almost entirely from measurements at mylonite locations.

## LINEATIONS

Within shear zones, stretching lineations are commonly seen on C surfaces (Berthe' et al., 1979), and regionally usually plot closely parallel with the orientation of the shear zone (Jegouzo 1980, Ponce de Leon and Choukroune 1980,





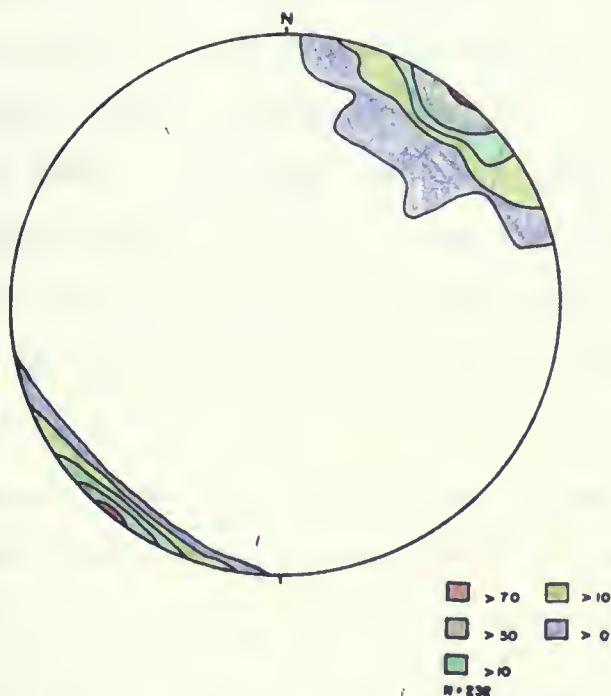


Fig. 28 "C'" fabric plotted as poles to a plane.  
Maximum=130/V.



Burg et al., 1981). When observed in relationship to a shear zone lineations of this type are considered to reflect the direction of maximum elongation, the X axis of the finite strain ellipsoid (Ramsay 1980).

Within the study area a well developed stretching lineation is defined by elongated pebbles in conglomerates and coarse grained sediments, elongated clasts in tuff and elongated minerals in both gabbro and tuff. A crinkle lineation of the same orientation is often seen in the pelitic sediments on C surfaces (Fig. 29). These stretching lineations are subhorizontal (Fig. 30), and parallel with the shear zone suggesting that the S fabric (X axis of the strain ellipse) becomes parallel to C.

Other types of lineation seen in the study area include slickensides and intersection lineations. Slickensides are seen only rarely, at locations along the Bankfield-Tombill fault. The slickensides are seen on the vertical C surfaces and are always subhorizontal, similar to the crinkle lineation. Within the layered sediments, a well developed lineation is often observed due to the intersection of folded layers and shear planes parallel with the C foliation. This lineation usually has a similar orientation and plunge (280/15-40) as local and regional fold axes.

#### SHEAR FABRICS IN THE GABBRO MYLONITE

A gabbro mylonite is exposed at several locations within or closely adjacent to the Bankfield-Tombill fault. At two of these locations (Fig. 55), the mylonite was mapped in detail

Burd et al., 1981). When observed in thin section, shear zone lineations of this type are considered to represent the direction of maximum elongation, the X axis of the finite strain ellipsoid (Ramsey, 1980).

Within the study area a well developed stretch lineation is defined by elongated pebbles in conglomerates and coarse grained sediments, elongated clasts in tuff and elongated minerals in both gabbro and tuff. A consistent lineation of the same orientation is often seen in the pelitic sediments on C surfaces (Fig. 29). These stretch lineations are subhorizontal (Fig. 30), and parallel with the shear zone suggesting that the S fabric (X axis of the strain ellipsoid) becomes parallel to C.

Other types of lineations seen in the study area include slickensides and intersection lineations. Slickensides are seen only rarely, at locations along the Bonfield fault. The slickensides are seen on the vertical C surfaces and are always subhorizontal, similar to the Clinch lineation. Within the layered sediment, a well developed lineation is often observed due to the intersection of foliation layers and shear planes parallel with the C foliation. This lineation usually has a similar orientation and sense (230/15-40) as local and regional fold axes.

#### SHEAR FABRICS IN THE GABBRU MYLONITE

A gabbro mylonite is exposed at several locations or closely adjacent to the Bonfield fault. In two of these locations (Fig. 31), the mylonite was mapped in detail.





Fig. 29. Crinkle lineation on C surface.

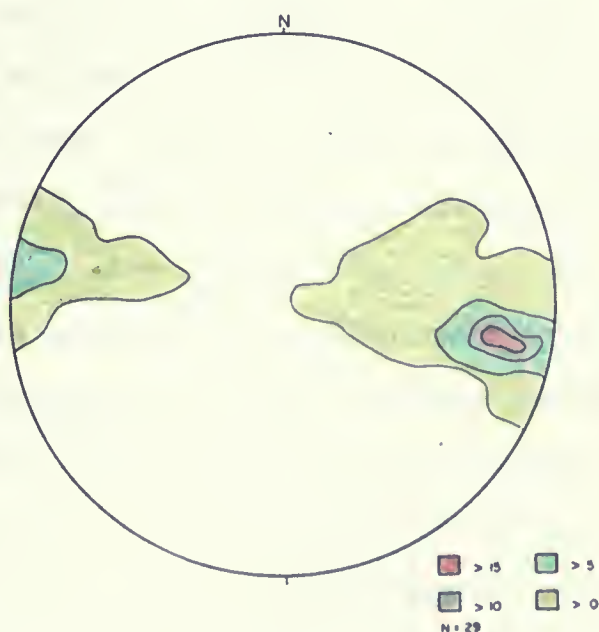


Fig. 30. Stretching lineations. Maximum = 100/20.



(Figs. 56 and 57), and studied in thin section. This mylonite provides the clearest examples of ductile shear fabrics. An S fabric is defined by elongated amphiboles and is observed to bend into a series of thin (<5cm) discrete shear zones (Fig. 31), producing the classic pattern described by Ramsay and Graham (1970). Displacement of the S fabric by a C fabric (Berthe et al., 1979, Simpson 1984) is not well defined at the outcrop scale but was seen in thin section (Fig. 59).

The discrete shears into which the S fabric is displaced, form an anastomosing pattern but in most cases are close to parallel with a strong local C fabric. The C is defined by a mineral elongation fabric (Fig. 60) and also a well developed mylonitic layering which at some locations is folded (Fig. 65). In many parts of the mylonite outcrops, the C foliation is disrupted by discrete surfaces of dextral displacement oblique to C by 10 to 45 degrees, a C' fabric. The intensity of disruption by the C' fabric varies over the mylonite outcrop. When the C fabric is defined by mineral elongation or a weak layering the C' surfaces are often short across strike and irregularly spaced (Fig. 60). At other locations within the same outcrop, well developed mylonitic layering is completely disrupted in clearly defined zones up to 1.5m wide (Fig. 64). The displacement of the C fabric by the C' fabric suggests that the C' fabric forms at a later stage of the deformation process. This is further supported by the presence of C' surfaces cutting folded mylonitic layers (Fig. 65). The average regional orientations of C and C' fabrics

(Page 55 and 56) ... provides the ... fabric is ... into a ... (1), producing the ... Graham (1970) ... (Borish et al., 1970, 1971, 1972) ... out-of-scale ... The electric ... form an ... parallel with a ... mineral elongation ... foliation layering ... (5). In ... is disrupted by ... due to C.F. ... of disruption ... petrology. When ... as a weak layering ... finite and ... within the ... completely ... (Fig. 54). The ... suggests that ... geological ... presence of ... (6). The ...



**Fig. 31. S fabric defined by elongated minerals bending into anastomosing shears.**



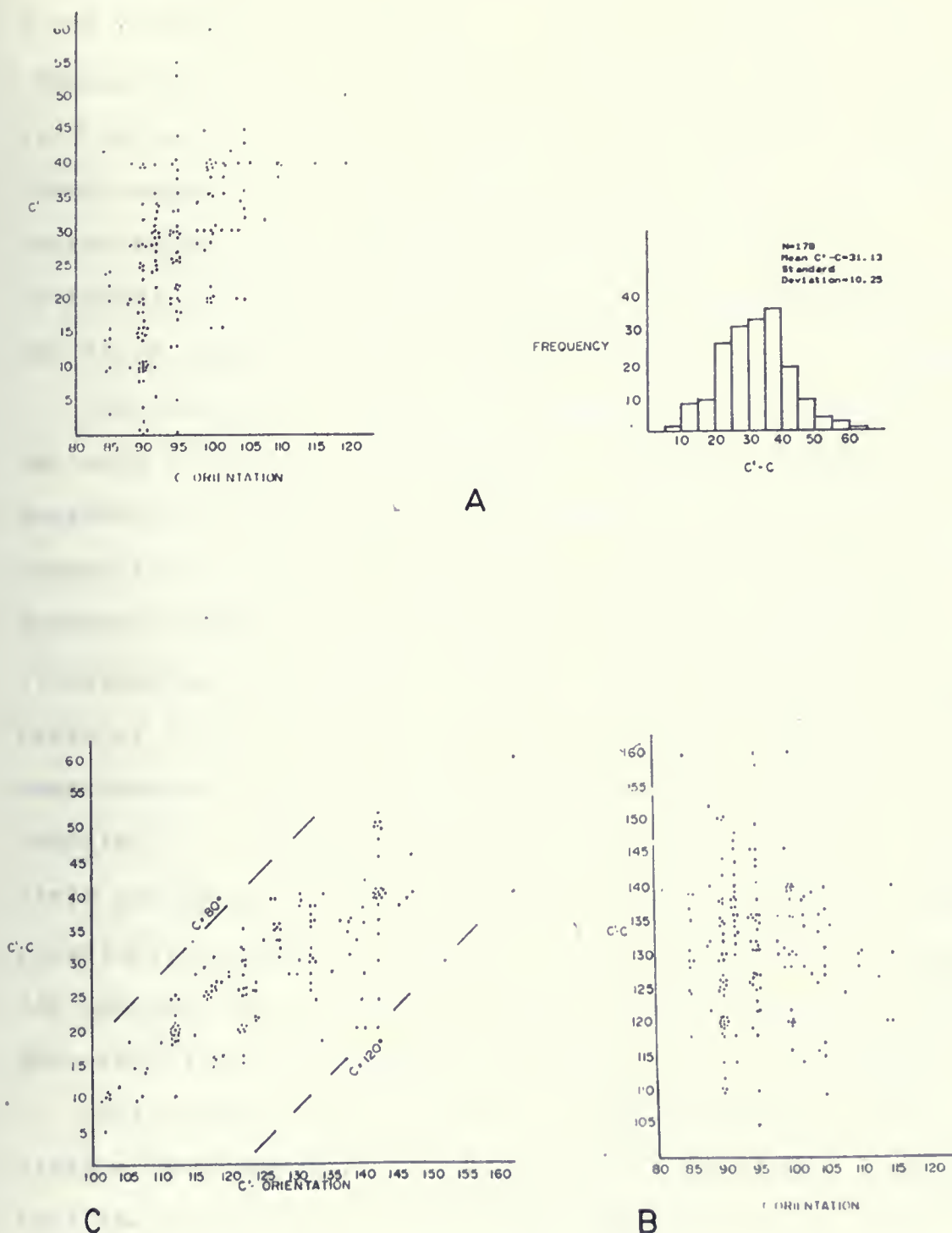
Fig. 31. S fabric defined by elongated minerals bending  
into anastomosing shears.

are shown in Figures 24 and 28. However in single exposures of the gabbro mylonite, the C foliation often undulates through various orientations. The C' fabric is also observed to vary greatly in orientation, even over 10's of centimeters.

In studies of mylonites by other workers, the average angle between the C and C' fabrics is usually observed to be less than 45 degrees (Gapais and White 1982). Commonly the average angle has been observed to be approximately 30 degrees (White et al., 1980). Platt (1984) suggests that when conjugate sets of C' develop, the angle between C and the dominant set of C' is 15 to 20 degrees.

The average angle between the C and C' fabrics in the gabbro mylonites of the present study area is 31 degrees with a standard deviation of 10 degrees (Fig. 32A). When the orientations of C and C' are plotted against each other (Fig. 32A), a weak correlation appears to be present, suggesting that the orientation of the C' fabric may be related to the orientation of C. To test this observation, the angle between the two fabrics was plotted against each separately. When the angle is plotted against the orientation of C, as in Figure 32B, the resulting scatter of measurements suggests that there is little or no relationship between the orientation of C and the angle made with C'. In fact, for any orientation of C it can be seen that the orientation of C' varies a great deal. For instance from Figure 32B, it can be seen that for a C orientation of 095 the angle between C and C' ranges from 5 to 60 degrees.

are shown in Figure 1 and 2. The results of the  
of the various systems are shown in Figure 3.  
for each system is shown in Table 1. The results of the  
to each system is shown in Table 2. The results of the  
In Figure 4, the results of the various systems are  
angle between the two systems is shown in Figure 5.  
from the 15 degree angle of the two systems.  
average of 15 degree angle of the two systems.  
(White et al., 1950). The results of the various  
contrast with the results of the various systems.  
between the two systems is shown in Figure 6.  
The results of the various systems are shown in Figure 7.  
between the two systems is shown in Figure 8.  
a standard deviation of 15 degree angle of the two systems.  
orientation of the two systems is shown in Figure 9.  
(1950), a mean deviation of 15 degree angle of the two systems.  
that the orientation of the two systems is shown in Figure 10.  
calculation of 15 degree angle of the two systems.  
the two systems is shown in Figure 11.  
angle is shown in Figure 12.  
350, the results of the various systems are shown in Figure 13.  
is shown in Figure 14.  
the results of the various systems are shown in Figure 15.  
can be seen that the results of the various systems are shown in Figure 16.  
from the 15 degree angle of the two systems.  
orientation of the two systems is shown in Figure 17.  
to the results of the various systems.



**Fig. 32.** Plots of  $C$  and  $C'$  orientations for all gabbros in the study area ( $C'-C$  is used on the plots to represent the angle between the two fabrics). A, plot of  $C$  vs  $C'$  plus a histogram plot of the  $C'-C$ . B, plot of the angle between the fabrics versus the orientation of  $C$ . C, plot of the angle between the fabrics versus the orientation of  $C'$ .





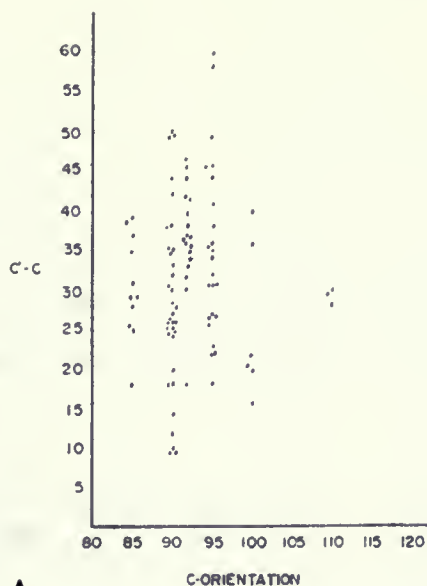
At first glance the plot of  $C'$  against the angle between  $C$  and  $C'$  (Fig. 32C), suggests a relatively strong correlation.

However the angle is measured in relation to the orientation of  $C$  which only ranges from 080 to 120. Therefore the linear trend suggested in Figure 32C, is actually the result of this narrow range of  $C$ . Within the boundaries of the  $C$  orientations the measurements describe a scatter, supporting the field impression that the orientation of  $C'$  is variable.

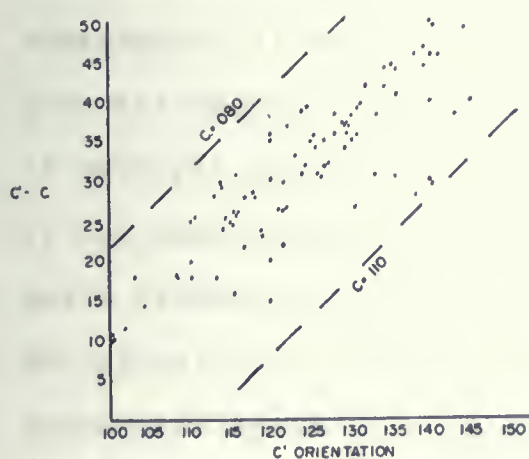
As pointed out earlier the composition of gabbros within the area is quite heterogeneous. As strain is in part dependent on lithology, this regional heterogeneity in composition may have an effect on  $C'$  formation and thus the scatter of data in Figures 32B and 32C, may reflect the lithological heterogeneity. To test this possibility, similar plots of  $C$ ,  $C'$  and the angle between  $C$  and  $C'$  were made using measurements from the single outcrop of gabbro mylonite at location 2. This outcrop was studied in detail both in the field and by thin section analysis and is considered to be relatively homogeneous locally. The results shown in Figures 33A and 33B, are virtually the same as the suggested by the data from all of the gabbro mylonites (Figs. 32B and 32C).

Detailed field analysis of  $C'$  structures (Platt and Vissers 1980) and theoretical geometry (Platt 1984), suggests that the  $C'$  fabric may rotate with continued deformation. Weljermeers and Rondeel (1984) have used this suggestion to conclude that since the angle between  $C$  and  $C'$  in the sheared pelites of the Macizo de Nevera of Spain remains consistently

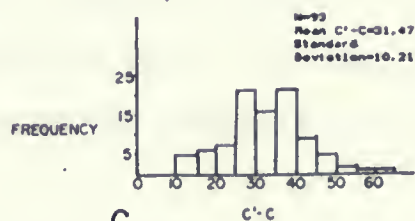




A



B



C

**Fig. 33. Plots of C and C' orientations for the gabbro at location 2. A, the angle between the fabrics versus C. B, the angle between the fabrics versus C'. C, histogram plot of the angle between the fabrics.**



at 18-25 degrees, there has been no rotation subsequent to formation of the C' fabric. However in the Betic Movement Zone (Platt and Vissers 1980), multiple sets of C' have been observed and interpreted as being the result of rotation during continued simple shearing. In this case the sets of C' at lower angles to the shear zone boundary (C foliation) represent an older set and higher angle sets represent later C' formation.

The variable orientation of C' in the present study may be interpreted as the result of rotation of an earlier set of C' with the subsequent formation of a later set. Support of this idea is suggested by a histogram plot of the angle between the C and C' fabrics in the gabbro mylonite of location 2 (Fig. 33C), which shows the presence of two populations at 25-30 and 35-40 degrees. If the conclusion that C' has been rotated due to continued deformation is acceptable, it seems logical to suggest that rocks showing the greatest degree of deformation should show; (i) the presence of multiple sets of C' and (ii) an increased frequency of C' at low angles to C. To investigate these possibilities the angle between C and C' was measured in three separate parts of the mylonite at location 2, representing progressively greater degrees of mylonitization.

In the first case, the gabbro is weakly foliated but has a well developed mineral fabric defining the C fabric. The C' fabric present at this stage is widely spaced, often occurring as single discrete surfaces (Fig. 60). The average angle



at 12-15 degrees, 1957, for land.

formation of the C. layer.

Zone (Plate and Vasey) which includes the C. layer.

observed and interpreted as being the result of

during continued slight erosion.

at lower angle to the west side of the valley.

represented in side 25, and side 26.

C. formation.

The section of the C. layer.

is interpreted as the result of erosion of the C. layer.

C. with the subsequent erosion of the C. layer.

this idea is suggested by the following facts:

between the C. and C. layer.

location (C. 1957) which shows the C. layer.

erosion at 25-30 and 35-40 degrees.

that C. has been forced down to a lower position.

consequently, it seems logical to expect that the C. layer

greater degree of dissection would show in the C. layer.

of which side 25 and (1957) side 26.

at low angle to C. 1957.

angle between C. and C. was measured in 1957.

the erosion at location 25, 1957, and 1957.

degree of dissection.

In the first case, the erosion is more pronounced.

a well developed (1957) form.

which is shown in 1957.

as shown in 1957.

between C and C' is 23.7 degrees with a relatively small standard deviation of 7.7 degrees. The histogram plot for this stage of deformation (Fig. 34A), shows a single population at 25-30 degrees. The second stage of mylonite is strongly foliated with a well developed chlorite-feldspar mylonitic layering. C' occurs more regularly than in the previous stage but is usually relatively widely spaced ( $>5\text{cm}$ ).

The average angle between C and C' for this stage is 34.7 with a standard deviation of 10.4 degrees. The histogram for this stage (Fig. 34B), shows the presence of two populations at 25-30 and 35-40 degrees. The third set of measurements comes from 1 meter wide zones of the well layered mylonite which have been totally disrupted by a closely spaced ( $<1\text{cm}$ ) C' foliation (Fig. 62). The average angle between C and C' is 29.9 degrees with a standard deviation of 10.0 degrees, similar to the results of the previous stage. However the histogram for this most deformed stage (Fig. 34C), more clearly defines two populations at 20-25 and 35-40 degrees. It also shows that there are more examples of C' at low angles to C at this stage.

## FOLDING

The most obvious evidence of deformation within the study area is the presence of abundant asymmetric Z style folding. As shown on Map 1, macroscopic (amplitudes  $>10\text{m}$ ) and megascopic regional scale folding, especially of banded iron formation is evident from surface mapping, drill core

WORLD LEAD

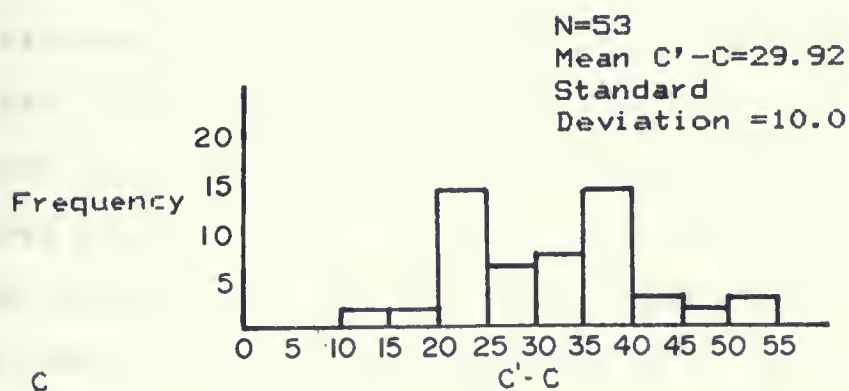
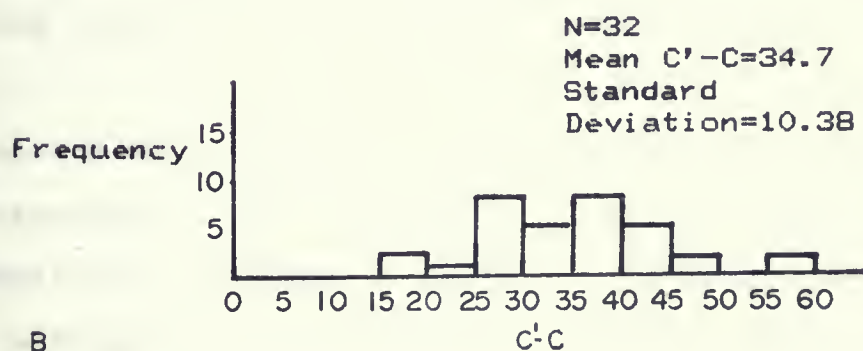
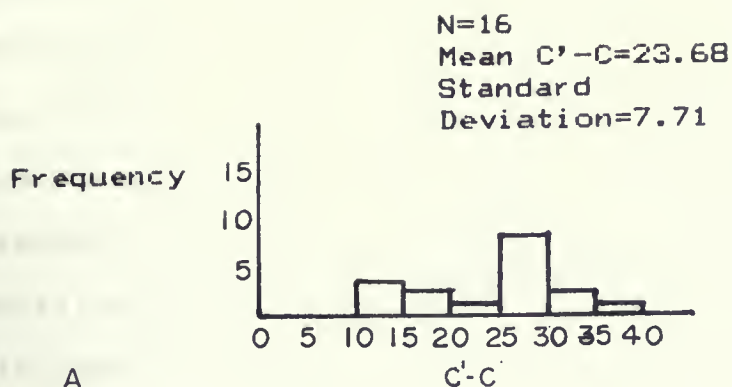


Fig. 34 Histogram plots of the angle between "C" and "C'" ( $C'-C$ ) for separate stages of the gabbro mylonite at location 2. A-C=progressive degrees of "C'" intensity.





information and magnetic survey. Asymmetric folding, related to shear zones and mylonites, has been observed by several workers (Berthe and Brun 1980, Cobbold and Quinquis 1980, Ponce de Leon and Choukroune 1980). The shape of these folds is related to the sense of displacement within a shear zone. Typically, S style folds prevail in a sinistral shear zone and Z style folds in a dextral shear zone (Cobbold and Quinquis 1980). Thus the prevalence of Z style folds in the study area indicates the presence of a dextral shear zone.

#### Mesoscopic Z Style Folding

Mesoscopic (amplitude <1m) Z style folding is present throughout the study area. However the intensity of folding varies and appears to be related to several factors including the degree of foliation development, distance from the Bankfield-Tombill Fault and the presence of banded iron formation. Closely adjacent to the Bankfield-Tombill Fault most rock types are well foliated and intensely folded. In exposures south of the fault, folding is observed to be most intense in the more thinly laminated sediments (Fig. 5) and in general the frequency of folding observed in outcrop decreases southwards. Approximately 1km south of the fault the sediments become more massive and folding is rarely observed.

To the north, both mesoscopic and macroscopic folding persist to the contact with the mafic volcanics, 3km north of the Bankfield-Tombill Fault. Exposures in this area are commonly strongly foliated, often by a well developed spaced



cleavage and intensely folded at a mesoscopic scale (Fig 35). Banded iron formation, absent in the sediments south of the fault is common in the north with exposures commonly revealing intense mesoscopic and macroscopic folding (Fig 13).

Although the attitude of these Z folds varies even at a single location, the stereo plot maximum for all of the mesoscopic Z fold axes measured is 257/20 (Fig. 36). The mean orientation of all Z fold axial traces is 078 or its complementary orientation 258. In most cases there is no evidence that these mesoscopic folds are parasitic to larger scale structures. Z folds of mesoscopic size occur in the layered sediments and iron formation, the conglomerate and tuff units where the well developed C foliation is folded, and also in the gabbro mylonite where the mylonitic layering is folded. Evidence supporting the observation that the C fabric is folded along with layering includes folding of a well developed spaced cleavage (Fig. 35), folded veins which have infilled the cleavage (Fig. 37), and folded conglomerate and tuff units in which clasts have been elongated parallel with C and folded (Figs. 11 and 38).

In some cases the Z folding affects areas several meters in width (Fig. 39). In other locations only one or two layers appear to be folded while surrounding layers are unaffected (Fig. 5). In the former case the axial trace of the folds is often observed to bend towards the C direction (Fig. 40), for example, changing in attitude from 250/w to 270/w. In most cases the folds with axial traces of orientations less than



cleavage and laminally folded (Fig. 10, 11, 12).

Based on the textural evidence, it is suggested that the

metamorphism is of the contact type, and that the

metamorphic and metamorphic conditions are

Although the thickness of the metamorphic zone is

variable, the metamorphic zone is generally

metamorphic (Fig. 10, 11, 12, 13, 14, 15, 16, 17, 18, 19, 20, 21, 22, 23, 24, 25, 26, 27, 28, 29, 30, 31, 32, 33, 34, 35, 36, 37, 38, 39, 40, 41, 42, 43, 44, 45, 46, 47, 48, 49, 50, 51, 52, 53, 54, 55, 56, 57, 58, 59, 60, 61, 62, 63, 64, 65, 66, 67, 68, 69, 70, 71, 72, 73, 74, 75, 76, 77, 78, 79, 80, 81, 82, 83, 84, 85, 86, 87, 88, 89, 90, 91, 92, 93, 94, 95, 96, 97, 98, 99, 100).

orientation of the metamorphic zone is

complementary orientation (Fig. 10, 11, 12, 13, 14, 15, 16, 17, 18, 19, 20, 21, 22, 23, 24, 25, 26, 27, 28, 29, 30, 31, 32, 33, 34, 35, 36, 37, 38, 39, 40, 41, 42, 43, 44, 45, 46, 47, 48, 49, 50, 51, 52, 53, 54, 55, 56, 57, 58, 59, 60, 61, 62, 63, 64, 65, 66, 67, 68, 69, 70, 71, 72, 73, 74, 75, 76, 77, 78, 79, 80, 81, 82, 83, 84, 85, 86, 87, 88, 89, 90, 91, 92, 93, 94, 95, 96, 97, 98, 99, 100).

evidence that these metamorphic zones are

scale structures. The scale of metamorphism is

layered and is not uniform, the metamorphic zone

is not uniform, the metamorphic zone is

also in the metamorphic zone (Fig. 10, 11, 12, 13, 14, 15, 16, 17, 18, 19, 20, 21, 22, 23, 24, 25, 26, 27, 28, 29, 30, 31, 32, 33, 34, 35, 36, 37, 38, 39, 40, 41, 42, 43, 44, 45, 46, 47, 48, 49, 50, 51, 52, 53, 54, 55, 56, 57, 58, 59, 60, 61, 62, 63, 64, 65, 66, 67, 68, 69, 70, 71, 72, 73, 74, 75, 76, 77, 78, 79, 80, 81, 82, 83, 84, 85, 86, 87, 88, 89, 90, 91, 92, 93, 94, 95, 96, 97, 98, 99, 100).

folded. Evidence supporting the metamorphic zone is

is folded along with the metamorphic zone (Fig. 10, 11, 12, 13, 14, 15, 16, 17, 18, 19, 20, 21, 22, 23, 24, 25, 26, 27, 28, 29, 30, 31, 32, 33, 34, 35, 36, 37, 38, 39, 40, 41, 42, 43, 44, 45, 46, 47, 48, 49, 50, 51, 52, 53, 54, 55, 56, 57, 58, 59, 60, 61, 62, 63, 64, 65, 66, 67, 68, 69, 70, 71, 72, 73, 74, 75, 76, 77, 78, 79, 80, 81, 82, 83, 84, 85, 86, 87, 88, 89, 90, 91, 92, 93, 94, 95, 96, 97, 98, 99, 100).

developed spaced cleavage (Fig. 10, 11, 12, 13, 14, 15, 16, 17, 18, 19, 20, 21, 22, 23, 24, 25, 26, 27, 28, 29, 30, 31, 32, 33, 34, 35, 36, 37, 38, 39, 40, 41, 42, 43, 44, 45, 46, 47, 48, 49, 50, 51, 52, 53, 54, 55, 56, 57, 58, 59, 60, 61, 62, 63, 64, 65, 66, 67, 68, 69, 70, 71, 72, 73, 74, 75, 76, 77, 78, 79, 80, 81, 82, 83, 84, 85, 86, 87, 88, 89, 90, 91, 92, 93, 94, 95, 96, 97, 98, 99, 100).

filled the cleavage (Fig. 10, 11, 12, 13, 14, 15, 16, 17, 18, 19, 20, 21, 22, 23, 24, 25, 26, 27, 28, 29, 30, 31, 32, 33, 34, 35, 36, 37, 38, 39, 40, 41, 42, 43, 44, 45, 46, 47, 48, 49, 50, 51, 52, 53, 54, 55, 56, 57, 58, 59, 60, 61, 62, 63, 64, 65, 66, 67, 68, 69, 70, 71, 72, 73, 74, 75, 76, 77, 78, 79, 80, 81, 82, 83, 84, 85, 86, 87, 88, 89, 90, 91, 92, 93, 94, 95, 96, 97, 98, 99, 100).

unit is with cleavage (Fig. 10, 11, 12, 13, 14, 15, 16, 17, 18, 19, 20, 21, 22, 23, 24, 25, 26, 27, 28, 29, 30, 31, 32, 33, 34, 35, 36, 37, 38, 39, 40, 41, 42, 43, 44, 45, 46, 47, 48, 49, 50, 51, 52, 53, 54, 55, 56, 57, 58, 59, 60, 61, 62, 63, 64, 65, 66, 67, 68, 69, 70, 71, 72, 73, 74, 75, 76, 77, 78, 79, 80, 81, 82, 83, 84, 85, 86, 87, 88, 89, 90, 91, 92, 93, 94, 95, 96, 97, 98, 99, 100).

and folded (Fig. 10, 11, 12, 13, 14, 15, 16, 17, 18, 19, 20, 21, 22, 23, 24, 25, 26, 27, 28, 29, 30, 31, 32, 33, 34, 35, 36, 37, 38, 39, 40, 41, 42, 43, 44, 45, 46, 47, 48, 49, 50, 51, 52, 53, 54, 55, 56, 57, 58, 59, 60, 61, 62, 63, 64, 65, 66, 67, 68, 69, 70, 71, 72, 73, 74, 75, 76, 77, 78, 79, 80, 81, 82, 83, 84, 85, 86, 87, 88, 89, 90, 91, 92, 93, 94, 95, 96, 97, 98, 99, 100).

In some cases the metamorphic zone is

or with (Fig. 10, 11, 12, 13, 14, 15, 16, 17, 18, 19, 20, 21, 22, 23, 24, 25, 26, 27, 28, 29, 30, 31, 32, 33, 34, 35, 36, 37, 38, 39, 40, 41, 42, 43, 44, 45, 46, 47, 48, 49, 50, 51, 52, 53, 54, 55, 56, 57, 58, 59, 60, 61, 62, 63, 64, 65, 66, 67, 68, 69, 70, 71, 72, 73, 74, 75, 76, 77, 78, 79, 80, 81, 82, 83, 84, 85, 86, 87, 88, 89, 90, 91, 92, 93, 94, 95, 96, 97, 98, 99, 100).

appear to be folded while metamorphism was

(Fig. 10, 11, 12, 13, 14, 15, 16, 17, 18, 19, 20, 21, 22, 23, 24, 25, 26, 27, 28, 29, 30, 31, 32, 33, 34, 35, 36, 37, 38, 39, 40, 41, 42, 43, 44, 45, 46, 47, 48, 49, 50, 51, 52, 53, 54, 55, 56, 57, 58, 59, 60, 61, 62, 63, 64, 65, 66, 67, 68, 69, 70, 71, 72, 73, 74, 75, 76, 77, 78, 79, 80, 81, 82, 83, 84, 85, 86, 87, 88, 89, 90, 91, 92, 93, 94, 95, 96, 97, 98, 99, 100).

often observed to fold towards the metamorphic zone

example, changing the metamorphic zone

cause the metamorphic zone to fold



Fig. 35 Folded spaced cleavage in greywacke.

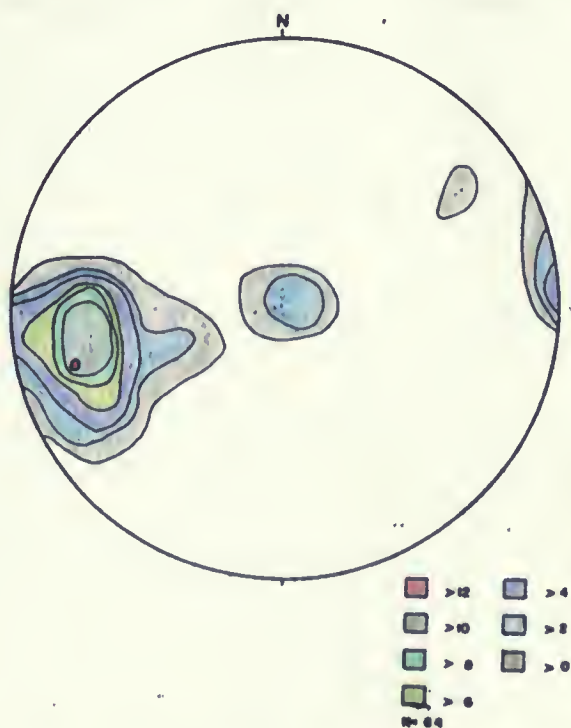


Fig. 36 "Z" shaped folds. Maximum=257/20.







**Fig. 37. Veins parallel with the C cleavage are folded in Z shapes.**

Fig. 37. Veins parallel with the C cleavage are folded in Z shapes.

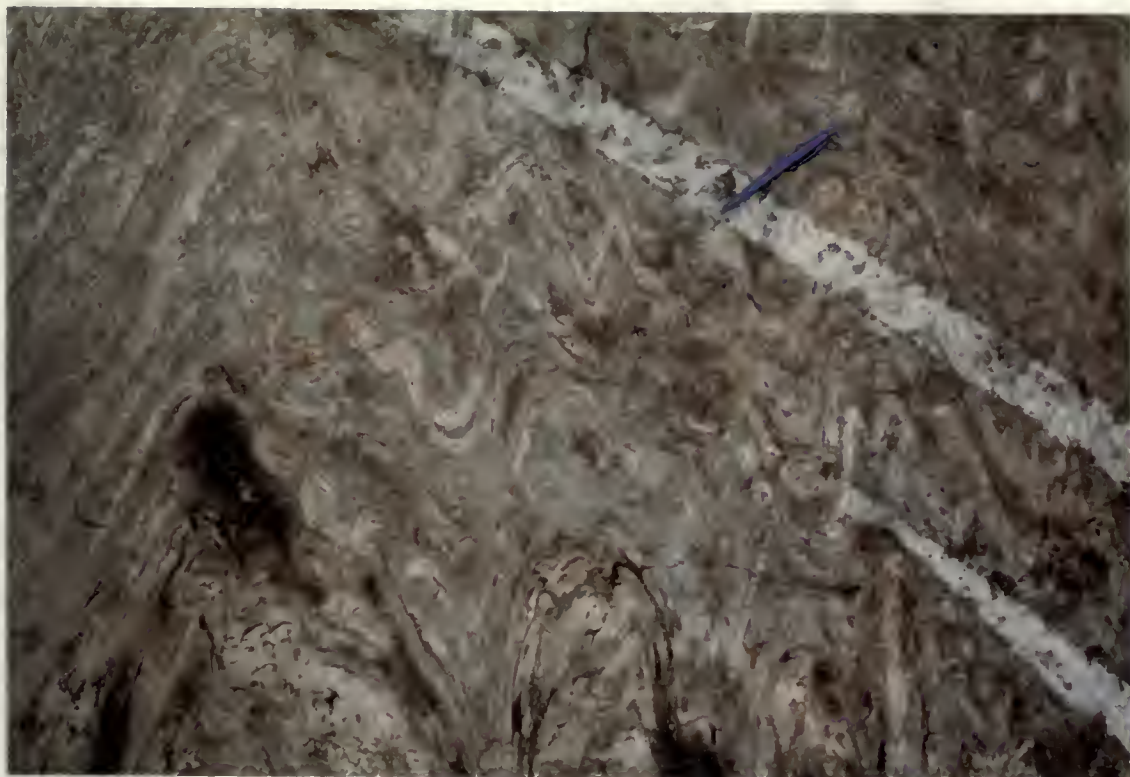


Fig. 38. Folded agglomerate unit. The clasts have been elongated parallel with the foliation which is folded.



Fig. 39. Wide zone of Z folding in greywackes.



Fig. 38. Folded aggregate unit. The clear, dark green elongated parallel with the foliation which is folded.

Fig. 39. Wide zone of folding in gneiss rock.



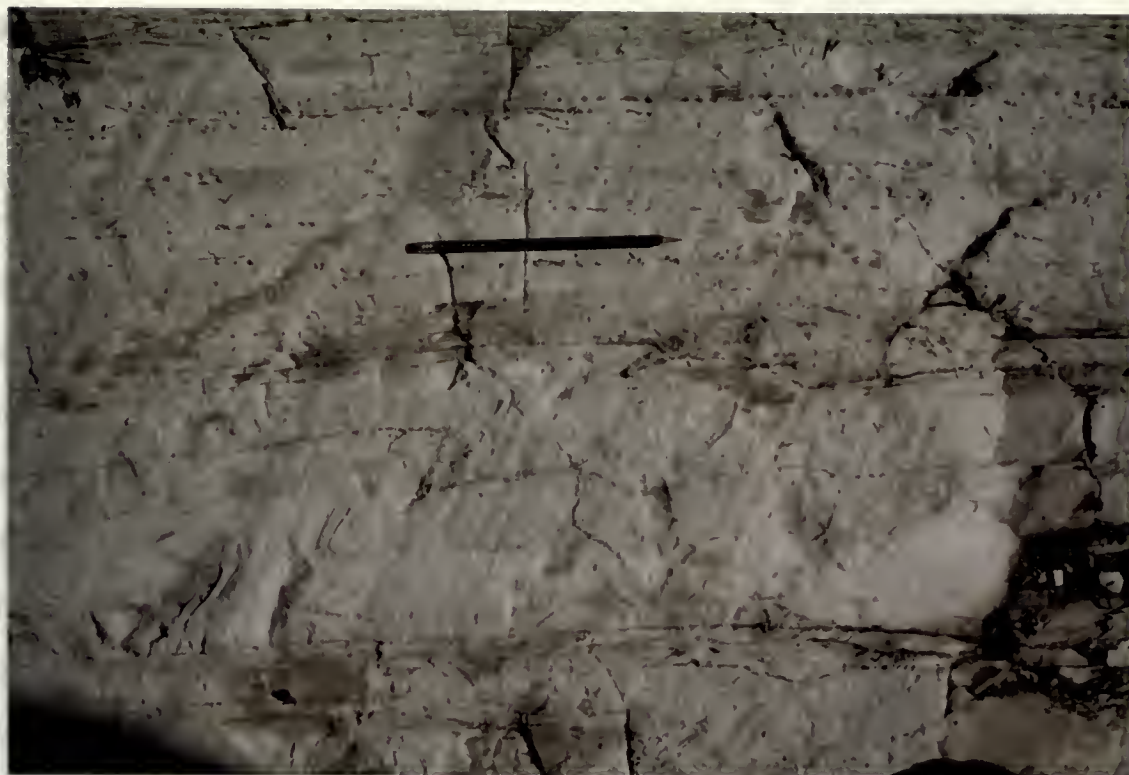


Fig. 40. The axial trace of Z folds are rotated towards the shear direction.



Fig. 41. Quartz filled fracture parallel with the short limb of a Z fold.

Fig. 10. The axial trace of a folde and related to the shear direction.

Fig. 11. Quartz filled fracture parallel with the slip line of a fold.

080 are more open whereas folds with axial traces of 090 are usually tighter.

At several locations, especially in the well layered sediments and the strongly foliated tuff, a weak axial planar fabric was observed in the hinges of mesoscopic Z folds. This fabric cuts both layering and the earlier formed C foliation and is usually best developed in the tightest fold hinges. Although displacement along this fabric was not observed, many of the mesoscopic Z folds have been disrupted by thin (<1cm) shear zones and brittle fractures which form parallel to the axial plane of the fold, but along the short limb (Fig. 41).

At several locations the tighter Z folds have axial traces approaching parallelism with the C foliation. In many cases the hinges of these folds become transposed or completely separated by shear planes parallel with the C foliation (Fig. 43). Folds with axial traces parallel with the foliation are also produced when folded layering is further displaced along the C foliation, producing class 2 or similar style folds. Quartz veins oblique to the C foliation are also often displaced along the foliation, producing similar folds.

Although rare, the presence of folds plunging towards the east was observed. In one case, a very small Z fold (amplitude <5cm) has successive hinges plunging in opposite directions. This structure occurs in an outcrop of intense mesoscopic folds and appears to be parasitic to these slightly larger folds. A possible explanation for the opposite



One or more open windows could be seen  
usually closed.

At several locations, especially in the west, the  
bedrooms and the dining room were  
further was covered in the shape of a large  
large cut-out section and the ceiling was a flat  
and its general level was in the same level as the  
Although displacement of the floor was not observed  
of the material in the floor have been displaced in the  
their cases and little evidence which indicates that  
level of the floor was the same level as the  
At several locations, the floor was a flat

traces appeared in the floor with the floor  
cases the floor of these rooms was displaced  
completely separated by some other material  
section (the floor was a flat level as the floor  
the floor was a flat level as the floor  
Further displaced along the floor was a flat  
level with the floor was a flat level as the floor  
are also other displaced along the floor was a flat  
level as the floor was a flat level as the floor

Although the floor was a flat level as the floor  
was observed in the floor was a flat level as the floor  
level as the floor was a flat level as the floor  
direction. This structure was a flat level as the floor  
second floor and appeared in the floor was a flat level  
larger than the floor was a flat level as the floor

plunging hinges, shown in Figure 42, is that the axis of the smaller fold is constrained at depth. This type of structure has not been observed at any other location, suggesting that conditions leading to the formation of such a structure are rare.

### Macroscopic and Megascopic Z Folding

As shown on Horwood and Pye's map (Map 1 ), macroscopic (amplitudes >10m) and megascopic (regional scale) folds, especially of banded iron formation appear to be abundant north of the Bankfield-Tombill Fault. However parts of this map have been interpreted from a magnetic survey using a dip needle. Large scale fold closures such as those shown on Map 1 west and south of Barton Bay, were rarely observed during the present study. Mapping during this study suggests that some of the supposed regional structures on Horwood and Pye's map can be reinterpreted. For instance field evidence is lacking to support the presence of the folding style shown south and west of Barton Bay, referred to above, and instead these have been reinterpreted as smaller scale macroscopic Z style folds (Fig. 23A-B). Outcrops at the locations referred to above are characterized by extensive mesoscopic Z folding (Fig. 39). Larger macroscopic folding of an iron formation unit is suggested by field mapping, but is usually disrupted by displacement along irregularly spaced shear planes oriented parallel to the local C foliation (090-100/80/s-V). Both the smaller Z folds and the larger folds have a similar range of



condition leading to the formation of a ...  
has not been observed on any other ...  
surface and is considered to be ...  
primary deposit, about 10 ...

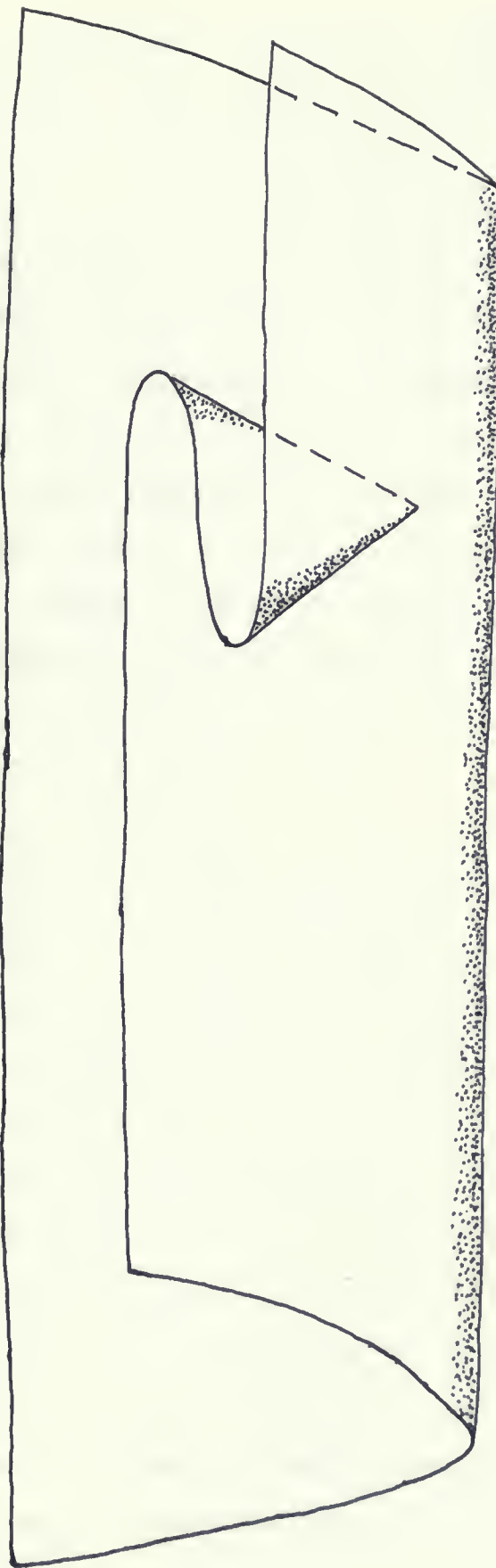


Fig. 42. A fold with hinges plunging in opposite directions, formed by dextral shearing parallel to the foliation but constrained at depth. The smaller fold is parasitic to a larger Z fold, causing the constraint at depth.



axial surface orientations, 060-100. All measurable axial plunges were towards the west and had orientations complementary to those indicated above.

Approximately 1 kilometer west along strike of the outcrops described above, stripping during the present study exposed the hinge of a macroscopic fold in iron formation (Fig. 13). This fold is not shown on Horwood and Pye's map but macroscopic Z folds are shown in iron formation both west and east of the newly exposed fold. Therefore it is believed that the one hinge exposed is also part of a similar Z style fold. The newly exposed fold hinge plunges to the west, 270/30 and the folded layering and what appears to be an earlier fabric parallel with the layering, is disrupted by shear planes parallel with the axial trace of the fold (Fig. 43), which is parallel with the C foliation locally. Displacement along these shear planes is dextral and is shown in detail in Figure 44. Within the fold, transposition along these shear planes has produced smaller scale folding in which limbs are often extremely stretched or even separated along the shear plane (Fig. 45). The disruption of folding by axial planar shear planes such as described here has also been observed in other areas of regional ductile shear (Soula et al., 1980). Outcrop of the well layered sediments at this location and nearby are characterized by intense mesoscopic Z folding. In many cases the short limb of these folds is also folded or displaced by shear planes producing a more complex structure (Fig. 46). The similarity between the newly exposed

axial surface of the crown of the tooth.

phases were towards the apex and had

completely to these features.

Approximately 1 kilometer west of the

outcrop described above, a small

exposed the base of a section of the

(Fig. 12). This is the same as

but somewhat. It is also

and most of the teeth exposed.

that the one side exposed is

fold. The newly exposed

1950 and the folded layer

earlier fabric. The

sheet phase parallel with

425, which is parallel with

Displacement of the

in detail in Figure 12. Within the

these sheet phases are

beds are often slightly

the sheet phase (Fig. 13).

planes shown above and

observed in this

all, 1950. Over

location and

folded. It

island of the

extension (Fig. 14).





Fig. 43. Discrete shear planes parallel to axial trace of large fold.

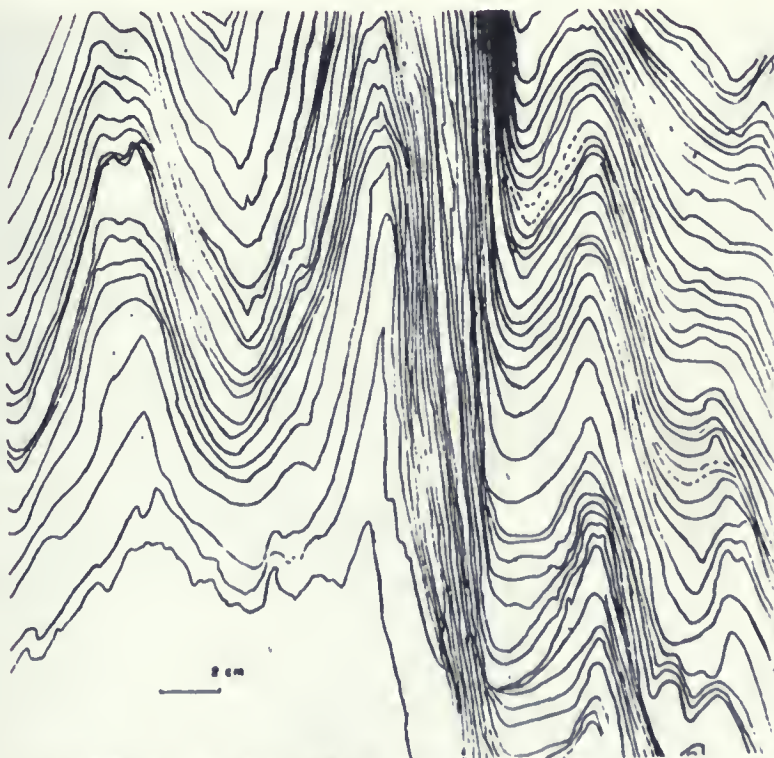


Fig. 44. Close up view of displacement caused by shear planes shown in Fig. 43. Line drawing is a tracing from the outcrop.

Fig. 22. Dorsal view of the head of the larva of the  
 genus *Phrynosoma*.



Fig. 23. Head of the larva of the genus *Phrynosoma*,  
 shown in Fig. 22, from a different angle.





**Fig. 45. Separation of fold hinges by discrete shear planes.**



**Fig. 46. Modified Z fold which may reflect the shape of larger scale folds.**

Fig. 45. Separation of fold hinges by discrete shear planes.

Fig. 46. Modified N fold which may reflect the shape of larger scale folds.

fold and those described south and west of Long Bay has led to the interpretation that all of these folds are generally Z style folds but may be modified, representing a larger scale example of the structure shown in Figure 46.

Other macroscopic folding observed or interpreted from mapping during the present study includes a large Z fold in iron formation, observed on the island in Barton Bay. The assumed boundaries of this fold are shown on Horwood and Pye's (1955) map and were outlined by drilling and magnetic survey. Trenches and areas exposed since the time of their map were mapped during the present study and support the original interpretation.

A very complex series of macroscopic folds were also observed in the tuffs and gabbros exposed by recent outcrop stripping and along the north eastern shoreline of the peninsula at the eastern end of Lake Kenogamisis. The folding here is extensive, but discontinuous over a strike width of approximately 1 kilometer. The folding is complicated by mixed lithologies, transposed layering and displacement along irregularly spaced shear planes similar to those seen in the folded iron formation. Mesoscopic Z style folding dominates, but macroscopic fold hinges with Z and S style parasitic folds were observed. The attitude of the smaller more common Z folds varies in orientation from 256-270 and in plunge from 10-40 to the west. The larger fold hinges at this location varied in orientation from 250-280 with plunges of 10-60 towards the west.



the interpretation that all of these facts are in fact  
style (and not in addition, representing a style of  
people of the literature shown in figure 2

The similarity of structures present at this location to the macroscopic folds described west of Lake Kenogamisis has led to a similar interpretation in Figure 23A-B. The overall structure is considered to be an open Z style fold with the shorter limb modified by smaller scale folding and displacement by shear planes parallel with the C foliation (Fig. 46).

### Other Fold Styles

Three other styles of folding were observed in the study area. At a single location near Mosher Lake (Map 1) and approximately 200m north of the Bankfield-Tombill Fault, a thin layer of iron formation appears to have been refolded (Fig. 47). One kilometer east of this location "unfolded" folds (H.Hugon, pers. comm. 1984) were observed in a sequence of layered sediments and iron formation (Fig. 48), suggesting passive folding of active Z folds. These styles of folding were observed only at these locations but indicate the degree of deformation that has taken place in areas close to the Bankfield-Tombill Fault.

Kink style folding is relatively common in the well foliated sediments of the study area, but is most common within 1km of the Bankfield-Tombill Fault. Due to the low lying nature of the outcrops and the dominantly vertical foliation and layering, the three dimensional orientation of these folds was difficult to measure. Therefore the kink band boundaries (trace of axial plane), were measured and plotted as poles assuming that the axial planes of the kinks were

The similarity of structures present at this location to the macroscopic folds described west of Lake Kogonchik led to a similar interpretation in Figure 23A-B. The overall structure is considered to be an open Z style fold with the shorter limb modified by smaller scale folding and displacement by shear planes parallel with the C foliation (Fig. 46).

### Other Fold Styles

Three other styles of folding were observed in the study area. At a single location near Mosher Lake (Map 1) and approximately 200m north of the Bankfield-Tombill Fault, a thin layer of iron formation appears to have been refolded (Fig. 47). One kilometer east of this location "unfolding" folds (H. Higon, pers. comm. 1984) were observed in a sequence of layered sediments and iron formation (Fig. 48), suggesting passive folding of active Z folds. These styles of folding were observed only at these locations but indicate the degree of deformation that has taken place in areas close to the Bankfield-Tombill Fault.

Kink style folding is relatively common in the well foliated sediments of the study area, but is not common within 1km of the Bankfield-Tombill Fault. Due to the tectonic nature of the outcrops and the dominantly vertical foliation and layering, the three dimensional orientation of these folds was difficult to measure. Therefore the fold band boundaries (trace of axial planes), were measured and plotted as poles assuming that the axial planes of the kink were





**Fig. 47. Refolded fold in iron formation.**



**Fig. 48. Unfolded folds in iron formation and greywacke.**



Fig. 47. Refolded fold in iron formation.

Fig. 48. Unfolded folds in iron formation and greywacke.

vertical. Although conjugate sets were rarely observed in a single outcrop, Figure 49 and 50 shows that regionally a conjugate set has developed. The dominant set has a sinistral sense and an average orientation of 144/V. The dextral set has an average orientation of 030/V.

The use of kink folds as stress orientation indicators has been well documented (Gay and Weiss 1974, Verbeek 1978, Weiss 1980, in Clifford and Wallace 1982). The maximum compressive stress,  $\sigma_1$  is defined as the bisectrix of the acute angle made by a conjugate set, the intermediate stress,  $\sigma_2$  as the axis of intersection of  $\sigma_1$  and 3, and the least compressive stress as the bisectrix of the obtuse angle of the set. The regional stress orientations suggested using this method are;  $\sigma_1 = 087/V$ ,  $\sigma_3 = 177/V$ .

The mechanism traditionally accepted for kink fold formation is one of compression parallel to a well developed foliation (Hobbs, Means and Williams 1976). With an average foliation orientation of 097/V, approximately parallel to the inferred  $\sigma_1$  087/V, the study area fits into this model quite well. However recent studies of kink folding in greenstone belts (Clifford and Wallace 1982) has led to some modifications to the traditional model. Clifford and Wallace found that kinking was related to sinistral movement along a regional ductile-brittle break, the Manitou Straights Fault. In this area they found; that kink folds were developed mainly in close proximity to the fault, dextral kink folds dominated and that the maximum compressive stress was parallel to a



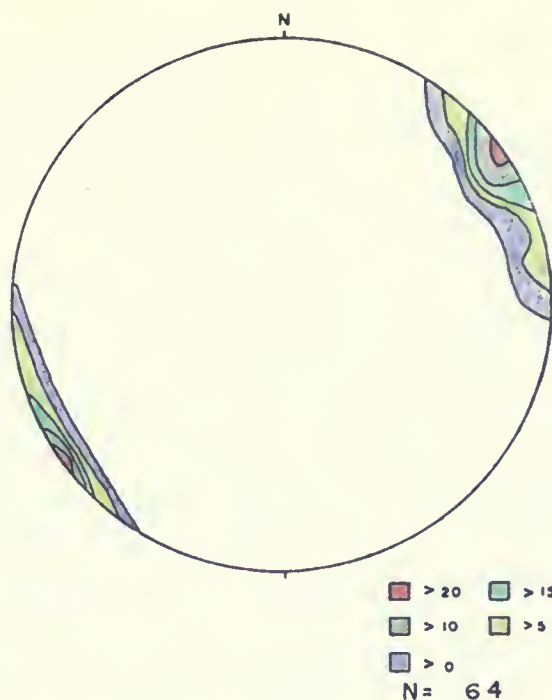


Fig. 49 Sinistral kinks plotted as poles to a plane representing the axial trace of the kink. Maximum=144/V.



Fig. 50 Dextral kinks plotted as poles to a plane representing the axial trace of the kink. Maximum=030/V.





strong regional schistosity.

The pattern of kinking in the present study area has several similarities to Clifford and Wallace's observations. Kinking is present mainly in association with the Bankfield-Tombill Fault, sinistral kinks dominate (in a dextral shear regime) and the determined  $\sigma_1$  is approximately parallel with the regional foliation. Following the argument of Clifford and Wallace this suggests that kink folding in the Geraldton area may be the result, not of a late east-west compression, but instead the result of dextral displacement along a ductile shear zone, the Bankfield-Tombill Fault, perhaps resulting from local compression associated with stick - slip mechanisms (Williams pers. comm.).

#### Discussion Of Folding

The variation in attitude of the mesoscopic and macroscopic Z folds observed in the study area, can be most easily explained in terms of reorientation of fold axes due to a simple shear process. The reorientation of fold axes in association with ductile shear zones and mylonites has been reported in several papers (Escher and Watterson 1974, Bell 1978, Berthe and Brun 1980). Progressive deformation by simple shearing produces a strain ellipse in which the direction of maximum elongation, the X axis, approaches parallelism with the direction of shearing (Fig. 51A). As shown by Escher and Watterson (1974), linear elements within a large sector of an originally undeformed circle will be

The pattern of ...

Several ...

Working ...

Geological ...

Geological ...

Geological ...

The argument ...

Feeling ...

East-west ...

displacement ...

They ...

with ...

## Discussion Of Results

The variation ...

Geological ...

Geological ...

Geological ...

Geological ...

Geological ...

Geological ...

Geological ...

Geological ...

Geological ...

Geological ...

Geological ...

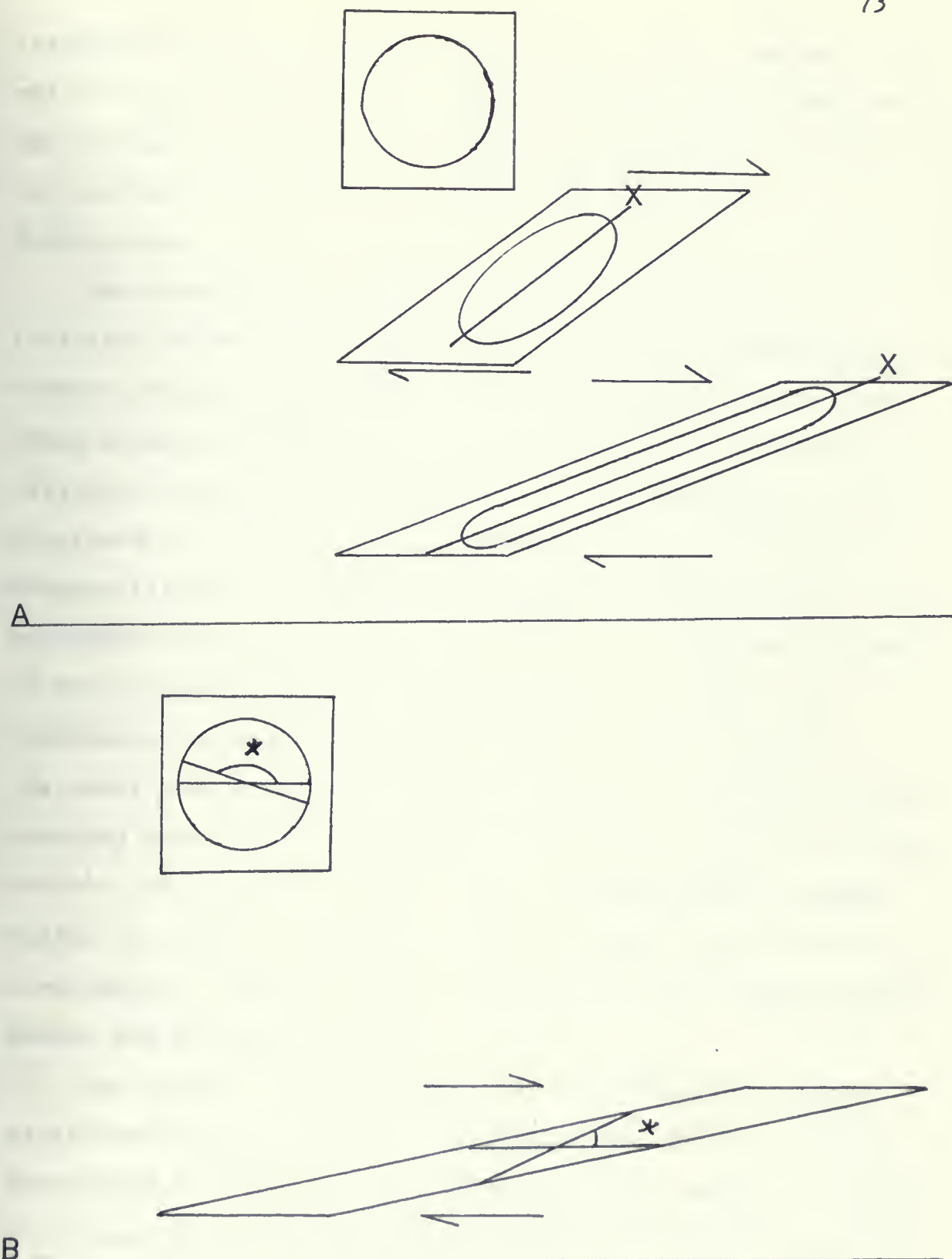


Fig. 51. A, rotation of the axis of elongation X towards the direction of shearing. B, all elements within sector \* will be rotated towards the shear direction (modified from Escher and Watterson 1974).





rotated in sympathy with the X axis (Fig. 51B). The degree of rotation or reorientation of linear elements such as the axes of original or contemporary folds will be dependent on both the degree of simple shear and the fold's original orientation.

The angle between the axial traces of folds and the C foliation in the study area varies from 40 to 0 degrees. As shown in Figure 40 the axial trace of mesoscopic Z folds was often observed to bend towards the C foliation. This is similar to the manner in which the simple shear S fabric is displaced by C as described by Berthe et al., (1979a) and Simpson (1984). In fact the average orientation of the mesoscopic Z fold axial traces is 078/V, which is very close to the average orientation of the S fabric, 084/V. This information suggests that most of the mesoscopic folding in the study area formed contemporaneously with a regional simple shearing event. The variation in attitudes of these folds may reflect the relative timing of the folding, those at higher angles to the C foliation having formed later than those at lower angles. Results similar to this have been suggested by Escher and Watterson (1974).

The larger macroscopic folds in the area usually have axial traces at much lower angles (15-0) to the C foliation. Considered in light of the simple shear model proposed, these folds may represent either the earliest contemporaneous folds or possibly original folds which have been reoriented closer to parallelism with the shear zone. Since these larger folds

rotated in synchrony with the  $\alpha$  axis (1957). The  
rotation of the lamellae at different angles was  
of original or contrapuntal fold axis as determined  
the degree of twist angle and the fold's original  
orientation.

The angle between the  $\alpha$  axis and the fold  
foliation in the good, first series (see 1957) was  
shown in Figure 4. The  $\alpha$  axis of the lamellae  
often appeared to bend towards the  $\alpha$  axis  
relative to the angles in which the  $\alpha$  axis was  
displaced by  $\alpha$  as determined by Davis in 1957. The  
displacement (1954) of the  $\alpha$  axis of the lamellae  
microscopic 2 fold axis (see 1957) was in the  
to the average orientation of the  $\alpha$  axis of the  
information suggests that part of the lamellae  
the study also formed contemporaneously with the fold  
shearing event. The lamellae in the fold axis  
reflect the fold - being of the fold (1954) and  
angles in the  $\alpha$  fold axis (see 1957) and  
lower angles. Possible reasons for this are discussed in  
Recher and Patterson (1954).

The lamellae are oriented in the fold axis  
fold traces at small angles (1957) and the fold axis  
considered in light of the fold axis (1957) and the  
folds are regarded as being for the fold axis (1957)  
or possibly of the fold axis (1957) and the fold axis  
as parallel with the fold axis (1957).

are mainly associated with the banded iron formation and tuff units, it may be that these lithologies have some bearing on the ease or timing of fold formation.

#### MINOR SHEARS

Further evidence of deformation in all rock types away from the Bankfield-Tombill Fault is suggested by the presence of numerous minor, discrete shear zones. These shears are generally less than 1cm wide and often only a few millimeters wide. They are commonly identified as schistose zones displacing veins in an otherwise undeformed rock (Fig. 52). The greatest number of these minor shears show a dextral sense of displacement and as shown in Figure 53A, are generally oriented at 100/V, parallel with the Bankfield-Tombill Fault and the regional C foliation. Shears with a sinistral displacement were also observed with most having orientations of 096/V and 040/V (Fig. 53B).

#### VEINS

Veining is common in most parts of the study area, but is most extensive in outcrops adjacent to the Bankfield-Tombill Fault (Fig. 37). Pure quartz veins are the most common but quartz-carbonate, quartz-epidote and quartz-tourmaline veins were also observed. Vein width varied from a few millimeters to tens of centimeters. The orientation of veins regionally, is extremely variable (Fig. 54), but generally can be broken down into those oblique to the C foliation and those parallel



...the same or being of the same kind...

...the same or being of the same kind...

...the same or being of the same kind...

...the same or being of the same kind...

...the same or being of the same kind...



**Fig. 52. Vein displaced by shear in gabbro.**

Fig. 52. Vein displaced by shear in gabbro.

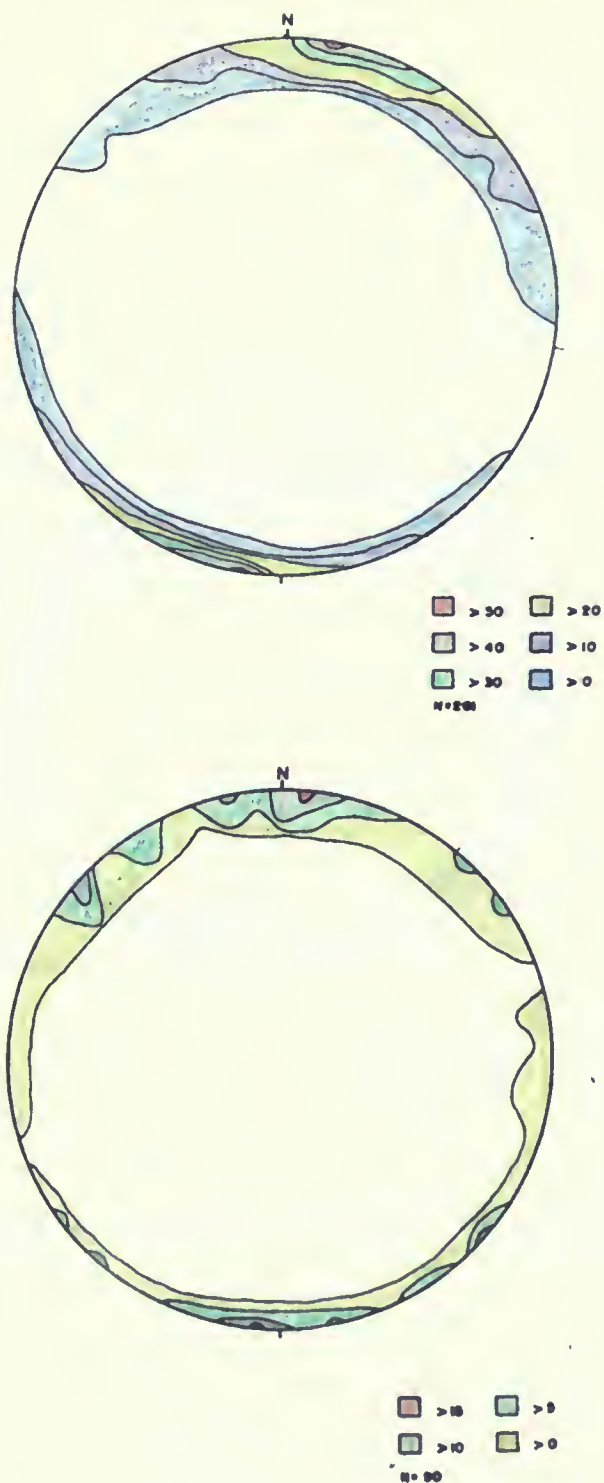


Fig. 53 Minor shears plotted as poles to a plane. (A) dextral shears, Maximum=100/V, (B), sinistral shears, Maximum=096/V.







Fig. 54 Veins plotted as poles to a plane.



with it. Veins oblique to the foliation are cut and often displaced by the foliation (Fig. 25). Displacement is most commonly dextral but sinistral displacements were observed. Most commonly veins were present parallel with and often folded with the foliation (Fig. 37). These foliation parallel veins often exhibit boudinage and pinch and swell structures (Fig. 6). The axes of the boudinage suggest extension parallel to the foliation. In zones of intense deformation such as some pelitic layers, veins have been totally disrupted by folding and discrete displacement (Fig. 6).

## Conclusions

The presence of shear related S, C and C' fabrics, both in the mylonite and surrounding rocks of the study area, indicates regional deformation by a large scale simple shear zone. The Z asymmetry of folds, relative orientations of the shear fabrics and displacement along these fabrics indicate that the predominant sense of displacement within this regional shear zone was dextral. Extension lineations, boudinage and pinch and swell structures indicate that extension as the result of the regional shearing was subhorizontal and parallel with the Bankfield-Tombill Fault. Structures related to regional shearing are recognized up to 2km south of the fault and northwards to the contact between sediments and volcanics, thus defining the boundaries of the Barton Bay Deformation Zone.





## STAGES OF GABBRO MYLONITIZATION

Separate stages of mylonitization have been outlined according to both field and microscopic evidence. In the field, outcrops of mylonite were subdivided according to texture and foliation development. Zones of increasing deformation within the gabbro were first described by Lavigne (1983), and the stages defined in this study are in part based on his original observations. Five separate zones of deformation-mylonitization were identified and were mapped in detail at two separate locations (Figs. 56 and 57). The least deformed gabbro is represented by a zone of thin (3-5cm) anastomosing shears which surround lithons of undeformed rock (Fig. 58). The next stage of deformation produces an elongated mineral fabric and in some cases a weak foliation, which is often displaced by a widely spaced irregular C' fabric. In some cases it appears as if the earlier anastomosing shears have been rotated parallel to each other. With further deformation a strong foliation-layering is produced which is often folded. In some places this zone is also cut by the C' fabric which causes displacement of the layering. At each of the outcrops mapped, the zones of most intense deformation are marked by the relatively uniform development of a closely spaced C' fabric. The layering within these zones is completely disrupted, producing the brecciated appearance noted by Pye (1952).

Samples from each of these zones were studied microscopically to determine any differences mineralogically,





Fig. 55 Location of gabbro mylonites mapped in detail.





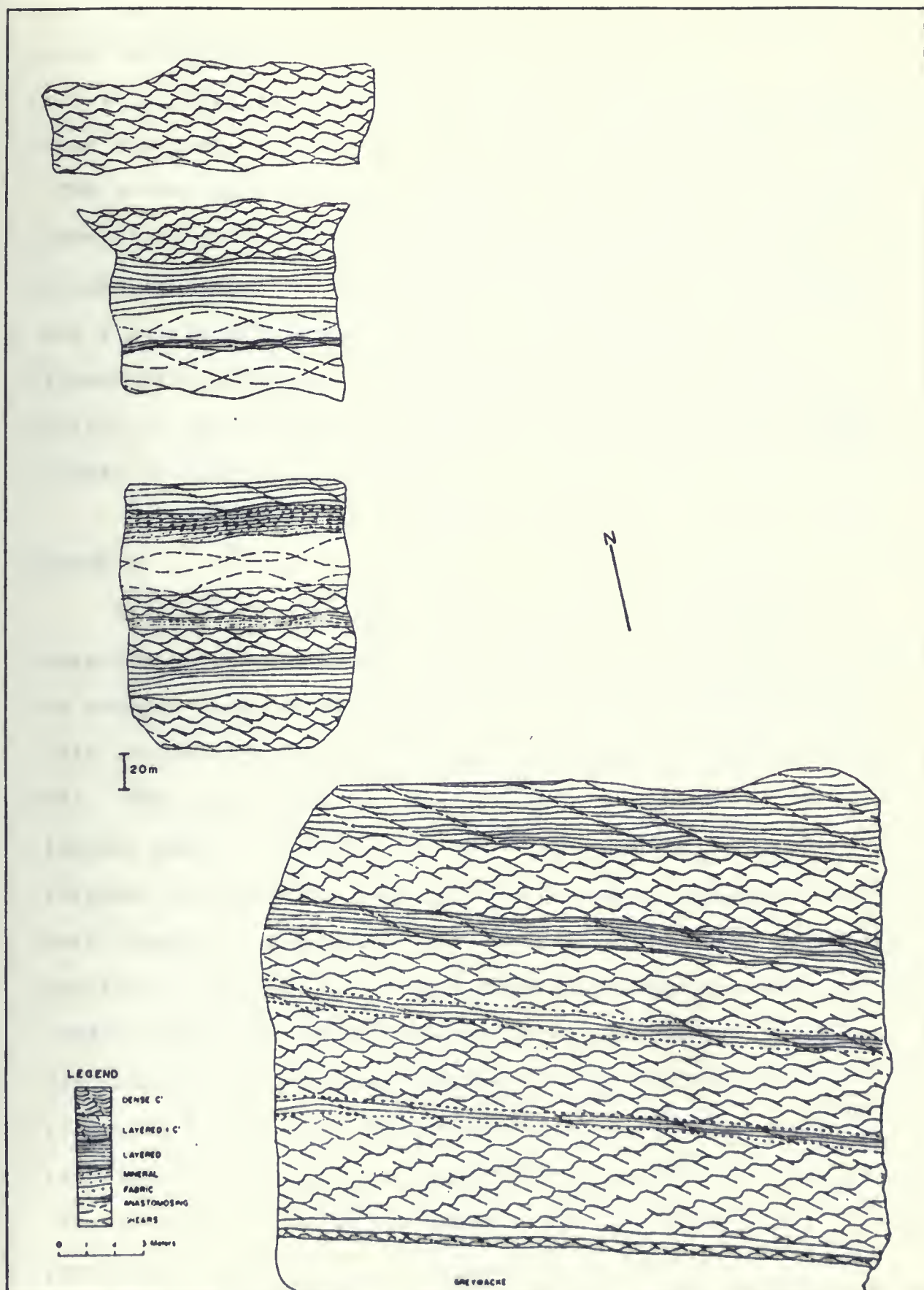


Fig. 57 Gabbro mylonite outcrop at location 1.



micro-structurally or in degrees of feldspar recrystallization. The axes of mineral grains and aggregates were measured in an attempt to define each zone statistically.

The microscopic evidence indicates that each of the zones identified in the field represent significantly different stages in the mylonitization of the gabbro. The character, and significant differences for each stage have been summarized in Table 1. Each stage has been expressed in mylonitic terminology by comparison with the classification scheme of Wise et al. (1984).

## STAGE I

This stage represents the least degree of deformation observed in outcrop and microscopically. In outcrop it occurs as zones of coarse grained lithons of gabbro surrounded by thin (3-5cm) discrete shears in an anastomosing pattern (Fig. 58). The gabbro near the center of these lithons exhibits a typical gabbroic texture of interlocking coarse grained feldspar and amphibole, and is considered to represent the best example of a stage I, undeformed gabbro. Rare elongated amphibole and leucoxene within this zone suggest that "undeformed" is a relative description. Closer to the discrete shears the gabbro becomes visibly deformed as elongated feldspar and amphibole define a strong S fabric rotating into parallelism with the shear boundaries (Fig. 31).

These discrete shears are generally oriented east-west, parallel with the regional shear direction, and have been





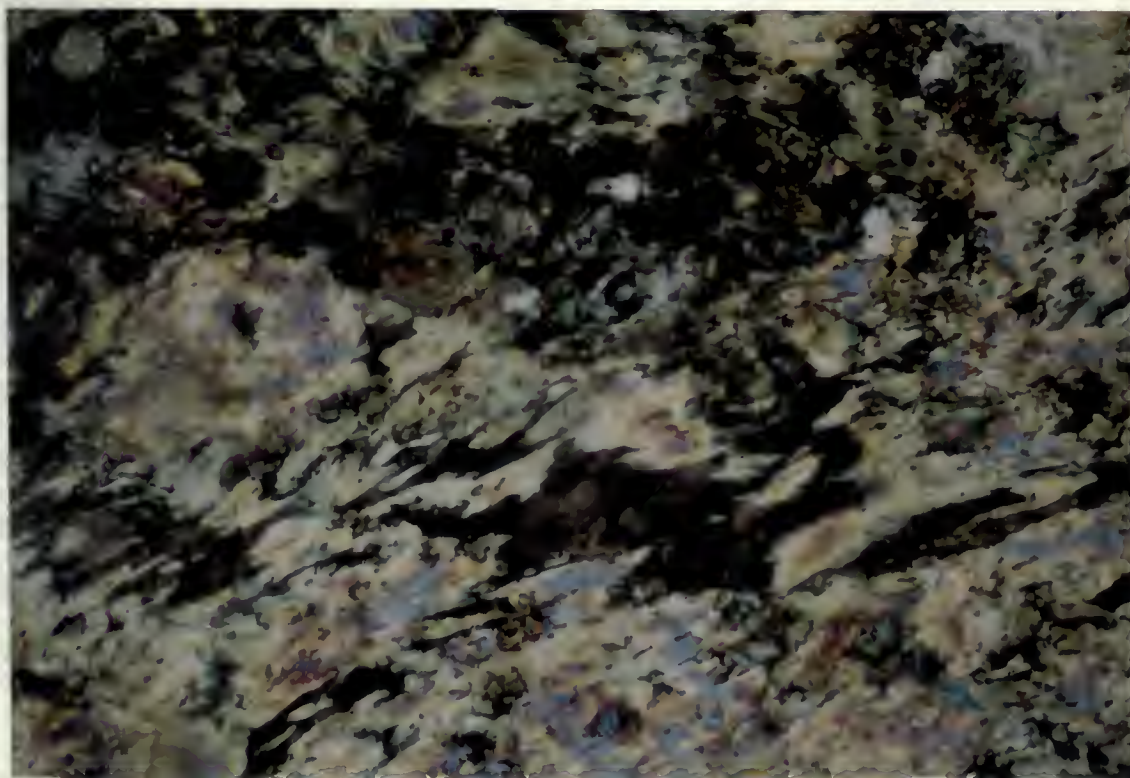
TABLE 1  
Summary of the characteristics of each stage of mylonitization. Mean grain size and recrystallization refer to feldspar.  
Grain size is in microns.

STAGE	OUTCROP DESCRIPTION	FABRICS	MEAN GRAIN SIZE	RECRYSTALLIZATION	MICROSCOPIC DESCRIPTION
I PROTOMYLONITE	Undeformed lithons between anastomosing shears.	Weak C and S.	111.0 x 68.0	Not observed.	Generally original texture.
II MYLONITE	C fabric defined by a well developed mineral elongation.	Strong C and a weak C'	65.0 x 23.2	Small degree of first order grains, 40 - 50 microns.	Elongated feldspar grains and aggregates of feldspar and actinolite.
III MYLONITE	Weak layering with mineral fabric.	Strong C foliation and widely spaced C'.	43.6 x 15.5	Increased first order plus a small degree of second order grains, 5 - 20 microns.	Weak chlorite-feldspar layering with very elongated aggregates of actinolite.
IV ULTRAMYLONITE	Thin layering which is sometimes folded and cut by C' fabric.	Strong C foliation and various degrees of C' fabric development.	48.8 x 18.2	Continuing first and second order recrystallization.	Well developed chlorite - feldspar layering and crenulation.
V ULTRAMYLONITE	Well developed thick layers displaced by C' fabric.	C foliation and wide spaced C' fabric.	40.9 x 13.5 in chlorite layers. 51.8 x 16.1 in feldspar layers.	Same as stage IV.	Thick layers of chlorite and feldspar. Strongly crenulated.





**Fig. 58. Anastomosing shears (on right side of figure).**



100  $\mu$ m

**Fig. 59. Weak S fabric defined by bent actinolite in stage I gabbro.**





considered separately from the remaining mylonite.

Samples taken from the lithon centers, when observed microscopically reveal only a small degree of deformation. Most minerals are roughly equidimensional and recrystallization of feldspar is rarely observed. Slightly elongated leucoxene and rare thin (5-10 micron) zones of higher strain define a very weak C fabric. A weak S fabric is also produced by the bending of amphiboles into the thin zones of higher strain (Fig. 59). Although significant recrystallization does not occur at this stage, the presence of the weak mylonitic fabrics suggest that stage I represents a protomylonite.

## STAGE II

In outcrop, stage II often but not always separates stage I from stage III and/or stage IV. Stage II consists of coarse elongated feldspar and amphibole in a finer, medium to dark green matrix. The elongated minerals define a strong C fabric (Fig. 60). An S fabric was not observed. The width of this stage varies from centimeters to tens of centimeters as it usually forms an alternating pattern with the weakly developed layering of stage III. In some cases where stage II is associated with stages III and IV it has been folded. Often it is weakly disrupted by a weak irregularly spaced C' fabric.

In thin section stage II is characterized by elongated feldspar grains, feldspar aggregates and actinolite aggregates (Fig. 61), which cause the strong fabric seen in outcrop. The

considered generally free in the system. The  
samples taken from the different samples of the  
microscopically examined with a light microscope. The  
most abundant are highly refractive  
crystallization of 1000 to 1500 Å. The  
disaggregated leucocytes and the other cells  
higher strains being a very small number. The  
also produced by the medium of aggregated cells  
of higher strains (Fig. 20). The  
crystallization does not occur in the  
of the very thin film of liquid, that is  
a protoplasmic.

## DISCUSSION

In summary, stage II cells are  
from stage III which stage II cells are  
disaggregated and aggregated. The  
green matrix. The aggregated cells  
Fig. 20. In Fig. 20 the cells are  
stage varies from crystalline to  
usually forms an alternating pattern with the  
lapping of stage III. In the case of stage III  
associated with stage II and III. The  
it is very difficult to see. The  
In this section, the  
disaggregated cells are  
Fig. 21. The cells are





**Fig. 60. Mineral fabric cut by wide spaced C' fabric.**



100UM

**Fig. 61. C fabric defined by parallel aggregates of feldspar and actinolite.**





actinolite aggregates have formed as the result of a large amount of recrystallization. However recrystallization in the feldspar aggregates is limited (Table 1). The C' fabric visible in outcrop is identified microscopically as thin planes of displacement, often infilled with fine grained chlorite. The structure is easily observed due to the sigmoidal shape of feldspar and actinolite grains (Fig. 62). Stage II exhibits a strong mylonitic fabric and some recrystallization, the surviving megacrysts of feldspar and actinolite make up less than 50% of the rock and therefore is considered to represent a mylonite.

### STAGE III

Rock representative of stage III consists of alternating dark and light green layers, oriented parallel with the shear zone boundaries. This layering is poorly developed, varies in width along its length and is often discontinuous (Fig. 63). In some places large elongated amphiboles within the lighter layers define a mineral fabric parallel with the layering. A similar layering effect has been observed in mylonites of the Arnaboll thrust (Dixon and Williams 1983). In that mylonite, layering is produced by alternating quartz plus feldspar and muscovite rich zones, in which mica concentrations are considered to mark high strain zones.

In thin section the dark green layering is seen to consist of masses of extremely elongated aggregates of actinolite which are being replaced by chlorite. Single

considered to represent a single

## DATE \_\_\_\_\_

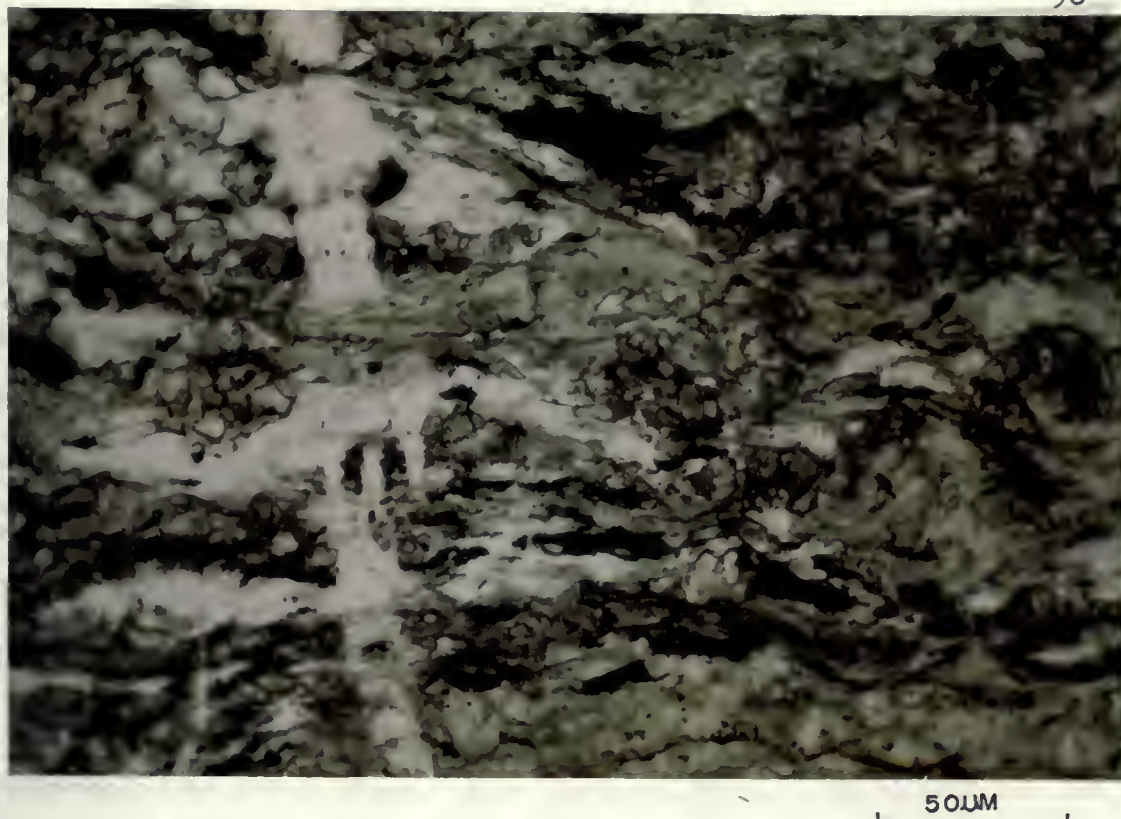


Fig. 62. Elongated feldspar with sigmoidal shape due to C' fabric. C is parallel with the base of the figure and C' is oriented NW -SE relative to the figure.



Fig. 63. Layering at stage III.





actinolite aggregates produce the mineral fabric in the lighter green layers which consist of chlorite and feldspar. Recrystallization of feldspar in these lighter layers has produced mainly first order grains (40 microns), and also a small degree of second order grains (15-20 microns). Original feldspar and actinolite grains are still present but make up less than 10% of the rock and therefore stage III represents an ultramylonite.

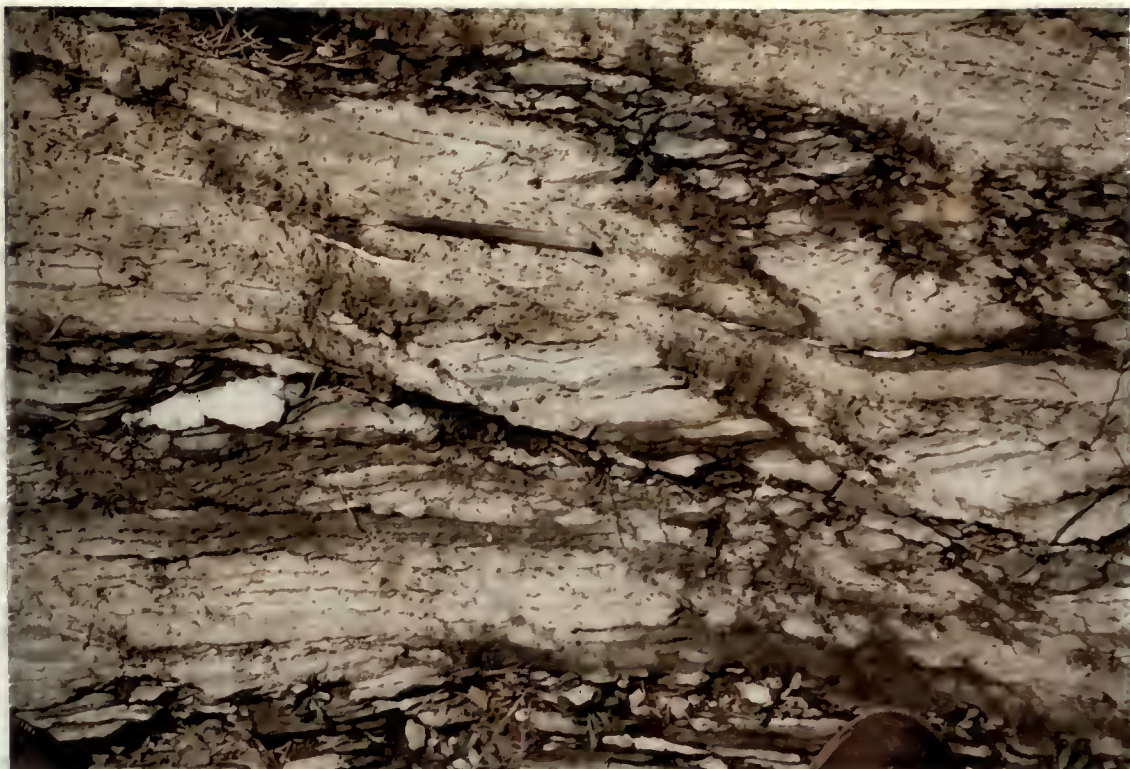
#### STAGE IV

The rock produced at this stage is considered to represent the most highly strained state of the gabbro. In outcrop it appears as a strongly layered rock in which the medium and pale green layers are usually relatively thin (<1cm), and often disrupted by a strong C' fabric (Fig. 64). The layering is less discontinuous than observed at stage III but the width continues to vary along the length of the layers. This well developed layering is often further deformed by Z style folds in which the axial trace bends towards parallelism with adjacent unfolded layering and is cut by the C' fabric (Fig. 65).

Microscopically the layering is revealed to be composed of alternating zones of chlorite and feldspar. The feldspar rich layers often center around extremely elongated aggregates of recrystallized feldspar. Within these aggregates, first order grains are the most common but a large degree of second order recrystallization has also taken place. Actinolite is







**Fig. 64. Thick layering of stage V mylonite surrounded by thin layering of stage IV cut by closely spaced C'.**



**Fig. 65. Folded layering is cut by C' fabric.**



Fig. 64. Thick layering of stage V mylonite surrounded by thin layering of stage IV cut by closely spaced C'.

Fig. 65. Folded layering is cut by C' fabric.

absent at stage IV and appears to have been totally replaced, producing the chlorite rich layers. Within both layers, elongated first and second order feldspar grains have become separated in a fine matrix of chlorite. Rare smaller aggregates of feldspar persist in which it can be seen that grains are being separated by chlorite at ends and margins. The long axes of both aggregates and grains are oriented parallel with a strong crenulation which is present at this stage. The strong foliation and degree of recrystallization at stage IV suggests that this rock is an ultramylonite.

#### STAGE V

Within the thinly layered stage IV rock at location 2, are zones of thicker layering (>1cm) in which the darker layers are a much darker green than in the surrounding stage IV layers. These zones are considered to mark a separate stage of mylonitization, stage V. The thicker layering becomes most obvious where it has been separated into "foliation fish" (Hanmer 1984) by the strongly developed C' fabric in the surrounding stage IV layers (Fig. 64). The stage V layering appears to be less affected by the C' which in most cases appears to stop at the layer boundary.

Microscopically this stage is similar to stage IV, with the same degrees of elongation and feldspar recrystallization.

Elongated aggregates are present in the feldspar rich layers but are usually shorter and thinner than those observed in stage IV. The most significant difference between these

## УДК 62-50

stages is the presence of actinolite in the chlorite rich layers of the stage V rock. This stage has been crenulated to a greater degree and in most places one set of limbs of the microfolds describes a distinctive crenulation cleavage.

Stages I through IV were used to describe rocks which have formed due to increasing strain within a gabbro. These stages were observed separately and together at several locations. The fifth stage described was clearly observed only at location 2, and appears to represent a similar degree of strain to stage IV. The thicker layering and presence of actinolite has led to defining of a separate stage. The apparent greater degree of separation of feldspar aggregates has led to defining this stage as a slightly higher degree of mylonitization than stage IV.

The thinly layered rock of stage IV is often cut and disrupted by zones of the closely spaced C' fabric (Fig. 64). The thick layering of stage V, observed at location 2 is surrounded by one of these zones but is only cut by the C' fabric at wide intervals (Fig. 64), producing the "foliation fish" appearance (Hanmer 1984). This effect appears to be related to the thickness of the layering, especially the chlorite rich layers in which the crenulation is best developed. According to Gapais and White (1982) the formation of a C' fabric in mylonites marks a change from homogeneous to inhomogeneous deformation and also a change in deformation mechanism from dislocation creep to grain boundary sliding. If these conclusions are applied to the present study, they





suggest that a sixth stage of mylonitization might be defined.

However evidence for the onset of grain boundary sliding in the examples studied by Gapais and White, came from observation of recrystallization within C' fabrics in a quartz mylonite. In the present study the zones of dense C' have been altered by carbonate which infilled the fabric and destroyed any original textures (Fig. 66). Because of this it is difficult to determine whether the zones of dense C' represent a further stage of mylonitization or a modification of stages IV and V.


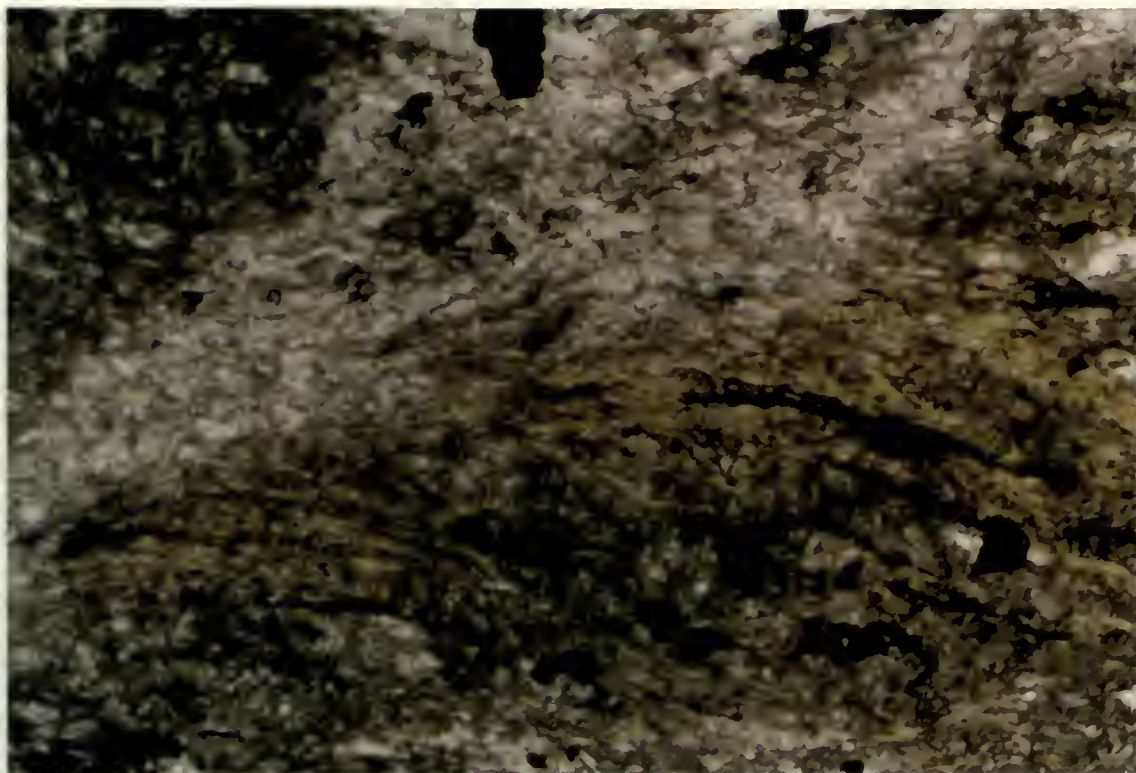


Fig. 66

...and a first series of experiments  
...for the purpose of determining  
...of the results obtained by the  
...of crystallization in the  
...In the present study the  
...been altered by conditions which  
...destroyed any original  
...In addition it is difficult to  
...represent a typical stage of  
...at stages IV and V.



100μm

**Fig. 66. C' fabric infilled by carbonate.**





## STATISTICAL ANALYSIS AND MINERALOGICAL DESCRIPTION

The gabbro mylonite from location 2 (Fig. 57) was chosen for detailed study due to the presence of all observed stages of mylonitization and also because of apparent homogeneity. The least deformed gabbro (stage I) consists of coarse grained albite-actinolite-chlorite-epidote-leucoxene +/- quartz. At this stage the gabbro maintains its primary igneous texture with weak fabrics defined by elongated actinolite and leucoxene. Mylonitization completely destroys the original texture producing an extremely fine grained well foliated rock, an ultramylonite. If not for the associated less deformed lithons of gabbro, the original progenitor of the ultramylonite (stage V), could not be easily discerned.

Thin sections were cut parallel with the lineation and perpendicular to the mylonite foliation. The axes of feldspar, actinolite, epidote, chlorite and leucoxene grains and aggregates were measured in an attempt to correlate statistically, the changes in shape with the degree of mylonitization. These measurements were also used to determine mean grain sizes of each stage. The mean ratio of length to width =  $R$ , the mean length =  $L$  and the mean width =  $W$  for each stage of mylonitization are shown in Table 2. The mean and standard deviation values are listed in Appendix 1.

The long and short axes of mineral grains and aggregates were measured optically, using the crosshair divisions provided. The measurements were then converted to microns. At high power and with a clear image, accuracy up to 2.5

The sample was placed in the center of the field of view of the camera and the distance between the camera and the sample was adjusted so that the image of the sample was in focus. The light from the sample was collected by a lens and focused on the entrance slit of the spectrograph. The light from the entrance slit was dispersed by a grating and focused on the photographic plate. The distance between the grating and the photographic plate was adjusted so that the spectrum was in focus. The photographic plate was developed and the spectrum was examined. The results of the measurements are given in the following table.

Table 1. Results of the measurements.

Wavelength (nm)	Intensity (a.u.)	Wavelength (nm)	Intensity (a.u.)
400	0.1	500	0.5
450	0.2	550	0.8
500	0.5	600	1.0
550	0.8	650	0.9
600	1.0	700	0.7
650	0.9	750	0.4
700	0.7	800	0.2
750	0.4	850	0.1
800	0.2	900	0.05
850	0.1	950	0.02
900	0.05	1000	0.01

The results of the measurements show that the intensity of the spectrum is maximum at 600 nm and decreases as the wavelength increases. The intensity is also minimum at 400 nm and increases as the wavelength decreases. The results of the measurements are in good agreement with the theoretical predictions.

microns was attained. The statistical data derived from these measurements is useful not only for indicating the effects of strain on individual minerals but also helps outline each of the separate mylonite stages.

In general, the R and L values of mineral types other than feldspar grains increase from stage I to stage IV (Table 2), indicating the increasing elongation of minerals through these stages. The sudden change in R and L in stage IV marks the formation of the crenulation and also indicates the increasing separation of grains by chlorite. An even better picture of the changes in mineral shape, is provided by histogram plots of R, L and W for each mineral through all stages of mylonitization (Appendix 1). Leucoxene provides a good example to illustrate the typical changes in R, L and W values. The values of R and L increased from 3.0 to 11.6 and 160.6 to 254.4 microns, respectively, from stage I to stage III. At the same time W decreased from 56.6 to 24.6 (Table 2). In stage IV each of the values shows a sudden decrease accompanying formation of the crenulation. Although the R, L and W values for stage V are greater than those in stage IV, they still show a marked decrease from stage III. It is also evident that the values are smaller in the chlorite layers where the crenulation is best developed (Table 2). The difference of R, L and W values between stage IV and stage V may be related to the relative layer thickness. The same pattern of increasing length and decreasing width shows up clearly in histogram plots for leucoxene (Fig. 67). The use



microns was obtained. The statistical data derived from these measurements is useful not only for indicating the effect of strain on individual minerals but also helps outlining a picture of the separate mylonitic stages.

In general, the R and L values of mineral types other than feldspar grains increase from stage I to stage IV (Table 2), indicating the increasing elongation of minerals through these stages. The sudden change in R and L in stage IV marks the formation of the crenulation and also indicates the increasing separation of grains by chlorite. An even better picture of the changes in mineral shape is provided by histogram plots of R, L and W for each mineral through the stages of mylonitization (Appendix I). Leuwaxen provides a good example to illustrate the typical changes in R, L and W values. The values of R and L increased from 3.7 to 11.5 and 160.6 to 224.4 microns, respectively, from stage I to stage III. At the same time W decreased from 56.6 to 24.1 microns.

2). In stage IV each of the values shows a sudden decrease accompanying formation of the crenulation. Although the R, L and W values for stage V are greater than those in stage IV, they still show a marked decrease from stage III. It is also evident that the values are smaller in the chlorite layer where the crenulation is best developed (Table 2). The difference of R, L and W values between stage IV and stage V may be related to the relative layer thickness. The same pattern of increasing length and decreasing width shows clearly in histogram plots for leuwaxen (Fig. 2). The data

TABLE 2

Mineral measurements for each stage of gabbro mylonitization. R=mean ratio, L=mean length and W=mean width. (L and W in microns).

Stages	:	:	I	:	II	:	III	:	IV	:	V-fel	V-chl
Feldspar	:R:		1.8:		3.2:		3.0:		3.0:		3.5:	3.4:
Grains	:L:		111.0:		65.3:		43.6:		48.8:		51.8:	40.9:
	:W:		68.0:		23.2:		15.5:		18.2:		16.1:	13.5:
Feldspar	:R:				5.9:		5.9:		4.8:		7.2:	8.8:
Aggregate	:L:				326.4:		545.9:		166.1:		508.8:	338.0:
	:W:				66.8:		90.9:		33.2:		73.7:	55.0:
Chlorite	:R:		2.6:		8.6:		9.6:		10.0:		6.3:	5.7:
	:L:		188.2:		173.8:		181.1:		93.6:		80.0:	102.3:
	:W:		91.0:		28.3:		24.2:		11.6:		17.5:	22.9:
Actinolite	:R:		3.2:		5.4:			:		:		8.2:
Grains	:L:		707.6:		400.3:			:		:		98.0:
	:W:		215.7:		92.6:			:		:		14.2:
Actinolite	:R:				8.1:		19.8:			:		:
Aggregates	:L:				676.0:		1240:			:		:
	:W:				124.0:		70.4:			:		:
Epidote	:R:		1.4:		1.8:		1.7:		1.9:		2.1:	2.0:
Grains	:L:		53.4:		84.1:		36.6:		44.9:		35.9:	35.4:
	:W:		40.0:		44.1:		23.1:		25.5:		19.2:	20.2:
Epidote	:R:		2.1:		3.0:		1.8:			:		:
Aggregates	:L:		172.7:		238.7:		97.8:			:		:
	:W:		90.9:		78.6:		57.6:			:		:
Leucoxene	:R:		3.0:		9.8:		11.6:		2.4:		8.3:	5.2:
	:L:		160.6:		190.5:		254.4:		32.1:		134.5:	98.8:
	:W:		56.6:		23.9:		24.6:		13.7:		16.1:	19.8:

TABLE 2

Mineral measurements for each stage of nephropathic mineralization.  
R=mean ratio, L=mean length and W=mean width (L and W in microns).

Stages			I	II	III	IV	V-fel	V-cel
Feldspar	R:	1.8:	3.2:	3.0:	3.0:	3.0:	3.2:	3.4:
	L:	111.0:	63.3:	43.6:	48.8:	51.8:	40.9:	
	W:	68.0:	23.3:	15.5:	18.2:	16.1:	13.7:	
Aggregate	R:		5.9:	7.9:	4.8:	7.2:	5.8:	
	L:	326.4:	545.9:	166.1:	508.8:	338.0:		
	W:	66.8:	90.9:	33.2:	73.7:	56.0:		
Chlorite	R:	2.6:	8.6:	9.6:	10.0:	6.3:	5.7:	
	L:	188.2:	173.8:	181.1:	93.6:	80.0:	102.5:	
	W:	91.0:	28.3:	24.3:	11.6:	17.5:	22.9:	
Actinolite	R:	3.2:	5.4:				8.2:	
	L:	707.6:	400.3:				99.0:	
	W:	215.7:	92.6:				14.7:	
Actinolite	R:		8.1:	19.8:				
	L:	676.0:	1240:					
	W:	124.0:	70.4:					
Epidote	R:	1.4:	1.8:	1.7:	1.9:	2.1:	2.0:	
	L:	53.4:	84.1:	36.6:	44.9:	35.9:	35.4:	
	W:	40.0:	44.1:	23.1:	25.2:	19.2:	20.2:	
Epidote	R:	2.1:	2.0:	1.8:				
	L:	172.7:	238.7:	97.8:				
	W:	90.9:	78.6:	27.6:				
Leucosane	R:	3.0:	9.8:	11.6:	2.4:	8.2:	5.2:	
	L:	160.6:	90.5:	254.4:	37.1:	134.2:	98.8:	
	W:	56.6:	23.2:	24.6:	13.7:	16.1:	19.8:	

LENGTH

WIDTH

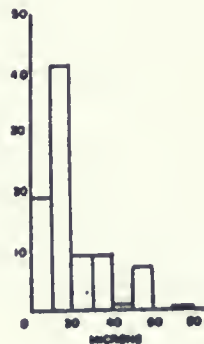
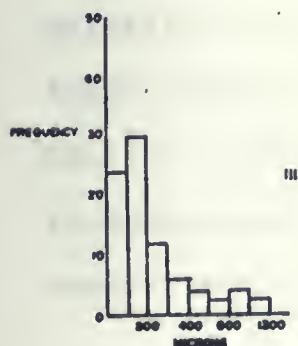
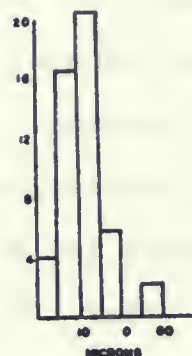
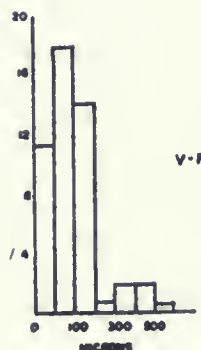
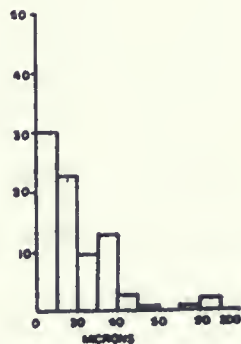
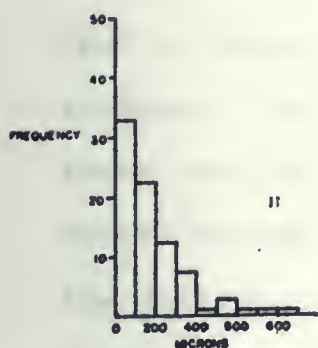
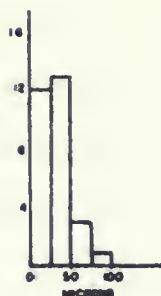
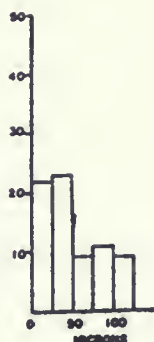
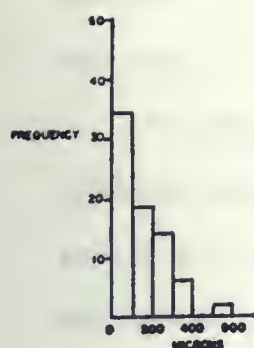


Fig. 87 Histograms of the length and width of leucoxene for each stage of mylonitization.





of R, L, W and histograms for length and width also proved useful in defining the different generations of feldspar recrystallization (Fig. 83 and Table 3).

Standard deviation values (Appendix 1) reveal a similar statistical pattern. In general the standard deviation of L and W are high for all stages of mylonitization. The standard deviation values for R are low for minerals in the least deformed rock but increase with increasing mylonitization. This effect is due to the contrasting ductilities of the different mineral types. Chlorite, actinolite and leucoxene tend to become elongated easily and earlier than feldspar and epidote. Individual R values of 20 to 50 are not uncommon for these ductile minerals (Appendix 1). However when forced to "flow" around the more rounded or blocky feldspars and epidote the ductile minerals pinch out or are separated in a more brittle fashion, producing grains of lower R values and thus larger values of standard deviation. The size of single feldspar grains and aggregates also show increased standard deviation in the later stages of mylonitization. In this case these seem to be the result of incomplete recrystallization. Smaller, undeformed new grains are produced from older elongated grains and aggregates causing two or more populations of grain size (Fig. 83).

#### EPIDOTE

Epidote is present throughout the gabbro mylonite. In the least deformed stages it is present both as single

891076

euohedral to subhedral grains (L=50, W=40 microns) and more commonly as radial aggregates (L=175, W=90 microns) of euohedral grains (Fig. 68). In plane light epidote is easily recognized due to its high relief, pale yellow colour and weak pleochroism. Throughout the early stages of mylonitization both single grains and compact aggregates are often observed surrounded by finer grained masses of chlorite and or actinolite as asymmetric pressure shadows, indicating rotation of the less ductile epidote within the more ductile matrix.

Of the minerals studied, single epidote grains showed the least effect of mylonitization. The small changes in R, L and W values listed in Table 2, appears to be the result of rotation of grains, so that the long axes are parallel with the foliation. The epidote grains themselves show no sign of strain or recrystallization.

The effects of mylonitization show more clearly through changes in the aggregates of epidote. A marked change in L and W values occurs between stages II and III (Table 2). This statistical evidence marks the breaking up of these aggregates into single grains. In stages IV and V aggregates of epidote are not present. Instead single grains are widely scattered throughout the rock with most grains oriented parallel with and emphasizing the crenulation (Fig. 69).

#### ACTINOLITE

At the least deformed stage, actinolite is present as fine acicular needles and more commonly as fibrous masses





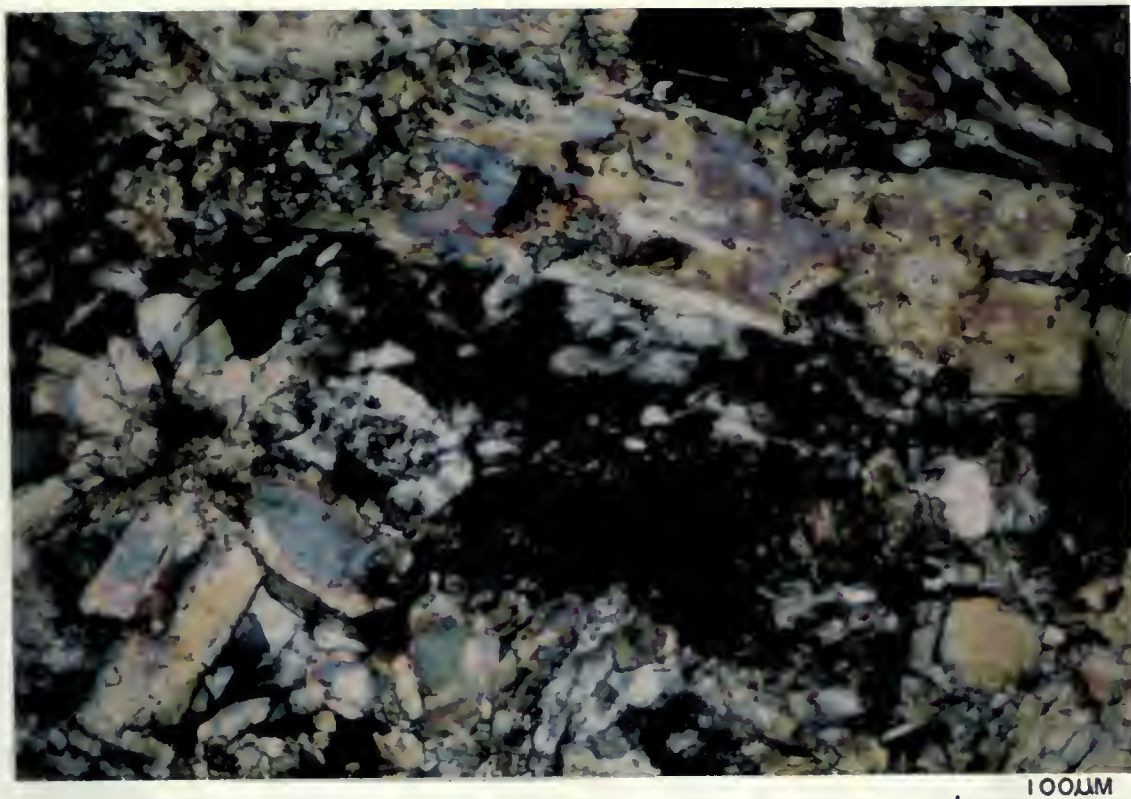


Fig. 68. Thin section of stage I gabbro. Note radial aggregate of epidote.



Fig. 69. Epidote grains with long axis parallel to crenulation in stage V.



(uralite) completely replacing original pyroxene. In plane light the actinolite has pale to dark green pleochroism. In most cases the original form and interstitial texture of the pyroxene is maintained (Fig. 68). Therefore the observed R, L and W values (Table 2) probably reflect the original texture of the gabbro. In some cases the coarse actinolite masses are deformed by short (<1mm) shears defining a weak C fabric. The masses become slightly elongated oblique to these shears, defining a weak S fabric 20 to 30 degrees from the C fabric (Fig. 59).

In the second stage actinolite is deforming rapidly, parallel to C, into elongated aggregates (R=10) up to 1.5mm in length. These aggregates form due to an accreting process in which large rounded masses form a central core with fine grained recrystallized tails which often combine to increase the overall length of the aggregate (Fig. 70). At stage II a weak C' fabric is often present which disrupts the C fabric, producing sigmoidal shaped feldspar and actinolite grains and aggregates (Fig. 62). Because of this disruption it is difficult to determine if an S fabric is present at stage II.

Actinolite aggregates appear to become completely recrystallized and continue to elongate in stage III (R = 25-36). The weak layering observed in stage III forms due to the accreting of thin (W = 40 microns) actinolite aggregates into larger aggregates (W = 100 microns). These in turn join to produce the weak layering. In most places the actinolite







50μm

**Fig. 70. Actinolite aggregates in stage II showing core of large grains with tails of finer grains.**

THE UNIVERSITY OF CHICAGO  
LIBRARY

is being replaced by chlorite at grain margins and along the actinolite cleavage.

At stage IV thin (2-3mm) chlorite and feldspar layers have formed. Actinolite is absent from both layers and appears to have been completely replaced by chlorite. However at stage V thicker layers have formed (1-2cm) with up to 15-20% actinolite in the chlorite rich layers. In this case the actinolite occurs as euhedral crystalline grains with their long axes parallel with the crenulation. In many cases these grains appear to be separating along their length in a brittle fashion (Fig. 71). In plane light these grains are a darker green-blue than in earlier stages. The actinolite present in stage V also has a higher extinction angle suggesting that these may be a higher grade actinolite or low grade hornblende.

#### CHLORITE

In the least deformed state, chlorite is present as anhedral grains interstitial to feldspar and actinolite (Fig. 68), as fine fibrous aggregates within thin shears and also as an alteration of the original pyroxene. At stages II and III, equidimensional chlorite grains are rare as most of the chlorite has become thin (25 microns) and elongated ( $R = 8.5-9.6$ ) parallel to C. Chlorite is also present, intergrown with or replacing actinolite, as fine aggregates forming pressure shadows around rotating epidote grains and within the C' fabric.

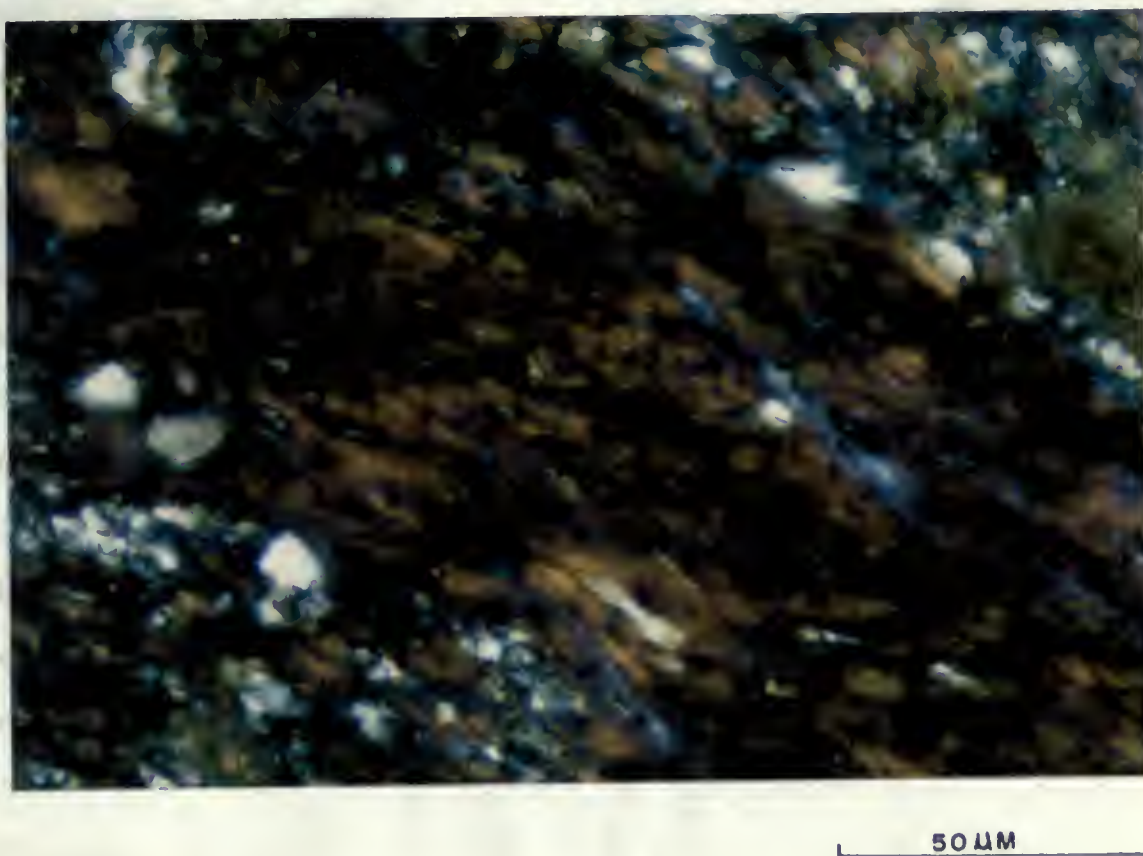


The results of the present study are in good agreement with those reported by other workers. The results of the present study are in good agreement with those reported by other workers.

SY 29D 21



**Fig. 71. Separation of actinolite grains at stage V.**



**Fig. 72. Two generations of chlorite in a carbonate rich gabbro mylonite.**



In stages IV and V chlorite alteration of actinolite has increased producing layers up to 75% chlorite. It occurs mainly as thin ( $W = 5-25$  micron) sinuous grains (Fig. 81) in the feldspar rich layers and as coarser aggregates surrounding isolated feldspar grains in the chlorite rich layers (Fig. 73). The chlorite layers in the zones of dense C' fabric are usually greater than 90% chlorite and often are made up of two generations of chlorite. The separate chlorites have distinctly different birefringence (Fig. 72), and the later generation appears to be related to alteration by carbonate infilling of the C' fabric.

#### FELDSPAR

In the least deformed rock (stage I), feldspar occurs as coarse grains ( $L = 111$ ,  $W = 65$  microns), forming an equigranular texture with coarse actinolite and chlorite. As the deformation increases to stage II elongated ( $R = 5.9$ ) aggregates of feldspar begin to form due to minor recrystallization and also due to an accreting or clotting together of previously separated grains. This second process is concentrated along the C fabric (Fig. 61). At the same time single grains have become elongated in a ductile fashion ( $R = 3.2$ ) parallel with the C fabric (Fig. 62). In some cases rounded feldspar grains have chlorite pressure shadows indicating rotation. The differing styles of deformation at this single stage of mylonitization indicate a heterogeneity of strain caused by the differing ductility of individual



is shown in the figure on the right.

Considered in the same way as the other

cases, we find that the same result is obtained

for the other two cases, and we conclude

that the same result is obtained in all cases.

The above result is a special case of the

more general result which we now state.

Theorem 1. Let  $f(x)$  be a function of  $x$  such that

$f(x) = 0$  for all  $x$  in the interval  $[a, b]$ .

Then the function  $f(x)$  is identically zero.

Proof. Let  $x_0$  be any point in the interval  $[a, b]$ .

## THEOREM 2

Let  $f(x)$  be a function of  $x$  such that

$f(x) = 0$  for all  $x$  in the interval  $[a, b]$ .

Then the function  $f(x)$  is identically zero.

Proof. Let  $x_0$  be any point in the interval  $[a, b]$ .

Then the function  $f(x)$  is identically zero.

Proof. Let  $x_0$  be any point in the interval  $[a, b]$ .

Then the function  $f(x)$  is identically zero.

Proof. Let  $x_0$  be any point in the interval  $[a, b]$ .

Then the function  $f(x)$  is identically zero.

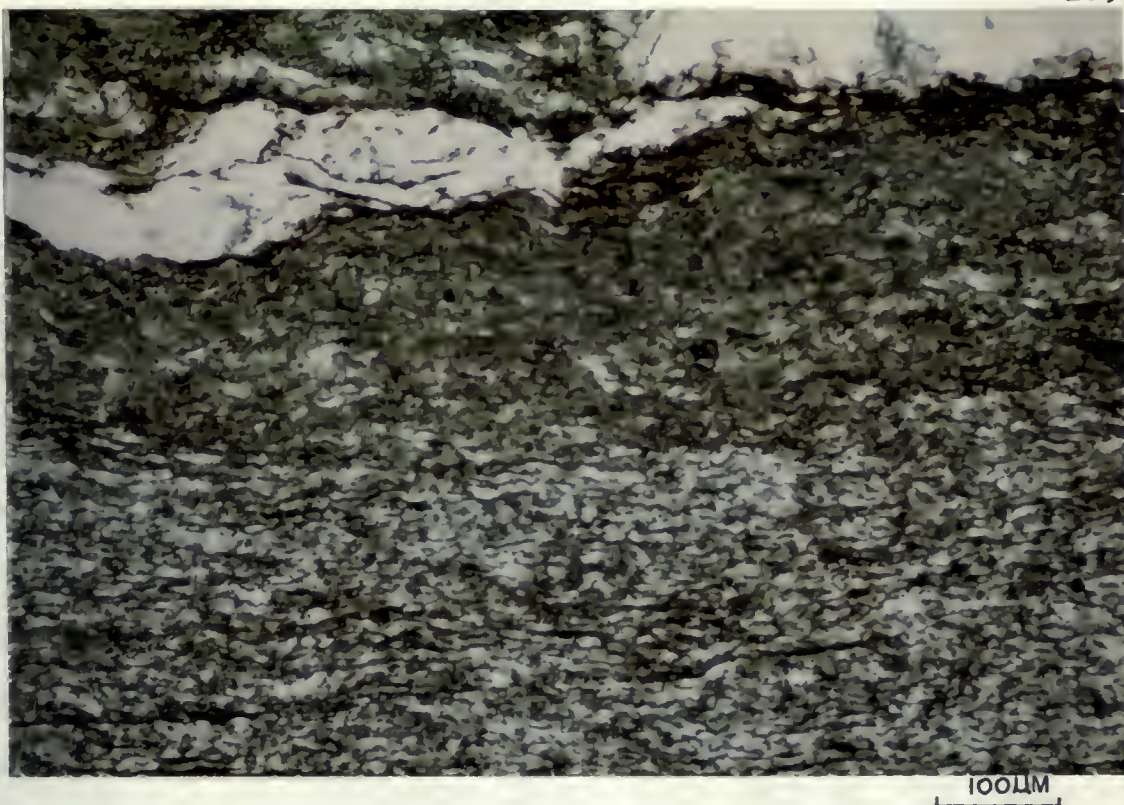
Proof. Let  $x_0$  be any point in the interval  $[a, b]$ .

Then the function  $f(x)$  is identically zero.

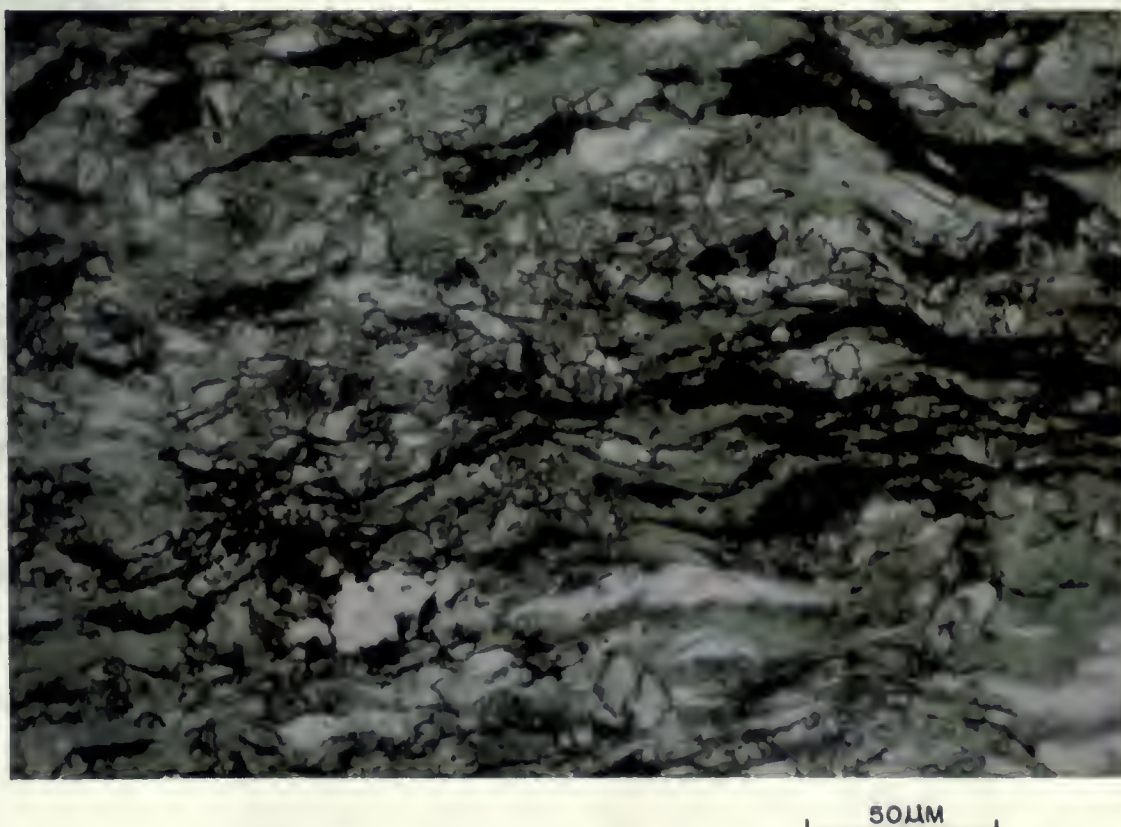
Proof. Let  $x_0$  be any point in the interval  $[a, b]$ .

Then the function  $f(x)$  is identically zero.

Proof. Let  $x_0$  be any point in the interval  $[a, b]$ .



**Fig. 73. Stage V layering. The feldspar rich layers are made up of isolated feldspar grains in coarse grained chlorite.**



**Fig. 74. Crenulated leucoxene at stage V.**





types of mineral.

By stage III accretion of feldspar aggregates has reached a point where discontinuous chlorite rich - feldspar rich layering has formed. The feldspar rich layering is up to 1-2mm wide at this stage. Smaller ( $<80$  microns) aggregates are also present in the chlorite rich layers. In both cases the elongation or layering is parallel with C. At the most deformed stages, the rock has become completely segregated into chlorite rich - feldspar rich layering. The individual aggregates within the feldspar layers are often separated by thin (5-25 micron) sinuous chlorite. Elongated feldspar grains within the chlorite layers have become totally separated from each other by coarse chlorite (Fig. 73).

#### LEUCOXENE

Aggregates of leucoxene are present in small amounts throughout the gabbro mylonite. In all stages it is present mainly as elongated aggregates of fine ( $<5$  micron), euhedral grains, which in all cases are oriented parallel with the C fabric. Even in the least deformed stage, slightly elongated aggregates ( $R = 3$ ), define a weak C fabric. The value of  $R$  increases from this stage to a value of 11.5 at the third stage. Observation of values for  $L$  and  $W$  in Table 2, reveal that this increase in  $R$  is due to rapidly increased length whereas the width decreases relatively slowly. This is due to the same process of accretion which causes elongation of feldspar and actinolite.





At stages IV and V a sudden decrease in R from 11.6 to 2.5 is accompanied by decreasing L and W values (Table 2). This change accompanys the development of a strong crenulation of the C fabric (Fig. 74). Values of R in the feldspar layers where the crenulation is weakly developed are higher than in the strongly crenulated chlorite layers.

In some cases the elongated aggregates remain continuous around the hinge of the crenulation (Fig. 74), but in most cases they become separated causing the decrease in R. The change in R may also be related to the reaching of a critical point of elongation, as in many cases the aggregates appear to be breaking up or pulling apart along their length. These show up as shorter aggregates with trails of smaller aggregates and single grains.



## DETAILED FELDSPAR MICROSTRUCTURES

The description of feldspar microstructures will be separated into stages corresponding with those defined in outcrop and supported by statistical analysis. Although recrystallization of feldspar is gradational, increasing towards areas of highest strain, these stages are representative of the minimum, intermediate and maximum degrees of deformation present in the gabbro mylonite. The feldspar microstructures present at each stage and their association with recrystallization have been summarized in Table 3.

The microstructural terminology used here to describe the recrystallization of feldspar in a gabbro mylonite has been widely used in studies of experimentally and naturally deformed rocks (Bell and Etheridge 1973, White 1976, Goetze 1978, Guillope and Poirier 1979). These terms have evolved from the study of dislocation and diffusion creep processes which are responsible for ductile deformation.

Briefly, dislocation creep is a process in which deformation is accomplished by slip along crystal lattice planes. The line between the slipped and unslipped parts of the crystal is called a dislocation (Hobbs et al., 1976) and these can be seen with the use of a transmission electron microscope. The dislocation creep process occurs at high pressures and temperatures and is accompanied by dynamic recrystallization which produces the fine grain size characteristic of mylonites.



101. The following table shows the results of the survey.

The results of the survey are as follows: The majority of the respondents (75%) are male, and the majority (65%) are aged between 25 and 40. The majority (80%) are employed, and the majority (70%) are married. The majority (60%) are of the Christian faith, and the majority (50%) are of the English nationality. The majority (40%) are of the middle social class, and the majority (30%) are of the working class. The majority (20%) are of the professional class, and the majority (10%) are of the managerial class. The majority (5%) are of the service class, and the majority (2%) are of the agricultural class. The majority (1%) are of the other class.

Table 1.

The following table shows the results of the survey. The majority of the respondents (75%) are male, and the majority (65%) are aged between 25 and 40. The majority (80%) are employed, and the majority (70%) are married. The majority (60%) are of the Christian faith, and the majority (50%) are of the English nationality. The majority (40%) are of the middle social class, and the majority (30%) are of the working class. The majority (20%) are of the professional class, and the majority (10%) are of the managerial class. The majority (5%) are of the service class, and the majority (2%) are of the agricultural class. The majority (1%) are of the other class.

TABLE 3  
FELDSPAR MICROSTRUCTURES

STAGE	UNDULATORY EXTINCTION	DEFORMATION BANDS	SUBGRAINS	RECRYSTALLIZATION
I	Present in most grains. grains.	Rarely and only in larger grains are in contact.	Rarely and only when large	Not observed.
II	Strong in all original grains, absent in new grains.	Rarely observed.	Common in single original grains and throughout aggregates.	Some recrystallization of single grains but more common in aggregates, new grains 40x20 microns.
III	Strong in original and first order grains.	Rarely observed.	Common in all original grains and aggregates but rare in new grains.	Mainly first order with some second order recrystallization in feldspar layer aggregates, second order 16x10 microns.
IV	Common in all grains.	Rarely observed.	Common in original and first order grains.	Continued recrystallization with second order grains mainly in aggregates.
V	Common in all grains.	Not observed.	Common in aggregates but rare in isolated single grains.	Very few original grains mainly single first and second order grains isolated in chlorite.



Undulatory extinction is produced when large densities of closely spaced dislocations form along prism planes. This causes lattice bending, visible optically. The build up of dislocations forms boundaries separating strain free areas of the lattice. These boundaries become slightly misoriented and are visible optically as subgrains. Elongated subgrains often form deformation bands parallel to prism planes and separated by less deformed parts of the crystal lattice (White 1976).

Dynamic recrystallization can occur in two ways. At lower stresses and temperatures, rotation recrystallization takes place (White, 1976, Guillope and Poirier, 1979). As deformation proceeds, dislocations build up in subgrain boundaries, causing increased misorientation across the boundaries until eventually a new grain forms.

Recrystallization can also occur due to grain boundary migration. This occurs when a major difference in dislocation density develops across grain boundaries. The grain boundary migrates towards the point of greatest dislocation density creating bulges which break off to form new grains.

Both of these recrystallization mechanisms can occur separately or together (White 1976). If the recrystallized mineral is continually strained, further recrystallization of both the original and the newer grains can occur. For the purpose of description in the present study, feldspar grains which are being recrystallized are defined as original grains.

The newer grains are considered to represent a first order of recrystallization. When these first order grains subsequently





recrystallize, a second order of grains is produced. In each case recrystallization has produced new grains smaller than their original host.

## STAGE I

At first glance, thin sections from samples taken at the center of the lithons representing the stage I gabbro appear undeformed (Fig. 68). Feldspar grains do not appear elongated (Table 2) and recrystallization is virtually absent. However the presence in the feldspar of undulatory extinction, deformation bands and subgrains indicates the presence of lattice distortion and dislocation creep processes.

Almost all of the feldspar shows weak to strong undulatory extinction. Deformation bands and lamellae are rare to absent but when recognized are confined to the largest isolated grains. Subgrain formation is relatively rare but is observed in many of the larger feldspar grains. Subgrains are commonly equidimensional and show up most clearly near grain margins and where one or more grains are in contact. Feldspar recrystallization is rare to absent in the sample taken to represent the best example of stage I mylonitization. Thin sections taken from samples away from the central part of the lithons do show increased recrystallization.

## STAGE II

This stage is characterized microscopically by the presence of elongated grains and aggregates of feldspar (Fig.

... of the ...

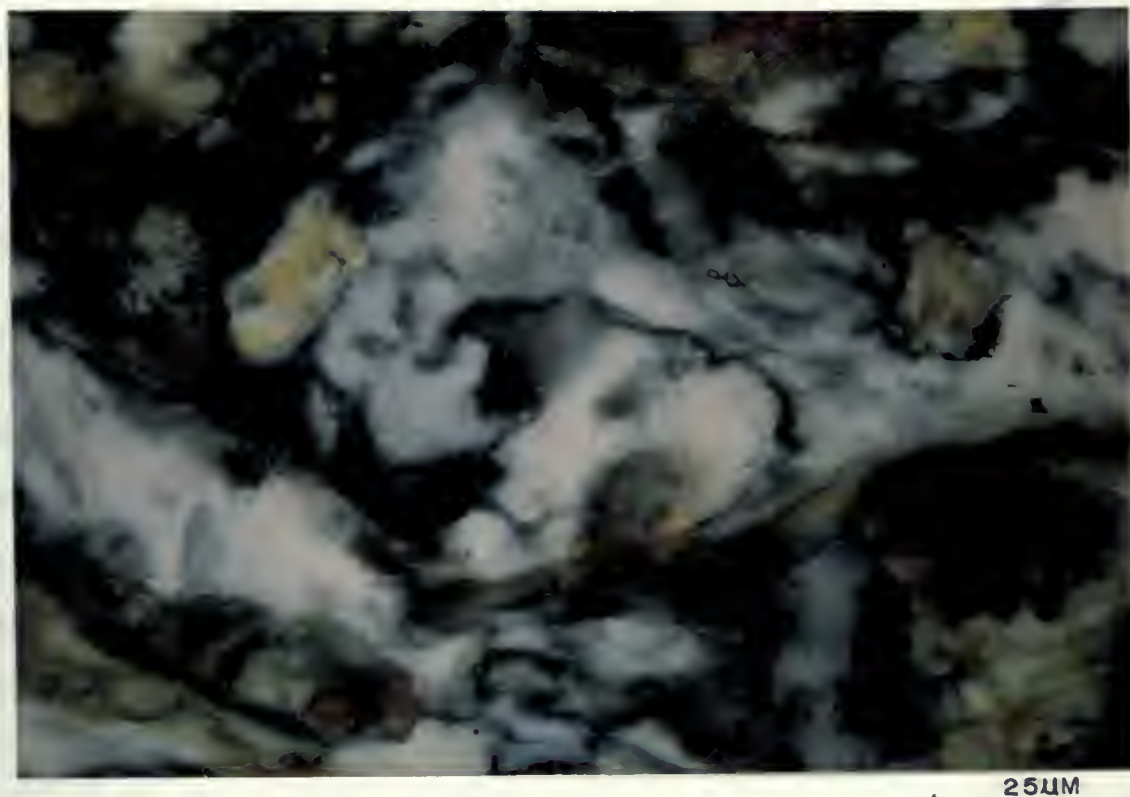
30.475

61). The formation of these as second stage strain features, after undulatory extinction, deformation bands and subgrain development in quartz, in mylonites has also been observed by Bell and Etheridge (1973) and White (1976). The elongated aggregates of feldspar are parallel in orientation to chlorite and actinolite growth, defining the first stages of a mylonite foliation or C fabric. Most single grains isolated by chlorite and or actinolite, are also elongated parallel with the C fabric. In many cases these are seen to bend in a ductile fashion into the discordant C' fabric weakly developed at this stage (Fig. 62).

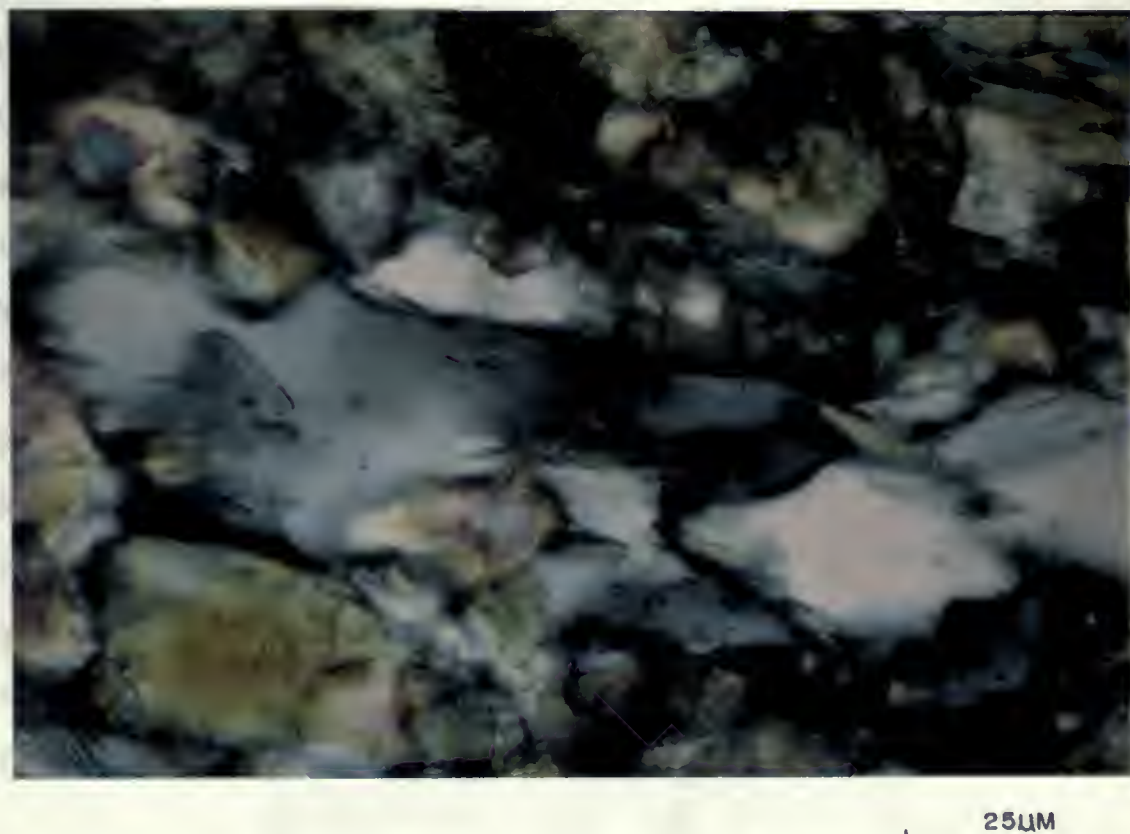
Recrystallization is present in association with single isolated grains and more commonly with aggregates. The aggregates appear to be made up of several large or small elongated grains. The new first order grains form mainly at grain margins and grain boundaries which are in contact. In many cases serrated grain boundaries indicate the presence of grain boundary bulging (Fig. 75). Many of the new grains especially those at the margins of single isolated grains are similar in size (42x28 micron) to subgrains which are well developed in all of the earliest unrecrystallized feldspar (Fig. 76). This appears to indicate that recrystallization at this stage is also due in part to the misorientation of subgrain boundaries to a point where new grains form at the original grain margins. All of the new first stage recrystallized grains appear unstrained, where as all of the original feldspar shows strong development of undulatory







**Fig. 75. Grain boundary bulging between grains of feldspar.**



**Fig. 76. Development of subgrains and first order grains of feldspar.**



extinction and subgrains. Deformation bands and lamellae are rare to absent at this stage.

### STAGE III

This stage marks the earliest formation of the weak feldspar rich - chlorite rich layering. Feldspar is present both as recrystallized aggregates making up the feldspar rich layers and also as rare smaller aggregates and isolated grains in the chlorite rich layers. Separate aggregates making up the feldspar layers are usually outlined by thin sinuous chlorite.

Feldspar microstructures differ distinctly in the different layers. In the chlorite rich layers most single isolated grains show strong subgrain formation, and commonly first order recrystallization similar to that seen in stage II. The new grains appear to be strain free. Feldspar aggregates within the chlorite rich layers show evidence of higher strains. Most of the original grains in these aggregates have recrystallized to first order grains which often have undulatory extinction and weak subgrain development. In some cases total recrystallization produces a "polygonal" texture described for quartz in mylonites by Lister and Price (1977) (Fig. 77). In several of the aggregates, new first order grains have serrated boundaries indicating the beginning of a second order of recrystallization (Fig 78).

The feldspar rich layers are made up mainly, of massed



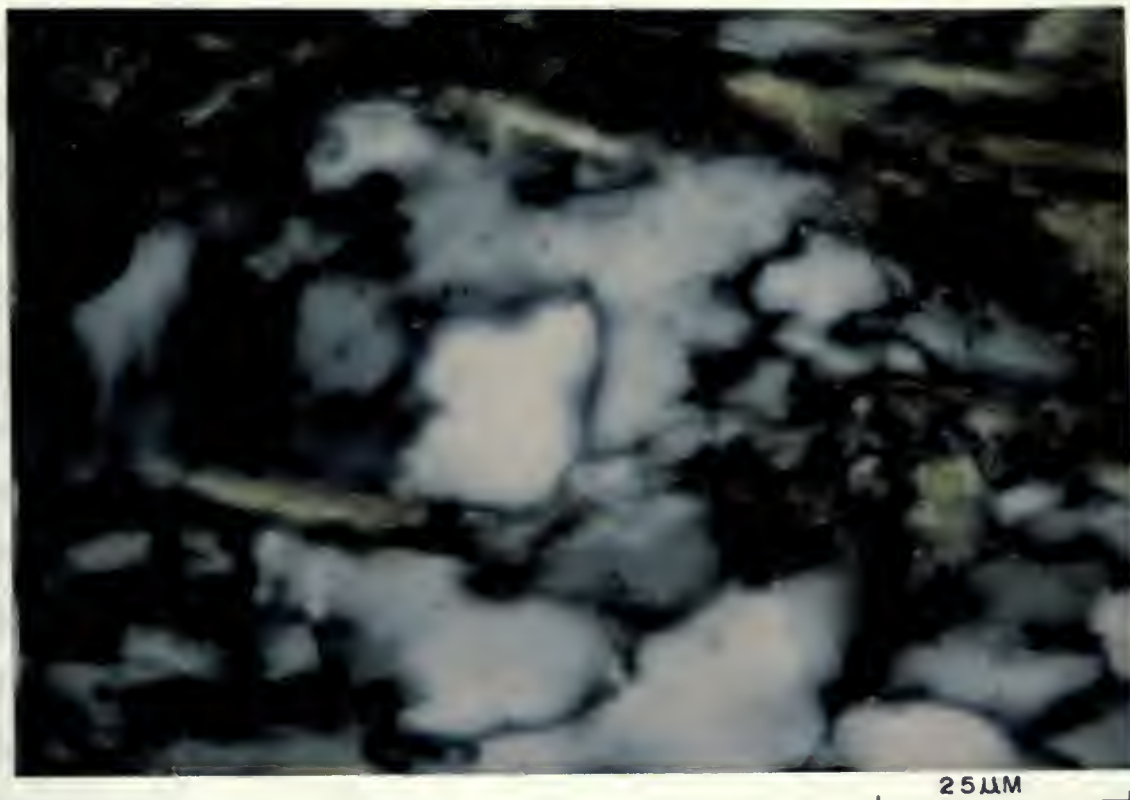
... and ...  
... at this stage

Stage III

This stage marks the earliest formation of ...  
... with ...  
... as ...  
... and also ...  
... the ...  
... are usually ...  
...

... microstructure ...  
... layers ...  
... that ...  
... first ...  
... the ...  
... within ...  
... most ...  
... aggregates ...  
... have ...  
... development ...  
... "polymer" ...  
... and ...  
... aggregates ...  
... indicating ...  
... microstructure ...

The ...



**Fig. 77. Polygonal texture in a feldspar aggregate. Note the grain boundary bulging in first order grains.**



**Fig. 78. Grain boundary bulging in first order feldspar grains (20 - 5 microns).**



aggregates of first order grains. Few of the original feldspar grains remain but those present show strong undulatory extinction and subgrain formation. The new first order grains also show strong undulatory extinction, subgrain formation and often are elongated with axial ratios of greater than 5 to 1. Grain boundary bulging occurs at first order grain contacts with the bulges ranging in size from 20 to 5 microns (Fig. 78). In some cases second order recrystallization has taken place and is concentrated at grain margins and grain contacts (Fig. 79). The mean length and width of these second order grains is 16x10 microns. Many of the first order grains have become separated from the aggregates by chlorite.

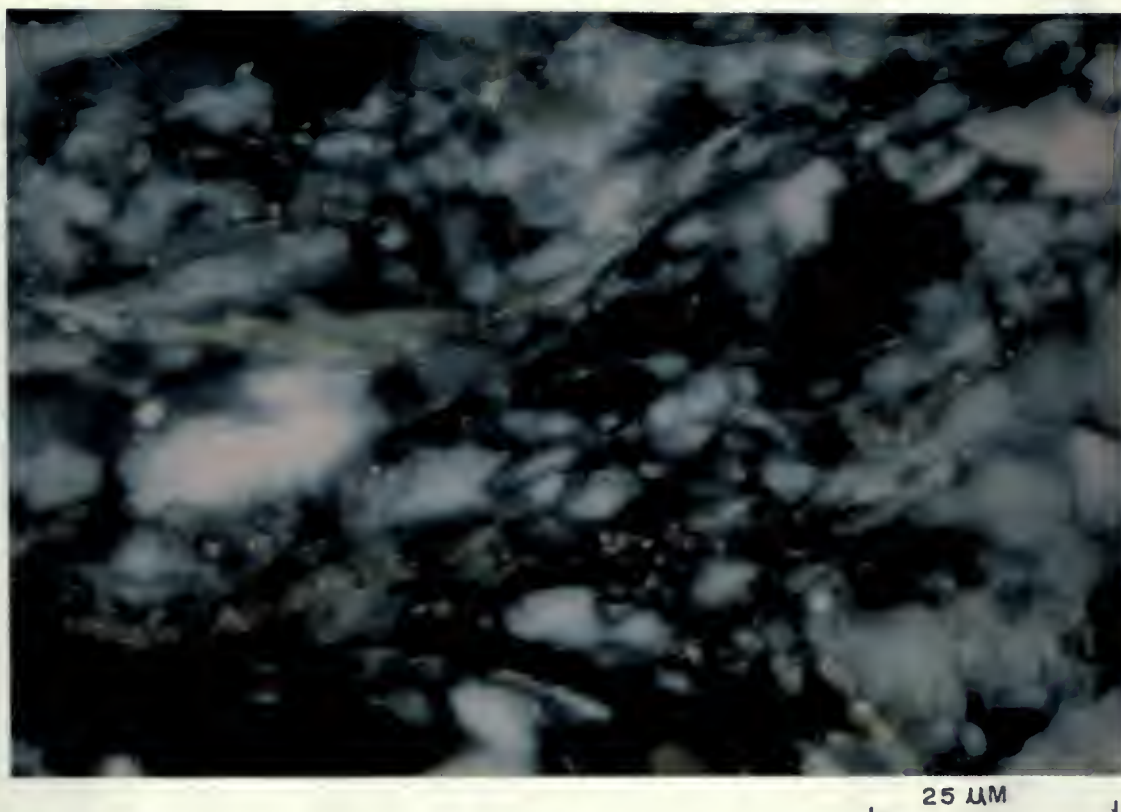
#### STAGE IV

At this stage well defined layers 2-3mm wide have formed.

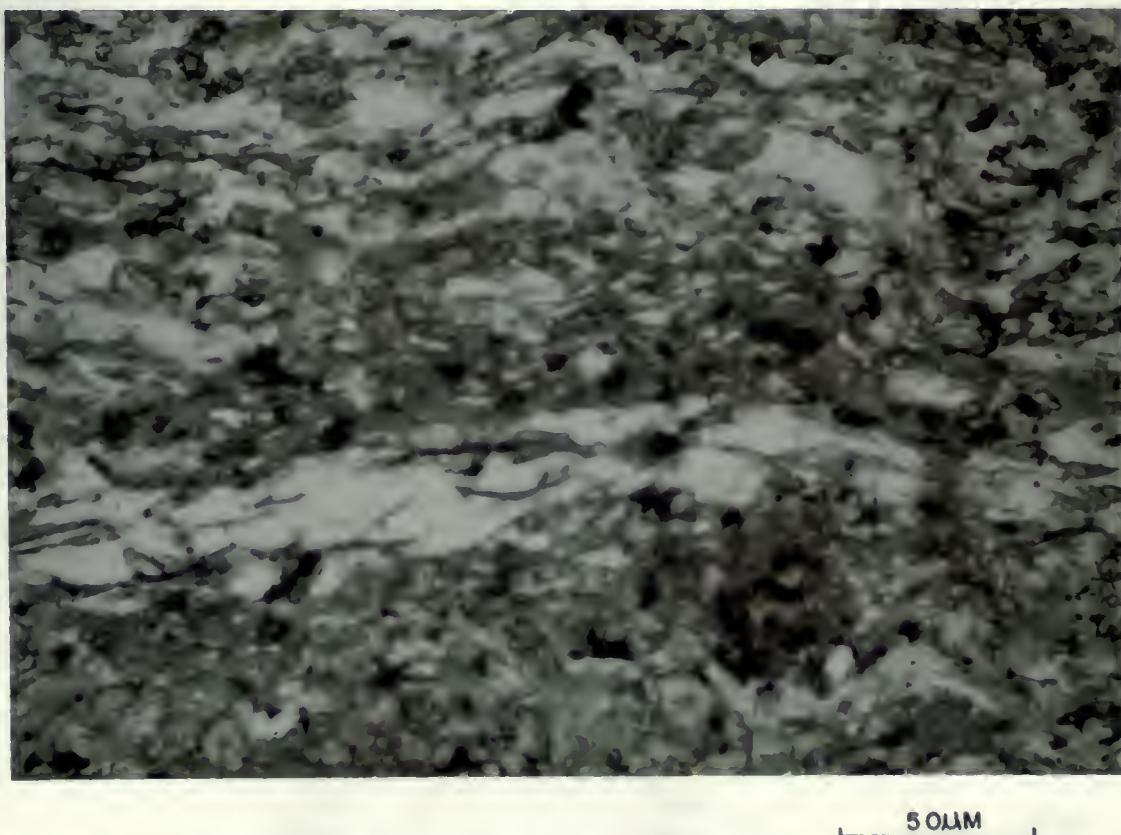
The feldspar rich layers are made up of elongated aggregates, 90-100% feldspar, surrounded by zones of separated feldspar grains and fine chlorite (Fig. 80). Feldspar within the chlorite rich layers is mainly single first order grains separated by coarse chlorite (Fig. 81). Most of these grains are elongated with their long axes parallel with the crenulation present at this stage. The average size of these grains is 45x15 microns. Both these and rare original grains show strong undulatory extinction and subgrain development. Rare grain boundary bulging is present where grains come in contact.







**Fig. 79. Chlorite separating first and second order feldspar grains from aggregate.**



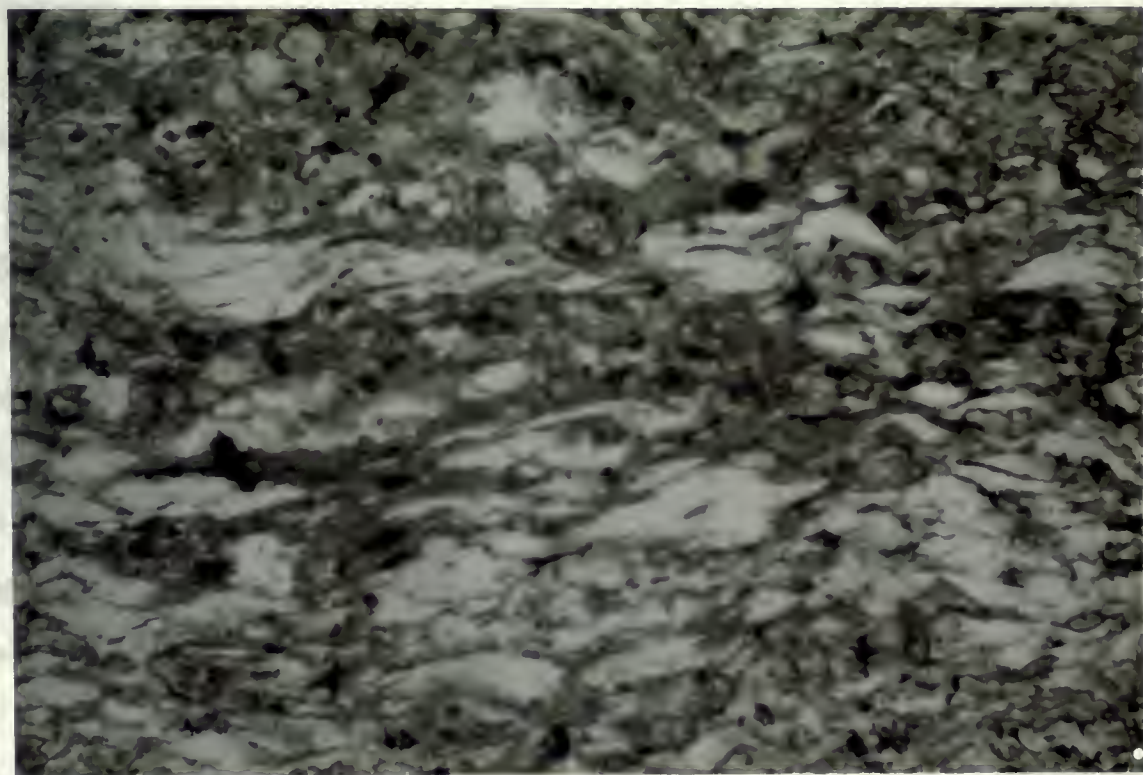
**Fig. 80. Layering at stage IV with chlorite separating feldspar grains from aggregates.**







**Fig. 81. Isolated first order feldspar grains in a matrix of chlorite.**



**Fig. 82. Thin chlorite surrounding feldspar grains near a feldspar aggregate.**





The feldspar rich zones surrounding the feldspar aggregates in the feldspar layers, consist of elongated first order and some remaining original feldspar grains in a matrix of thin (5 micron) chlorite (Fig. 82). All of the feldspar grains have well developed undulatory extinction and subgrain formation. The aggregates of feldspar are often greater than 1cm long and consist of all three orders of recrystallized grains. The cores of the aggregates are made up of large original and first order grains with some second order grains at grain contacts and also at the margins and ends of the aggregate (Fig. 79). All of the grains in the aggregates have undulatory extinction and subgrain formation can be seen in all but the second order grains. In many places grains at the margins of the aggregates are becoming separated by fine chlorite.

#### STAGE V

The layering at this stage has increased in width up to 2-3cm. Feldspar is present in the chlorite rich layers as elongated single grains in a matrix of coarse grained chlorite. The feldspar rich layers are also mainly elongated single grains in a matrix of finer chlorite. The aggregates of feldspar are shorter than at the previous stage and a greater degree of grains are being separated from the aggregates by chlorite. Undulatory extinction, subgrain formation and recrystallization appear to be unchanged from that described for stage IV.



The effects of recrystallization on feldspar grain size show up clearly through changes in the R, L and W values, listed in Table 2, and also in histograms for feldspar grains shown in Figure 83. The values of L and W decrease from 111-68 microns at stage I to 41-14 microns at stage V. The histograms show more clearly the effect of first and second order recrystallization on the average feldspar grain size. In Figure 83B the presence of first order grains (42x28 microns) shows up as an increased number of grains with lengths of less than 50 microns, and widths less than 20 microns. In Figure 83C it is possible to recognize two separate populations of grain size, one with lengths up to 50 microns and widths up to 20 microns reflecting the new grains and another group with lengths of 50-150 microns and widths of 35-45 microns, reflecting the earliest unrecrystallized grains. The addition of an increased amount of second order recrystallization (16x10 microns) in stages IV and V shows up in Figure 83D-F, as an increase in grains with lengths less than 25 microns and widths less than 10-5 microns.

The microstructural observations provided in this section indicate that the production of a mylonite from gabbro has been accomplished by a dislocation creep mechanism, accompanied by dynamic recrystallization. The recrystallization occurred both by grain boundary bulging and also by subgrain rotation. The core and mantle texture of recrystallization (White 1976) was observed in feldspar aggregates but was destroyed by thin chlorite in the later



The river is (approximately) 100 m wide.

show up (Figure 1) and (Figure 2).

Figure 1 shows the river and the surrounding area.

Figure 2 shows the river and the surrounding area.

Figure 3 shows the river and the surrounding area.

Figure 4 shows the river and the surrounding area.

Figure 5 shows the river and the surrounding area.

Figure 6 shows the river and the surrounding area.

Figure 7 shows the river and the surrounding area.

Figure 8 shows the river and the surrounding area.

Figure 9 shows the river and the surrounding area.

Figure 10 shows the river and the surrounding area.

Figure 11 shows the river and the surrounding area.

Figure 12 shows the river and the surrounding area.

Figure 13 shows the river and the surrounding area.

Figure 14 shows the river and the surrounding area.

Figure 15 shows the river and the surrounding area.

Figure 16 shows the river and the surrounding area.

Figure 17 shows the river and the surrounding area.

Figure 18 shows the river and the surrounding area.

Figure 19 shows the river and the surrounding area.

Figure 20 shows the river and the surrounding area.

Figure 21 shows the river and the surrounding area.

Figure 22 shows the river and the surrounding area.

Figure 23 shows the river and the surrounding area.

Figure 24 shows the river and the surrounding area.

Figure 25 shows the river and the surrounding area.

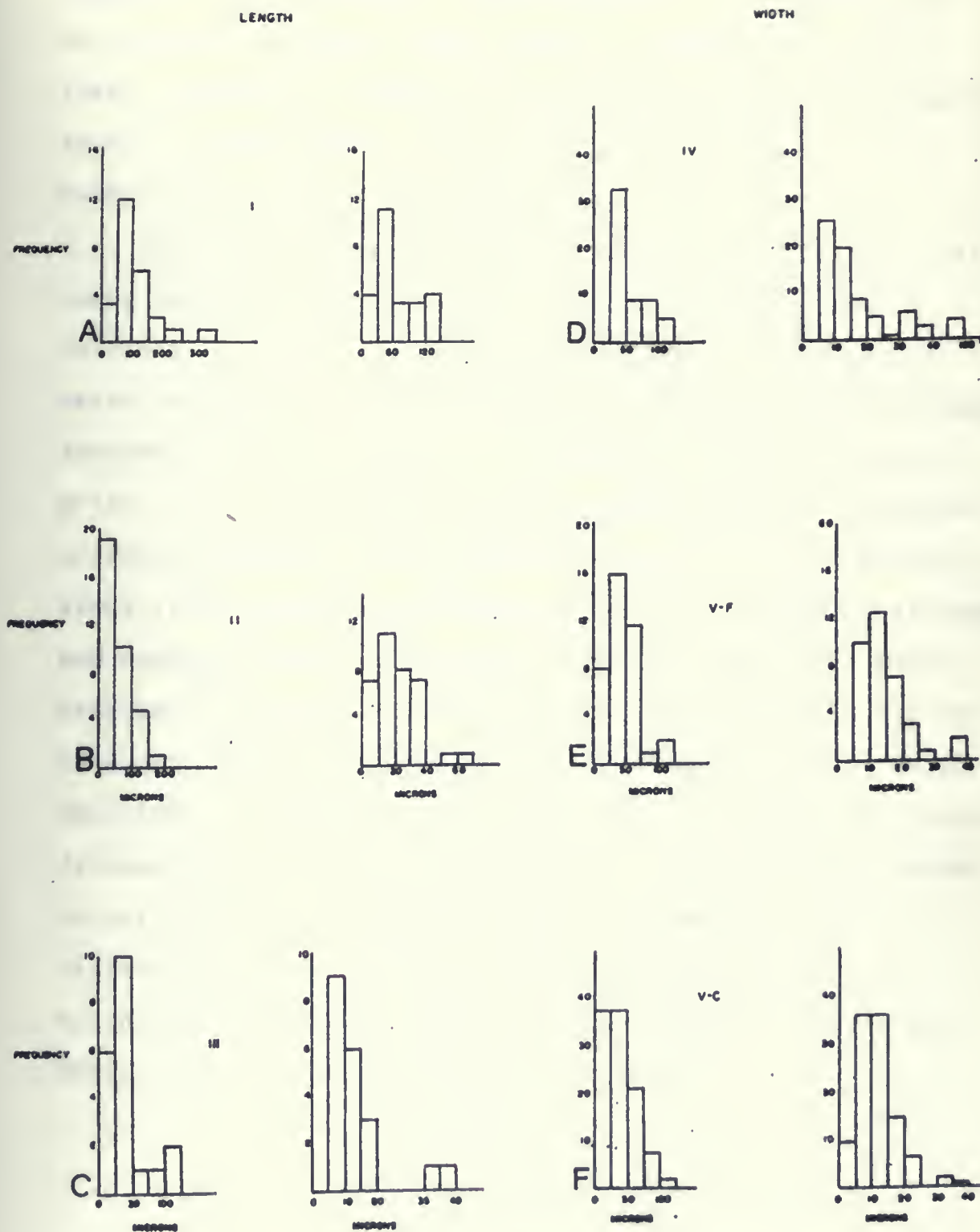


Fig. 83. Histograms of feldspar grain size at each stage of mylonitization.



Small, faint text at the bottom right, possibly a page number or reference.

stages of mylonitization. This mechanism of separation by chlorite may act to pin the ultimate recrystallized grain size. The grains of feldspar separated by chlorite appeared to be relatively strain free and a third order of recrystallization was not observed.

According to Gapais and White (1982) the development of shear bands - C' fabrics, occurs due to a change from dislocation creep to grain boundary sliding. Evidence of grain boundary sliding, within shear bands according to Gapais and White, is indicated by the presence of recrystallized grains with a rectangular or square shape and grain margins oriented parallel with the shear direction. In the present study it was difficult to determine if grain boundary sliding had occurred, as in most cases, well developed shear bands have been infilled by late carbonate. Where this is not the case, the shear bands are most often occupied by fine grained chlorite. In stage V where a crenulation cleavage is present, feldspar grains are oriented parallel to the crenulation but do not exhibit any excessive recrystallization. These differences may be related to the polymineralogy of the mylonite studied here, where as that studied by Gapais and White was a monomineralic quartz-mylonite.





## DISCUSSION

With the aid of underground workings and drilling, Pye (1952) and Horwood and Pye (1955), suggested that the rocks of the Geraldton area had been regionally folded into a series of east-west trending shallow plunging anticlines and synclines. They noted however, that Z shaped folds, north of the Bankfield-Tombill Fault were not compatible as parasitic folds to the larger scale structures interpreted. They suggested that these folds were related to steep thrusting on the Bankfield-Tombill Fault.

During the present study, no regional scale fold closures were observed and little evidence was seen suggesting regional anticlines and synclines. Instead, observations made during the present study suggest that all or most of the structures in the study area can be more easily explained in relationship to ductile simple shearing associated with the Bankfield-Tombill Fault.

Much of the evidence for Horwood and Pye's interpretation came from the attitude and younging direction suggested by graded greywacke units. As shown during the present study, the presence of simple shear fabrics suggest that even the apparently undeformed sediments may have been modified. The presence of structures related to simple shearing, observed during the present study, outline the Barton Bay Deformation Zone, a zone up to 5km wide which was included in the area interpreted by Horwood and Pye. Folding within the Barton Bay Deformation Zone is dominated by asymmetric Z shaped folds

With the aid of an electron microscope and the

10000000 and 10000000 (1955) (1955) (1955) (1955)

the electron microscope and the electron microscope

electron microscope and the electron microscope

They noted however that the electron microscope

Electron microscope and the electron microscope

to the electron microscope and the electron microscope

that the electron microscope and the electron microscope

Electron microscope and the electron microscope

During the first few days of the electron microscope

were observed and the electron microscope and the electron microscope

Electron microscope and the electron microscope

The electron microscope and the electron microscope

in the electron microscope and the electron microscope

to the electron microscope and the electron microscope

Electron microscope and the electron microscope

Electron microscope and the electron microscope

Electron microscope and the electron microscope

Electron microscope and the electron microscope

Electron microscope and the electron microscope

Electron microscope and the electron microscope

Electron microscope and the electron microscope

Electron microscope and the electron microscope

Electron microscope and the electron microscope

Electron microscope and the electron microscope

Electron microscope and the electron microscope

Electron microscope and the electron microscope

Electron microscope and the electron microscope

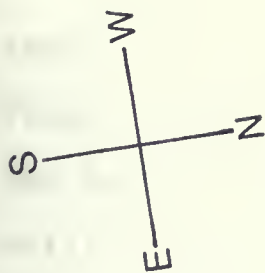
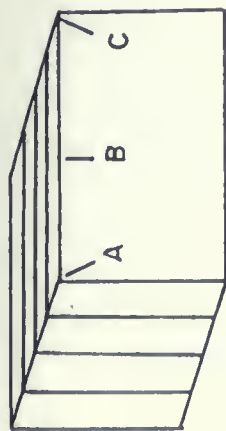
which plunge shallowly to the west. The presence of east-west trending subhorizontal to slightly east plunging slickensides and stretching lineations, suggest that these folds are related to slightly oblique strike slip movement along and parallel with the Bankfield-Tombill Fault (Fig. 84). The orientations of shear related fabrics, fold shape and kinematic indicators in the deformed conglomerate units indicate that the sense of movement along the fault was dextral.

The presence of deformed intrusives and varying fold axes orientations, suggest that the deformation associated with the movement along the fault was either continuous over a long period or reactivated many times. The presence of the gabbro mylonite within the fault zone and shear fabrics outside of the fault indicate that the major component of deformation was of a ductile nature.

The difference in intensity of folding and shearing between the areas north and south of the fault appears to be related to lithological differences. Iron formation, present only in the sediments north of the fault appears to act as a focus for intense folding. This effect may be due to ductility contrast between the iron formation and the surrounding greywacke. Pelitic layers of greywacke were also more common north of the fault and intense deformation was often observed within these layers. Pelitic layers and also Z folding was less common south of the fault. It could be suggested that the pelitic layers were also planes of strike







# BANKFIELD-TOMBILL FAULT

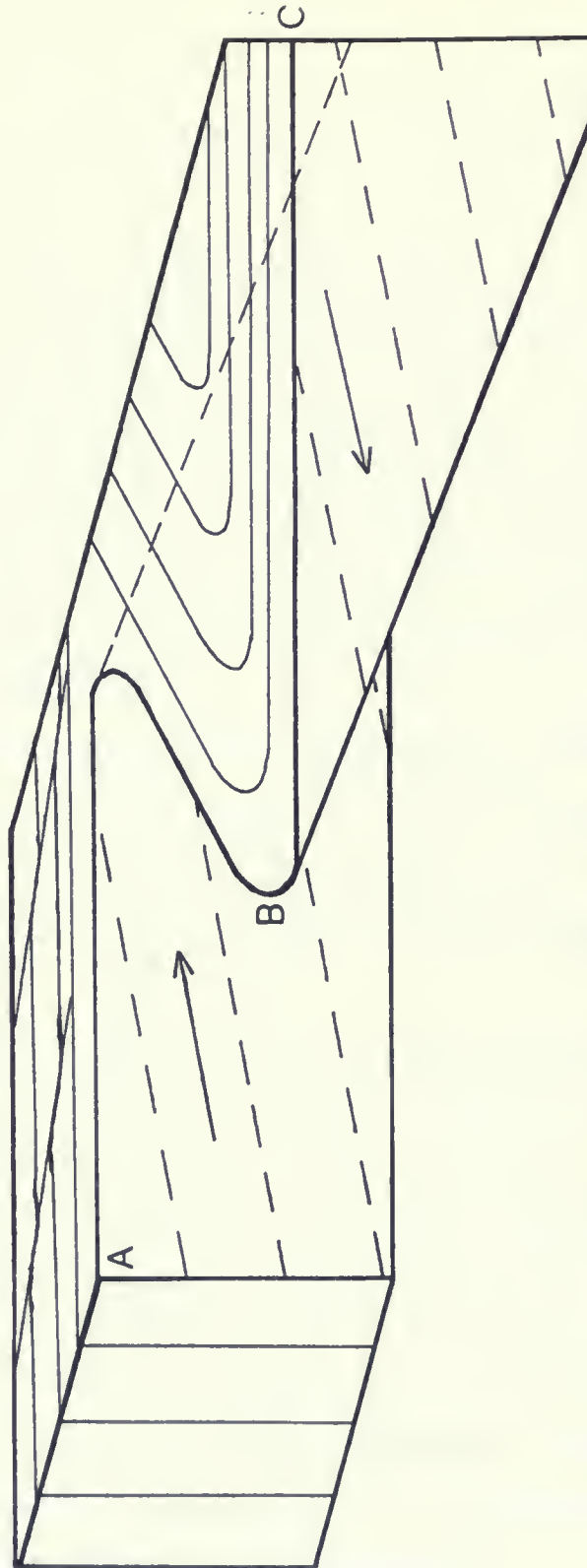


Fig. 84. Formation of Z folds due to oblique strike slip movement along the Bankfield-Tombill Fault. The arrows show the relative sense of displacement.



slip movement separate from, but parallel with the Bankfield-Tombill Fault.

A wide zone of gabbro mylonite within the fault zone indicates that the greatest degree of ductile deformation was focused within this zone. However it is difficult to assess the degree of deformation that may have occurred within the pelitic layers. The fine grain size necessary for ductile deformation was original in the pelitic layers whereas the mylonite has developed through grain size reduction of an originally coarse grained gabbro.

A sequence of structural events, suggested by the progressive deformation of the gabbro to an ultramylonite can also be applied to structures present outside of the fault.

1. The formation of an elongated mineral fabric, S in the gabbro.

The S fabric is reflected in the sediments by a preferred orientation of clasts.

2. The S fabric is rotated into shear planes which develop parallel with the shear zone boundary.

The C fabric forms in the sediments and any earlier planar or linear structures are rotated closer to parallel with the Bankfield-Tombill Fault.

3. The development of the C foliation increases to a mylonitic layering which is subsequently folded.

The development of folding in the sediments may have occurred at earlier stages due to the



A

indicated that the system of geologic mapping was  
developed within this area. However, it is also  
the degree of distortion that may have occurred  
within the area. The first step in the process  
was original in the geologic mapping of the  
system. It has developed through the years  
originally, and is now being used.

A system of geologic mapping was developed in the  
progressive development of the system in the  
also is applied to the geologic mapping of the  
1. The location of the system is shown in

to the system.

The system is shown in the system.

by a system of geologic mapping.

2. The system is shown in the system.

which geologic mapping is shown in the system.

The system is shown in the system.

which geologic mapping is shown in the system.

which geologic mapping is shown in the system.

3. The system is shown in the system.

which geologic mapping is shown in the system.

which

The system is shown in the system.

which geologic mapping is shown in the system.

original anisotropy of bedding. Several generations of folding may have occurred, each being rotated by continuous deformation.

4. In the mylonite the oblique C' fabric develops (possibly more than one set).

The C' fabric is not observed outside of the mylonite. However discrete shear planes develop parallel with the axial traces of some tight folds. These were not observed in the mylonite and may reflect axial planar cleavages which have rotated parallel to the shear direction becoming planes of displacement.

#### CONCLUSIONS

1. Structures within the Barton Bay Deformation Zone are related to ductile simple shearing along or parallel with the Bankfield-Tombill Fault.

2. Movement along the Bankfield-Tombill Fault was in a south over north, oblique strike slip fashion with a dextral sense of displacement.

3. Tuffs and tuff - breccias within the Barton Bay Deformation Zone are in many cases a gabbro mylonite.

4. The grain size of the original gabbro has been reduced by a combination of dislocation creep and dynamic recrystallization.

5. The most intensely deformed stage of the mylonite is



marked by two or more sets of a closely spaced C' fabric.





## REFERENCES

- Bell, T.H. 1978. Progressive deformation and reorientation of fold axes in a ductile mylonite zone: The Woodroffe Thrust. *Tectonophysics*, 44, pp.285-320.
- Bell, T.H. and Etheridge, M.A. 1973. Microstructures of mylonites and their descriptive terminology. *Lithos*, 6, pp.337-348.
- Berth, D., Choukroune, P. and Jegouzo, P. 1979a. Orthogneiss, mylonite and non coaxial deformation of granites: the example of the South Armorican Shear Zone. *J. Struct. Geol.* 1, 31-42.
- Berth, D., Choukroune, P. and Gapais, D. 1979b. Orientations preferentialles du quartz et orthogneissification progressive en regime cisailant. *Bull. Mineral.* 102, pp. 265-272.
- Berthe, D. and Brun, J.P. 1980. Evolution of folds during progressive shear in the South Armorican Shear Zone, France. *J. Struct. Geol.* 2, pp.127-133.
- Bruce, E.L. 1936. New developments in the Little Long Lac Area. *Ont. Dept. Mines.* 45, pt. 2, pp. 118-140.
- Burg, J.P., Iglesias, M., Laurent, Ph., Matte, Ph. and Ribeiro, A. 1981. Variscan intercontinental deformation: The Coimbra-Cordoba Shear Zone (SW Iberian Peninsula). *Tectonophysics* 78, pp. 161-177.
- Cobbold, P.R. and Quinquis, H. 1980. Development of sheath folds in shear regimes. *J. Struct. Geol.* 2, pp. 119-126.
- Dixon, J. and Williams, G. 1983. Reaction softening in mylonites from the Arnaboll thrust, Sutherland. *Scott. J. Geol.* 19, (2), pp. 157-168.
- Escher, A. and Watterson, J. 1974. Stretching fabrics, folds and crustal shortening. *Tectonophysics* 22, pp. 223-231.
- Fralick, P.W. and Barrett, T.J. 1983. The sedimentology of banded iron formation in the Beardmore-Geraldton greenstone belt: a preliminary appraisal. in *Summary of Field Work, 1983*, by the Ontario Geological Survey, edited by John Wood, Owen L. White, R.B. Barlow, and A.C. Colvine, Ontario Geological Survey, Miscellaneous Paper 116, 313p.
- Gapais, D. and White, S.H. 1982. Ductile shear bands in a naturally deformed quartzite. *Textures and Microstructures* 5, pp. 1-17.

Bill, W.H. 1950. *Journal of the American Water Resources Association*.  
Vol. 1, No. 1, pp. 1-10.

Bill, T.H. and Bill, W.H. 1950. *Journal of the American Water Resources Association*.  
Vol. 1, No. 1, pp. 11-20.

Bill, W.H. 1950. *Journal of the American Water Resources Association*.  
Vol. 1, No. 1, pp. 21-30.

Bill, W.H. 1950. *Journal of the American Water Resources Association*.  
Vol. 1, No. 1, pp. 31-40.

Bill, W.H. 1950. *Journal of the American Water Resources Association*.  
Vol. 1, No. 1, pp. 41-50.

Bill, W.H. 1950. *Journal of the American Water Resources Association*.  
Vol. 1, No. 1, pp. 51-60.

Bill, W.H. 1950. *Journal of the American Water Resources Association*.  
Vol. 1, No. 1, pp. 61-70.

Bill, W.H. 1950. *Journal of the American Water Resources Association*.  
Vol. 1, No. 1, pp. 71-80.

Bill, W.H. 1950. *Journal of the American Water Resources Association*.  
Vol. 1, No. 1, pp. 81-90.

Bill, W.H. 1950. *Journal of the American Water Resources Association*.  
Vol. 1, No. 1, pp. 91-100.

Bill, W.H. 1950. *Journal of the American Water Resources Association*.  
Vol. 1, No. 1, pp. 101-110.

Bill, W.H. 1950. *Journal of the American Water Resources Association*.  
Vol. 1, No. 1, pp. 111-120.

- Goetze, C. 1978. The mechanisms of creep in olivine. *Phil. Trans. R. Soc. Lond. A*, 288, pp.99-119.
- Guillope, M. and Poirier, J.P. 1979 Dynamic recrystallization during creep of single crystalline halite; An experimental study. *J. Geophys. Res.* 84, pp. 5557-5567.
- Hanmer, S.K. 1984. Tpotential use of planer and elliptical structures as indicators of strain regime and kinematics of tectonic flow; in *Current Research, Part B, Geological Survey of Canada, Paper 84-1B*, pp. 133-142.
- Hobbs, B.E., Means, W.D. and Williams, P.F. 1976. An outline of structural geology. John Wiley, New York. 571 pp.
- Horwood, H.C. and Pye, E.G. 1955. Geology of Ashmore Township, Little Long Lac Area, Thunder Bay District. in Ontario Department of Mines, Annual Report for 1951, 60, pt. 5, pp.105. Accompanied by Map 1951-2, scale 1 inch to 1000 feet.
- Jegouzo, P. 1980. The South Armorican Shear Zone. *J. Struct. Geol.* 2, pp.39-47.
- Lavigne, Jr. M.J. 1983. Gold deposits of the Geraldton Area. in Summary of Field Work, 1983, by the Ontario Geological Survey, edited by John Wood, Owen L. White, R.B. Barlow, and A.C. Colvine, Ontario Geological Survey, Miscellaneous Paper 116, 313 pp.
- Macdonald, A.J. 1982. The MacLeod-Cockshutt and Hard Rock Mines, Geraldton: Examples of an iron formation related gold deposit. in Summary of Field Work, 1982, by the Ontario Geological Survey, edited by John Wood, Owen L. White, R.B. Barlow, and A.C. Colvine, Ontario Geological Survey, Miscellaneous Paper 106, 235 pp.
- Macdonald, A.J. 1983. A re-appraisal of the Geraldton Gold Camp. in Summary of Field Work, by the Ontario Geological Survey, edited by John Wood, Owen L. White, R.B. Barlow and A.C. Colvine, Ontario Geological Survey, Miscellaneous Paper 116, 313 pp.
- Mackasey, W.O. 1976. Geology of Walters and Leduc Townships, District of Thunderbay. Ministry of Natural Resources Division of Mines Geoscience Report 149, 64 pp.
- Platt, J.P. 1979. Extensional crenulation cleavage. *J. Struct. Geol.* 1, pp.95.
- Platt, J.P. 1984. Secondary cleavages in ductile shear zones. *J. Struct. Geol.* 6, pp.439-442.
- Platt, J.P. and Vissers, R.L.M. 1980. Extensional structures in anisotropic rocks. *J. Struct. Geol.* 2, pp.397-410.



October 10, 1977: In accordance with the  
order of the Board of Directors, the following

Director, Mr. [Name] has been elected to the  
Board of Directors for the term ending 1980.  
The Board of Directors has also elected Mr. [Name]  
as Vice President for the term ending 1980.

Director, Mr. [Name] has been elected to the  
Board of Directors for the term ending 1980.  
The Board of Directors has also elected Mr. [Name]  
as Vice President for the term ending 1980.

Director, Mr. [Name] has been elected to the  
Board of Directors for the term ending 1980.  
The Board of Directors has also elected Mr. [Name]  
as Vice President for the term ending 1980.

Director, Mr. [Name] has been elected to the  
Board of Directors for the term ending 1980.  
The Board of Directors has also elected Mr. [Name]  
as Vice President for the term ending 1980.

Director, Mr. [Name] has been elected to the  
Board of Directors for the term ending 1980.  
The Board of Directors has also elected Mr. [Name]  
as Vice President for the term ending 1980.

Director, Mr. [Name] has been elected to the  
Board of Directors for the term ending 1980.  
The Board of Directors has also elected Mr. [Name]  
as Vice President for the term ending 1980.

Director, Mr. [Name] has been elected to the  
Board of Directors for the term ending 1980.  
The Board of Directors has also elected Mr. [Name]  
as Vice President for the term ending 1980.

Director, Mr. [Name] has been elected to the  
Board of Directors for the term ending 1980.  
The Board of Directors has also elected Mr. [Name]  
as Vice President for the term ending 1980.

Director, Mr. [Name] has been elected to the  
Board of Directors for the term ending 1980.  
The Board of Directors has also elected Mr. [Name]  
as Vice President for the term ending 1980.

Director, Mr. [Name] has been elected to the  
Board of Directors for the term ending 1980.  
The Board of Directors has also elected Mr. [Name]  
as Vice President for the term ending 1980.

Director, Mr. [Name] has been elected to the  
Board of Directors for the term ending 1980.  
The Board of Directors has also elected Mr. [Name]  
as Vice President for the term ending 1980.

Director, Mr. [Name] has been elected to the  
Board of Directors for the term ending 1980.  
The Board of Directors has also elected Mr. [Name]  
as Vice President for the term ending 1980.

- Ponce De Leon, M.I. and Choukroune, P. 1980. Shear zones in the Iberian arc. *J. Struct. Geol.* 2, pp. 63-68.
- Pye, E.G. 1952. Geology of Errington Township, Little Long Lac Area, Thunder Bay District; in Ontario Department of Mines, Annual Report for 1951, 60, pt. 6, 140 pp. Accompanied by Map 1951-7, scale 1 inch to 1000 feet.
- Ramsay, J.G. and Graham, R. 1970. Strain variation in shear belts. *Can. J. Earth Sci.* 7, pp. 786-813.
- Ramsay, J.G. 1980. Shear zone geometry: a review. *J. Struct. Geol.* 2, pp. 83-100.
- Simpson, C. 1984. Borrego Springs-Santa Rosa mylonite zone: A late Cretaceous west-directed thrust in southern California. *Geology* 12, pp. 8-11.
- Simpson, C. and Schmid, S.M. 1983. An evaluation of criteria to deduce the sense of movement in sheared rocks. *Bull. Geol. Soc. Amer.* 95, pp. 1281-1288.
- Soula, J.C. and Bessiere, G. 1980. Sinistral horizontal shearing as a dominant process of deformation in the Alpine Pyrenees. *J. Struct. Geol.* 2, pp. 69-74.
- Turner, F.J. 1968. *Metamorphic Petrology*. McGraw-Hill Book Co., N.Y., 321 pp.
- Vernon, R.H., Williams, V.A. and D'Arcy, W.F. 1982. Grain-size reduction and foliation development in a deformed granitoid batholith. *Tectonophysics* 92, pp. 123-145.
- Weljermars, R. and Rondeel, H.E. 1984. Shear band foliation as an indicator of shear: Field observations in central Spain. *Geology* 12, pp. 603-606.
- White, S. 1976. The effects of strain on the microstructures, fabrics and deformation mechanisms in quartzites. *Phil. Trans. R. soc. lond. A.* 283, pp. 69-86.
- White, S.H., Burrows, S.E., Carreras, J. Shaw, N.D. and Humphreys, F.J. 1980. On mylonites in ductile shear zones. *J. Struct. Geol.* 2, pp. 175-188.
- Wise, D.U., Dunn, D.E., Engelder, J.T., Geiser, P.A., Hatcher, R.D., Kish, S.A., Odom, A.L. and Schamel, S. 1984. Fault related rocks: Suggestions for terminology. *Geology* 12, pp. 391-394.



## APPENDIX I

### Histograms and Statistics for R, L and W



## APPENDIX I

Histograms and Statistics for P. L and W

## APPENDIX I

Histograms have been produced and printed by computer for the length, width and axial ratio of minerals at each stage of mylonitization. The base of each histogram for length and width is in microns.

The number of measurements made for each mineral at each stage and the statistical parameters calculated for each set of data is provided in a tabular form. The mean and standard deviation listed in these tables are in micron units. Stage V has been subdivided into feldspar rich layers-V-F and chlorite rich layers-V-C.

[illegible]

THE UNIVERSITY OF CHICAGO LIBRARY

1. *Mathematics* (1991) 19, 103–110.

100-100000

## FELDSPAR GRAINS-STATISTICS

## I VARIABLE RATIO

MEAN	1.786	STD ERROR	0.122	STD DEV	0.611
VARIANCE	0.774	KURTOSIS	0.481	SKENNESS	1.148
RANGE	2.160	MINIMUM	1.090	MAXIMUM	3.250
SUM	44.650				

VALID OBSERVATIONS - 25

MISSING OBSERVATIONS - 0

## VARIABLE LENGTH

MEAN	111.000	STD ERROR	13.288	STD DEV	66.442
VARIANCE	4414.583	KURTOSIS	2.862	SKENNESS	1.332
RANGE	290.000	MINIMUM	30.000	MAXIMUM	320.000
SUM	2775.000				

VALID OBSERVATIONS - 25

MISSING OBSERVATIONS - 0

## VARIABLE WIDTH

MEAN	68.000	STD ERROR	8.026	STD DEV	40.130
VARIANCE	1610.417	KURTOSIS	-0.494	SKENNESS	0.676
RANGE	140.000	MINIMUM	10.000	MAXIMUM	150.000
SUM	1700.000				

VALID OBSERVATIONS - 25

MISSING OBSERVATIONS - 0

## II VARIABLE RATIO

MEAN	3.179	STD ERROR	0.254	STD DEV	1.500
VARIANCE	2.231	KURTOSIS	0.521	SKENNESS	0.847
RANGE	6.200	MINIMUM	1.000	MAXIMUM	7.200
SUM	111.260				

VALID OBSERVATIONS - 35

MISSING OBSERVATIONS - 0

## VARIABLE LENGTH

MEAN	65.286	STD ERROR	6.790	STD DEV	40.169
VARIANCE	1613.319	KURTOSIS	0.739	SKENNESS	1.113
RANGE	163.500	MINIMUM	17.500	MAXIMUM	180.000
SUM	2285.000				

VALID OBSERVATIONS - 35

MISSING OBSERVATIONS - 0

## VARIABLE WIDTH

MEAN	23.214	STD ERROR	2.470	STD DEV	14.610
VARIANCE	213.445	KURTOSIS	2.387	SKENNESS	1.365
RANGE	65.000	MINIMUM	5.000	MAXIMUM	70.000
SUM	812.500				

VALID OBSERVATIONS - 35

MISSING OBSERVATIONS - 0

## III VARIABLE RATIO

MEAN	2.961	STD ERROR	0.332	STD DEV	1.483
VARIANCE	2.201	KURTOSIS	-0.700	SKENNESS	0.543
RANGE	5.000	MINIMUM	1.000	MAXIMUM	6.000
SUM	59.210				

VALID OBSERVATIONS - 20

MISSING OBSERVATIONS - 0

## VARIABLE LENGTH

MEAN	43.625	STD ERROR	7.728	STD DEV	34.560
VARIANCE	1194.391	KURTOSIS	4.491	SKENNESS	2.133
RANGE	137.500	MINIMUM	12.500	MAXIMUM	150.000
SUM	872.500				

VALID OBSERVATIONS - 20

MISSING OBSERVATIONS - 0

## VARIABLE WIDTH

MEAN	15.500	STD ERROR	2.101	STD DEV	7.734
VARIANCE	95.132	KURTOSIS	4.550	SKENNESS	2.120
RANGE	37.500	MINIMUM	7.500	MAXIMUM	45.000
SUM	310.000				

VALID OBSERVATIONS - 20

MISSING OBSERVATIONS - 0



1. The first of these is the fact that the American Medical Association is a non-profit-making organization. It is not a corporation, and its assets are held in trust for the benefit of the medical profession. This means that the Association is not subject to the same financial pressures as a for-profit corporation, and it is able to devote its resources to the advancement of the medical profession without the distraction of profit-making.

2. The second of these is the fact that the American Medical Association is a representative organization. It is composed of representatives of the medical profession from all parts of the United States, and it is able to speak for the entire profession. This means that the Association is able to bring to the attention of the public the needs and interests of the medical profession as a whole, and it is able to advocate for the profession in a way that is representative of the entire profession.

3. The third of these is the fact that the American Medical Association is a professional organization. It is composed of medical professionals, and it is able to speak for the profession in a way that is based on professional standards and ethics. This means that the Association is able to advocate for the profession in a way that is based on the highest standards of medical practice, and it is able to ensure that the public is protected by the highest standards of medical care.

4. The fourth of these is the fact that the American Medical Association is a voluntary organization. It is composed of medical professionals who have chosen to join the Association, and it is able to speak for the profession in a way that is based on the interests of its members. This means that the Association is able to advocate for the profession in a way that is based on the interests of the medical professionals who are most directly affected by the issues it is addressing.

5. The fifth of these is the fact that the American Medical Association is a national organization. It is composed of medical professionals from all parts of the United States, and it is able to speak for the profession in a way that is representative of the entire profession. This means that the Association is able to bring to the attention of the public the needs and interests of the medical profession as a whole, and it is able to advocate for the profession in a way that is representative of the entire profession.

6. The sixth of these is the fact that the American Medical Association is a professional organization. It is composed of medical professionals, and it is able to speak for the profession in a way that is based on professional standards and ethics. This means that the Association is able to advocate for the profession in a way that is based on the highest standards of medical practice, and it is able to ensure that the public is protected by the highest standards of medical care.

7. The seventh of these is the fact that the American Medical Association is a voluntary organization. It is composed of medical professionals who have chosen to join the Association, and it is able to speak for the profession in a way that is based on the interests of its members. This means that the Association is able to advocate for the profession in a way that is based on the interests of the medical professionals who are most directly affected by the issues it is addressing.

8. The eighth of these is the fact that the American Medical Association is a national organization. It is composed of medical professionals from all parts of the United States, and it is able to speak for the profession in a way that is representative of the entire profession. This means that the Association is able to bring to the attention of the public the needs and interests of the medical profession as a whole, and it is able to advocate for the profession in a way that is representative of the entire profession.

9. The ninth of these is the fact that the American Medical Association is a professional organization. It is composed of medical professionals, and it is able to speak for the profession in a way that is based on professional standards and ethics. This means that the Association is able to advocate for the profession in a way that is based on the highest standards of medical practice, and it is able to ensure that the public is protected by the highest standards of medical care.

IV

## FELDSPAR GRAINS - STATISTICS

## VARIABLE RATIO

MEAN	3.009	STD ERROR	0.205	STD DEV	1.762
VARIANCE	3.104	KURTOSIS	4.017	SKEWNESS	1.890
RANGE	9.000	MINIMUM	1.000	MAXIMUM	10.000
SUM	222.630				

VALID OBSERVATIONS -	74	MISSING OBSERVATIONS -	0
----------------------	----	------------------------	---

## VARIABLE LENGTH

MEAN	48.796	STD ERROR	3.886	STD DEV	33.428
VARIANCE	1117.448	KURTOSIS	2.400	SKEWNESS	1.494
RANGE	170.000	MINIMUM	10.000	MAXIMUM	180.000
SUM	3610.900				

VALID OBSERVATIONS -	74	MISSING OBSERVATIONS -	0
----------------------	----	------------------------	---

## VARIABLE WIDTH

MEAN	18.223	STD ERROR	1.499	STD DEV	12.893
VARIANCE	166.241	KURTOSIS	2.185	SKEWNESS	1.604
RANGE	59.500	MINIMUM	0.500	MAXIMUM	60.000
SUM	1340.500				

VALID OBSERVATIONS -	74	MISSING OBSERVATIONS -	0
----------------------	----	------------------------	---

V-F

## VARIABLE RATIO

MEAN	3.468	STD ERROR	0.211	STD DEV	1.304
VARIANCE	1.700	KURTOSIS	0.311	SKEWNESS	0.727
RANGE	5.670	MINIMUM	1.000	MAXIMUM	6.670
SUM	131.770				

VALID OBSERVATIONS -	38	MISSING OBSERVATIONS -	0
----------------------	----	------------------------	---

## VARIABLE LENGTH

MEAN	51.842	STD ERROR	4.933	STD DEV	30.412
VARIANCE	924.893	KURTOSIS	7.729	SKEWNESS	2.263
RANGE	160.000	MINIMUM	20.000	MAXIMUM	180.000
SUM	1970.000				

VALID OBSERVATIONS -	38	MISSING OBSERVATIONS -	0
----------------------	----	------------------------	---

## VARIABLE WIDTH

MEAN	16.118	STD ERROR	1.319	STD DEV	8.131
VARIANCE	66.114	KURTOSIS	2.305	SKEWNESS	1.377
RANGE	35.000	MINIMUM	5.000	MAXIMUM	40.000
SUM	612.500				

VALID OBSERVATIONS -	38	MISSING OBSERVATIONS -	0
----------------------	----	------------------------	---

V-C

## VARIABLE RATIO

MEAN	3.390	STD ERROR	0.213	STD DEV	2.177
VARIANCE	4.740	KURTOSIS	3.536	SKEWNESS	1.795
RANGE	11.000	MINIMUM	1.000	MAXIMUM	12.000
SUM	352.570				

VALID OBSERVATIONS -	104	MISSING OBSERVATIONS -	0
----------------------	-----	------------------------	---

## VARIABLE LENGTH

MEAN	40.913	STD ERROR	2.376	STD DEV	24.226
VARIANCE	586.900	KURTOSIS	0.996	SKEWNESS	1.143
RANGE	115.000	MINIMUM	10.000	MAXIMUM	125.000
SUM	4255.000				

VALID OBSERVATIONS -	104	MISSING OBSERVATIONS -	0
----------------------	-----	------------------------	---

## VARIABLE WIDTH

MEAN	13.486	STD ERROR	0.642	STD DEV	6.342
VARIANCE	42.891	KURTOSIS	3.189	SKEWNESS	1.349
RANGE	37.500	MINIMUM	2.500	MAXIMUM	40.000
SUM	1402.500				

VALID OBSERVATIONS -	104	MISSING OBSERVATIONS -	0
----------------------	-----	------------------------	---



## FELDSPAR GRAINS - RATIO

```

I AAAAAA ( 12)
I 1 THRU 1.5
I AAAAAA ( 7)
I 1.5 THRU 2
I AAAAAA ( 3)
I 2 THRU 2.5
I AAAAAA ( 2)
I 2.5 THRU 3
I AAAAAA ( 1)
I 3 THRU 3.5
I .....1.....12.....16.....1
I .....4.....8.....12.....16.....1
0 FREQUENCY

```

—

```

I AAAAAA ( 1)
I 0 THRU 1
I AAAAAA ( 4)
I 1 THRU 1.5
I AAAAAA ( 3)
I 1.5 THRU 2
I AAAAAA ( 4)
I 2.5 THRU 3
I AAAAAA ( 2)
I 3 THRU 3.5
I AAAAAA ( 2)
I 3.5 THRU 4
I AAAAAA ( 4)
I 4 THRU HIGHEST
I .....1.....1.....1.....1.....1
I .....2.....4.....6.....8.....10
0 FREQUENCY

```

==

```

I AAAAAA ( 1)
I 0 THRU 1
I AAAAAA ( 4)
I 1 THRU 1.5
I AAAAAA ( 3)
I 2 THRU 2.5
I AAAAAA ( 7)
I 2.5 THRU 3
I AAAAAA ( 10)
I 3 THRU 3.5
I AAAAAA ( 5)
I 3.5 THRU 4
I AAAAAA ( 8)
I 4 THRU HIGHEST
I .....1.....1.....1.....1.....1
I .....2.....4.....6.....8.....10
0 FREQUENCY

```

V-F

```

I AAAAAA ( 1)
I 0 THRU 1
I AAAAAA ( 3)
I 1 THRU 1.5
I AAAAAA ( 4)
I 1.5 THRU 2
I AAAAAA ( 6)
I 2 THRU 2.5
I AAAAAA ( 5)
I 2.5 THRU 3
I AAAAAA ( 4)
I 3 THRU 3.5
I AAAAAA ( 4)
I 3.5 THRU 4
I AAAAAA ( 8)
I 4 THRU HIGHEST
I .....1.....1.....1.....1.....1
I .....2.....4.....6.....8.....16
0 FREQUENCY

```

==

```

I AAAAAA ( 1)
I 0 THRU 1
I AAAAAA ( 11)
I 1 THRU 1.5
I AAAAAA ( 13)
I 1.5 THRU 2
I AAAAAA ( 11)
I 2 THRU 2.5
I AAAAAA ( 15)
I 2.5 THRU 3
I AAAAAA ( 9)
I 3 THRU 3.5
I AAAAAA ( 3)
I 3.5 THRU 4
I AAAAAA ( 11)
I 4 THRU HIGHEST
I .....1.....1.....1.....1.....1
I .....4.....8.....12.....16.....20
0 FREQUENCY

```

IV

```

I AAAAAA ( 4)
I 0 THRU 1
I AAAAAA ( 12)
I 1 THRU 1.5
I AAAAAA ( 17)
I 1.5 THRU 2
I AAAAAA ( 13)
I 2 THRU 2.5
I AAAAAA ( 16)
I 2.5 THRU 3
I AAAAAA ( 5)
I 3 THRU 3.5
I AAAAAA ( 12)
I 3.5 THRU 4
I AAAAAA ( 25)
I 4 THRU HIGHEST
I .....1.....1.....1.....1.....1
I .....10.....20.....30.....40.....50
0 FREQUENCY

```

V-C



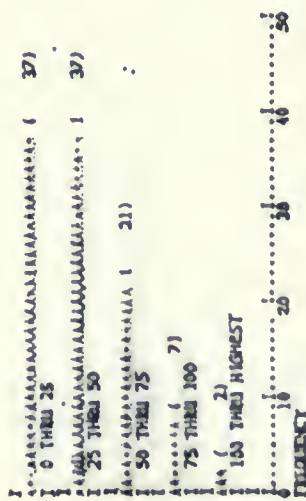


# FELDSPAR GRAINS- LENGTH

III



V-C



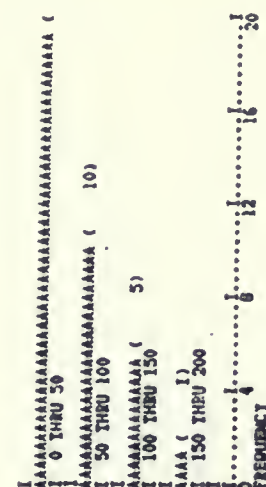
IV



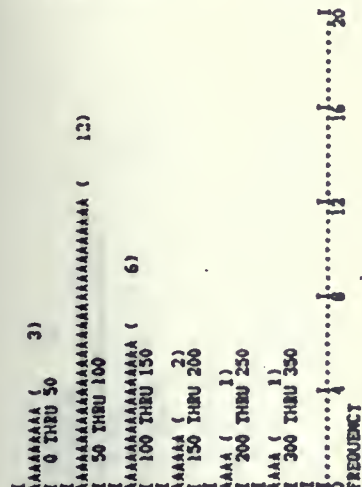
II



=

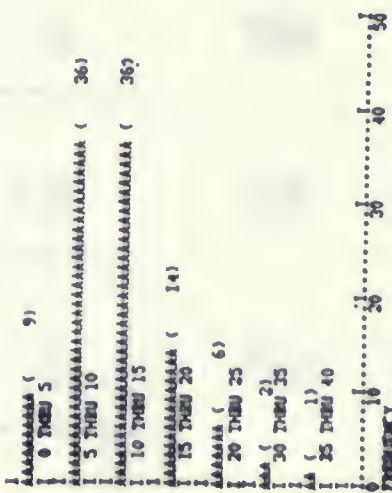
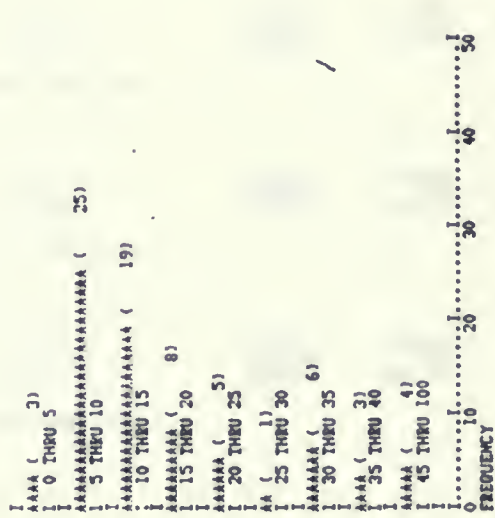
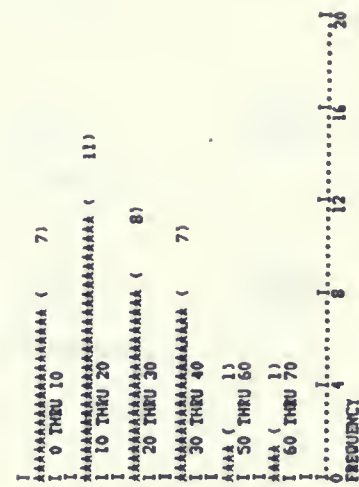
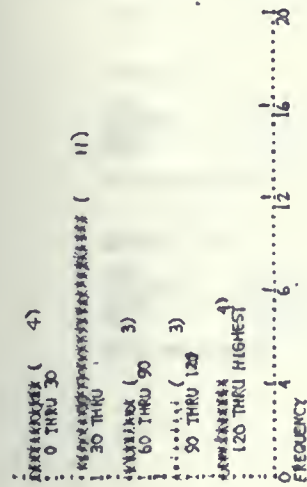


-





# FEDSPAR GRAINS- WIDTH







# FELDSPAR AGG. - STATISTICS

143

## II VARIABLE RATIO

MEAN	5.866	STD ERROR	0.531	STD DEV	3.188
VARIANCE	10.165	KURTOSIS	7.279	SKEWNESS	1.925
RANGE	17.860	MINIMUM	1.140	MAXIMUM	19.000
SUM	211.170				

VALID OBSERVATIONS - 36 MISSING OBSERVATIONS - 0

## VARIABLE LENGTH

MEAN	326.389	STD ERROR	70.455	STD DEV	470.730
VARIANCE	221586.587	KURTOSIS	24.917	SKEWNESS	4.714
RANGE	2785.000	MINIMUM	65.000	MAXIMUM	2850.000
SUM	11750.000				

VALID OBSERVATIONS - 36 MISSING OBSERVATIONS - 0

## VARIABLE WIDTH

MEAN	66.806	STD ERROR	16.539	STD DEV	99.232
VARIANCE	9847.004	KURTOSIS	25.172	SKEWNESS	4.753
RANGE	590.000	MINIMUM	10.000	MAXIMUM	600.000
SUM	2405.000				

VALID OBSERVATIONS - 36 MISSING OBSERVATIONS - 0

## III VARIABLE RATIO

MEAN	5.862	STD ERROR	0.658	STD DEV	5.267
VARIANCE	27.742	KURTOSIS	12.374	SKEWNESS	3.147
RANGE	31.660	MINIMUM	1.670	MAXIMUM	33.330
SUM	375.160				

VALID OBSERVATIONS - 64 MISSING OBSERVATIONS - 0

## VARIABLE LENGTH

MEAN	545.938	STD ERROR	104.175	STD DEV	833.397
VARIANCE	694550.694	KURTOSIS	19.692	SKEWNESS	3.860
RANGE	5475.000	MINIMUM	25.000	MAXIMUM	5500.000
SUM	34940.000				

VALID OBSERVATIONS - 64 MISSING OBSERVATIONS - 0

## VARIABLE WIDTH

MEAN	90.859	STD ERROR	12.859	STD DEV	102.870
VARIANCE	10582.186	KURTOSIS	8.967	SKEWNESS	2.635
RANGE	590.000	MINIMUM	10.000	MAXIMUM	600.000
SUM	5815.000				

VALID OBSERVATIONS - 64 MISSING OBSERVATIONS - 0

## IV VARIABLE RATIO

MEAN	4.834	STD ERROR	0.418	STD DEV	2.955
VARIANCE	8.729	KURTOSIS	3.422	SKEWNESS	1.605
RANGE	14.750	MINIMUM	1.250	MAXIMUM	16.000
SUM	241.710				

VALID OBSERVATIONS - 50 MISSING OBSERVATIONS - 0

## VARIABLE LENGTH

MEAN	166.100	STD ERROR	34.252	STD DEV	242.197
VARIANCE	58659.480	KURTOSIS	11.505	SKEWNESS	3.284
RANGE	1235.000	MINIMUM	20.000	MAXIMUM	1255.000
SUM	8305.000				

VALID OBSERVATIONS - 50 MISSING OBSERVATIONS - 0

## VARIABLE WIDTH

MEAN	33.150	STD ERROR	4.517	STD DEV	31.938
VARIANCE	1030.043	KURTOSIS	3.014	SKEWNESS	1.041
RANGE	140.000	MINIMUM	5.000	MAXIMUM	145.000
SUM	1657.500				

VALID OBSERVATIONS - 50 MISSING OBSERVATIONS - 0



# FELDSPAR AGG. - STATISTICS

144

V-F.

## VARIABLE RATIO

MEAN	7.211	STD ERROR	1.021	STD DEV	4.690
VARIANCE	21.904	KURTOSIS	4.863	SKEWNESS	1.844
RANGE	20.500	MINIMUM	2.000	MAXIMUM	22.500
SUM	151.430				

VALID OBSERVATIONS - 21

MISSING OBSERVATIONS - 0

## VARIABLE LENGTH

MEAN	508.810	STD ERROR	114.542	STD DEV	524.897
VARIANCE	275517.262	KURTOSIS	5.328	SKEWNESS	2.140
RANGE	2180.000	MINIMUM	70.000	MAXIMUM	2250.000
SUM	10685.000				

VALID OBSERVATIONS - 21

MISSING OBSERVATIONS - 0

## VARIABLE WIDTH

MEAN	73.690	STD ERROR	12.680	STD DEV	58.109
VARIANCE	3376.637	KURTOSIS	0.523	SKEWNESS	0.996
RANGE	207.500	MINIMUM	12.500	MAXIMUM	220.000
SUM	1547.500				

VALID OBSERVATIONS - 21

MISSING OBSERVATIONS - 0

V-C

## VARIABLE RATIO

MEAN	8.762	STD ERROR	3.084	STD DEV	7.554
VARIANCE	57.068	KURTOSIS	1.914	SKEWNESS	1.545
RANGE	19.500	MINIMUM	3.000	MAXIMUM	22.500
SUM	52.570				

VALID OBSERVATIONS - 6

MISSING OBSERVATIONS - 0

## VARIABLE LENGTH

MEAN	338.000	STD ERROR	137.241	STD DEV	336.170
VARIANCE	113010.000	KURTOSIS	5.054	SKEWNESS	2.196
RANGE	908.000	MINIMUM	100.000	MAXIMUM	1008.000
SUM	2028.000				

VALID OBSERVATIONS - 6

MISSING OBSERVATIONS - 0

## VARIABLE WIDTH

MEAN	55.000	STD ERROR	22.286	STD DEV	54.589
VARIANCE	2980.000	KURTOSIS	3.782	SKEWNESS	1.867
RANGE	150.000	MINIMUM	10.000	MAXIMUM	160.000
SUM	330.000				

VALID OBSERVATIONS - 6

MISSING OBSERVATIONS - 0









## FELDSPAR AGG. - LENGTH

[illegible][illegible]

I	AAAAA ( 1 )	
I	50 THRU 100	1
I	AAAAA ( 1 )	
I	100 THRU 200	1
I	AAAAA ( 2 )	
I	200 THRU 300	1
I	AAAAA ( 1 )	
I	300 THRU 400	1
I	AAAAA ( 1 )	
I	1000 THRU HIGHEST	1
I		2
I		4
I		6
I		8
I		10

V-C

IV

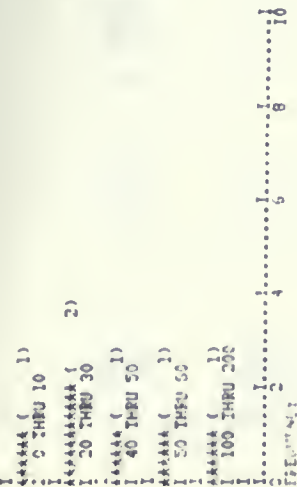
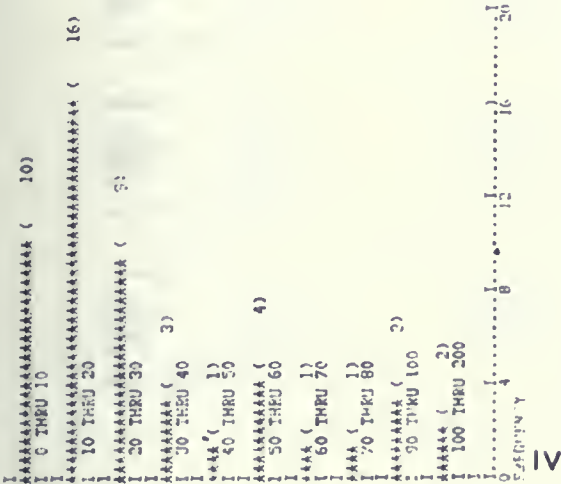
[illegible][illegible]

V-F





FELDSPAR AGG. WIDTH



V-C

V-F



## ACTINOLITE GRAINS - STATISTICS

## I VARIABLE RATIO

MEAN	3.152	STD ERROR	0.279	STD DEV	1.672
VARIANCE	2.795	KURTOSIS	0.767	SKEWNESS	1.060
RANGE	6.780	MINIMUM	1.220	MAXIMUM	8.000
SUM	113.460				

VALID OBSERVATIONS - 36

MISSING OBSERVATIONS - 0

## VARIABLE LENGTH

MEAN	707.639	STD ERROR	113.088	STD DEV	678.526
VARIANCE	460397.837	KURTOSIS	1.385	SKEWNESS	1.481
RANGE	2540.000	MINIMUM	60.000	MAXIMUM	2600.000
SUM	25475.000				

VALID OBSERVATIONS - 36

MISSING OBSERVATIONS - 0

## VARIABLE WIDTH

MEAN	215.694	STD ERROR	24.707	STD DEV	148.243
VARIANCE	21975.933	KURTOSIS	-0.306	SKEWNESS	0.726
RANGE	530.000	MINIMUM	20.000	MAXIMUM	550.000
SUM	7765.000				

VALID OBSERVATIONS - 36

MISSING OBSERVATIONS - 0

## II VARIABLE RATIO

MEAN	5.416	STD ERROR	0.405	STD DEV	3.924
VARIANCE	15.401	KURTOSIS	7.831	SKEWNESS	2.274
RANGE	25.000	MINIMUM	1.000	MAXIMUM	26.000
SUM	505.070				

VALID OBSERVATIONS - 94

MISSING OBSERVATIONS - 0

## VARIABLE LENGTH

MEAN	400.266	STD ERROR	34.230	STD DEV	231.877
VARIANCE	110142.133	KURTOSIS	2.778	SKEWNESS	1.651
RANGE	1525.000	MINIMUM	35.000	MAXIMUM	1560.000
SUM	37625.000				

VALID OBSERVATIONS - 94

MISSING OBSERVATIONS - 0

## VARIABLE WIDTH

MEAN	92.617	STD ERROR	8.729	STD DEV	84.628
VARIANCE	7161.906	KURTOSIS	9.430	SKEWNESS	2.430
RANGE	550.000	MINIMUM	10.000	MAXIMUM	560.000
SUM	8706.000				

VALID OBSERVATIONS - 94

MISSING OBSERVATIONS - 0

## V-C VARIABLE RATIO

MEAN	0.188	STD ERROR	0.688	STD DEV	5.544
VARIANCE	30.735	KURTOSIS	1.469	SKEWNESS	1.351
RANGE	25.800	MINIMUM	0.200	MAXIMUM	26.000
SUM	532.190				

VALID OBSERVATIONS - 65

MISSING OBSERVATIONS - 0

## VARIABLE LENGTH

MEAN	97.962	STD ERROR	6.843	STD DEV	55.172
VARIANCE	3043.924	KURTOSIS	0.954	SKEWNESS	1.043
RANGE	255.000	MINIMUM	25.000	MAXIMUM	280.000
SUM	6367.500				

VALID OBSERVATIONS - 65

MISSING OBSERVATIONS - 0

## VARIABLES WIDTH

MEAN	14.185	STD ERROR	1.135	STD DEV	9.153
VARIANCE	83.778	KURTOSIS	0.824	SKEWNESS	3.377
RANGE	55.000	MINIMUM	5.000	MAXIMUM	60.000
SUM	922.000				

VALID OBSERVATIONS - 65

MISSING OBSERVATIONS - 0

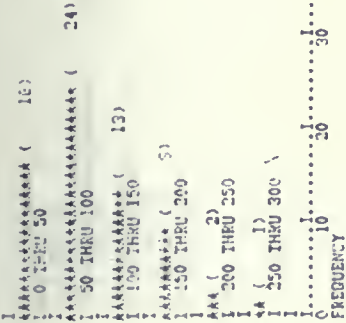




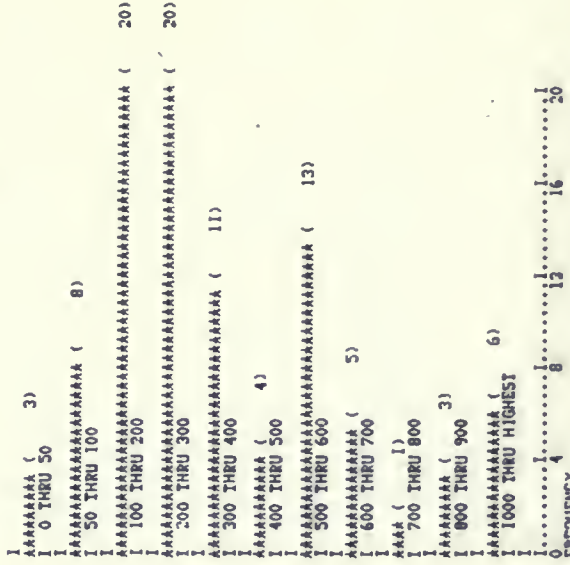
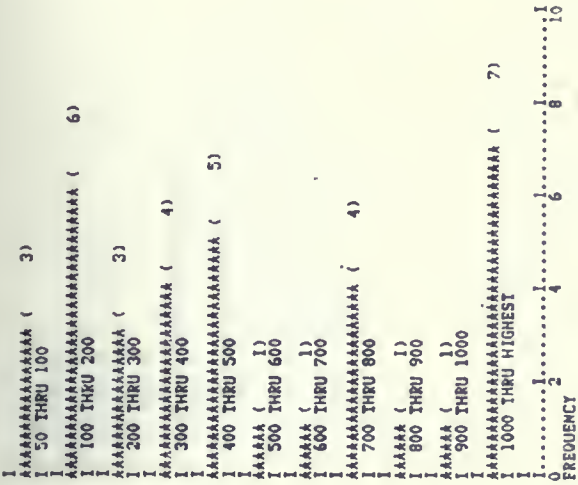




ACTINOLITE GRAINS - LENGTH



V-C

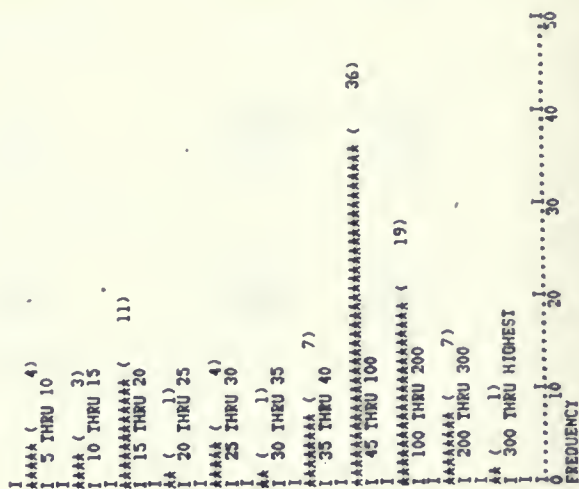






# ACTINOLITE GRAINS - WIDTH

151





## ACTINOLITE AGG.-STATISTICS

## II VARIABLE RATIO

MEAN	8.126	STD ERROR	1.027	STD DEV	4.593
VARIANCE	21.095	KURTOSIS	0.734	SKEWNESS	0.949
RANGE	17.100	MINIMUM	2.900	MAXIMUM	20.000
SUM	162.520				

VALID OBSERVATIONS -	20	MISSING OBSERVATIONS -	0
----------------------	----	------------------------	---

## VARIABLE LENGTH

MEAN	676.000	STD ERROR	79.334	STD DEV	354.793
VARIANCE	125877.895	KURTOSIS	0.431	SKEWNESS	0.932
RANGE	1280.000	MINIMUM	220.000	MAXIMUM	1500.000
SUM	13520.000				

VALID OBSERVATIONS -	20	MISSING OBSERVATIONS -	0
----------------------	----	------------------------	---

## VARIABLE WIDTH

MEAN	124.000	STD ERROR	20.956	STD DEV	93.719
VARIANCE	8783.158	KURTOSIS	-0.084	SKEWNESS	0.968
RANGE	320.000	MINIMUM	20.000	MAXIMUM	340.000
SUM	2480.000				

VALID OBSERVATIONS -	20	MISSING OBSERVATIONS -	0
----------------------	----	------------------------	---

## III VARIABLE RATIO

MEAN	19.793	STD ERROR	1.965	STD DEV	16.558
VARIANCE	274.158	KURTOSIS	3.979	SKEWNESS	1.802
RANGE	86.000	MINIMUM	2.000	MAXIMUM	88.000
SUM	1405.320				

VALID OBSERVATIONS -	71	MISSING OBSERVATIONS -	0
----------------------	----	------------------------	---

## VARIABLE LENGTH

MEAN	1240.000	STD ERROR	150.653	STD DEV	1269.426
VARIANCE	AAAAA	KURTOSIS	0.606	SKEWNESS	1.203
RANGE	4950.000	MINIMUM	50.000	MAXIMUM	5000.000
SUM	88040.000				

VALID OBSERVATIONS -	71	MISSING OBSERVATIONS -	0
----------------------	----	------------------------	---

## VARIABLE WIDTH

MEAN	70.352	STD ERROR	7.231	STD DEV	60.932
VARIANCE	3712.731	KURTOSIS	2.234	SKEWNESS	1.407
RANGE	295.000	MINIMUM	5.000	MAXIMUM	300.000
SUM	4995.000				

VALID OBSERVATIONS -	71	MISSING OBSERVATIONS -	0
----------------------	----	------------------------	---

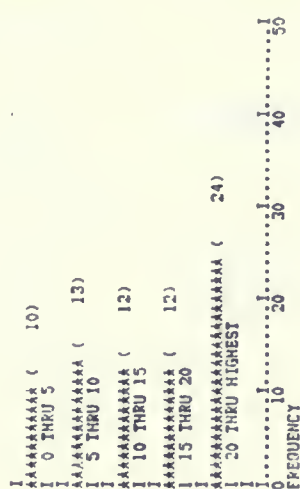




## ACTINOLITE AGG.-RATIO

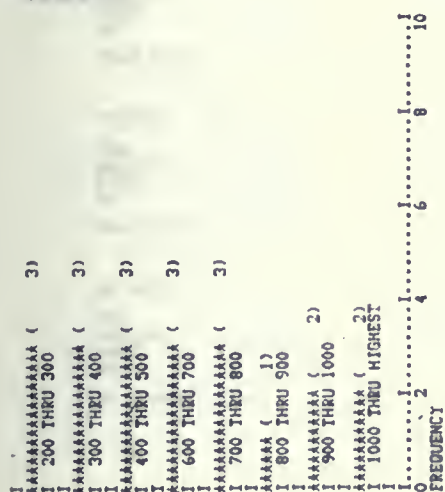


II

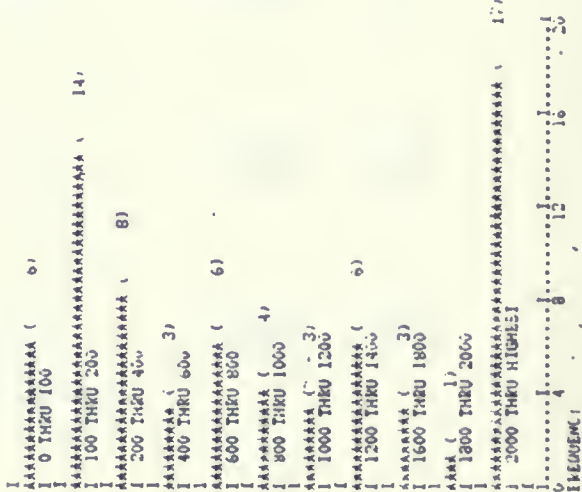


III

## LENGTH

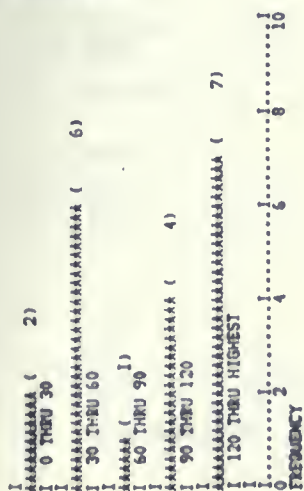


II



III

## WIDTH



II



III



# EPIDOTE GRAINS-STATISTICS

154

## I VARIABLE RATIO

MEAN	1.368	STD ERROR	0.060	STD DEV	0.306
VARIANCE	0.094	KURTOSIS	-0.548	SKEWNESS	0.748
RANGE	1.000	MINIMUM	1.000	MAXIMUM	2.000
SUM	35.560				

VALID OBSERVATIONS - 26 MISSING OBSERVATIONS - 0

### VARIABLE LENGTH

MEAN	53.365	STD ERROR	5.573	STD DEV	28.416
VARIANCE	807.471	KURTOSIS	0.735	SKEWNESS	0.932
RANGE	112.500	MINIMUM	12.500	MAXIMUM	125.000
SUM	1387.500				

VALID OBSERVATIONS - 26 MISSING OBSERVATIONS - 0

### VARIABLE WIDTH

MEAN	40.000	STD ERROR	4.315	STD DEV	22.000
VARIANCE	484.000	KURTOSIS	0.327	SKEWNESS	1.425
RANGE	80.000	MINIMUM	10.000	MAXIMUM	90.000
SUM	1040.000				

VALID OBSERVATIONS - 26 MISSING OBSERVATIONS - 0

## II VARIABLE RATIO

MEAN	1.799	STD ERROR	0.151	STD DEV	0.892
VARIANCE	0.795	KURTOSIS	1.702	SKEWNESS	1.425
RANGE	3.300	MINIMUM	1.000	MAXIMUM	4.300
SUM	62.960				

VALID OBSERVATIONS - 35 MISSING OBSERVATIONS - 0

### VARIABLE LENGTH

MEAN	84.071	STD ERROR	10.236	STD DEV	60.555
VARIANCE	3666.943	KURTOSIS	3.847	SKEWNESS	1.656
RANGE	280.000	MINIMUM	20.000	MAXIMUM	300.000
SUM	2942.500				

VALID OBSERVATIONS - 35 MISSING OBSERVATIONS - 0

### VARIABLE WIDTH

MEAN	44.143	STD ERROR	3.704	STD DEV	21.912
VARIANCE	480.126	KURTOSIS	-0.947	SKEWNESS	0.423
RANGE	75.000	MINIMUM	10.000	MAXIMUM	85.000
SUM	1545.000				

VALID OBSERVATIONS - 35 MISSING OBSERVATIONS - 0

## III VARIABLE RATIO

MEAN	1.746	STD ERROR	0.097	STD DEV	0.576
VARIANCE	0.332	KURTOSIS	1.312	SKEWNESS	1.101
RANGE	2.500	MINIMUM	1.000	MAXIMUM	3.500
SUM	61.100				

VALID OBSERVATIONS - 35 MISSING OBSERVATIONS - 0

### VARIABLE LENGTH

MEAN	36.643	STD ERROR	2.919	STD DEV	17.267
VARIANCE	298.141	KURTOSIS	2.325	SKEWNESS	1.341
RANGE	80.000	MINIMUM	10.000	MAXIMUM	90.000
SUM	1282.500				

VALID OBSERVATIONS - 35 MISSING OBSERVATIONS - 0

### VARIABLE WIDTH

MEAN	23.143	STD ERROR	2.402	STD DEV	14.211
VARIANCE	201.964	KURTOSIS	5.042	SKEWNESS	1.993
RANGE	70.000	MINIMUM	5.000	MAXIMUM	75.000
SUM	810.000				

VALID OBSERVATIONS - 35 MISSING OBSERVATIONS - 0





# EPIDOTE GRAINS-STATISTICS

155

IV

## VARIABLE RATIO

MEAN	1.853	STD ERROR	0.104	STD DEV	0.699
VARIANCE	0.489	KURTOSIS	3.409	SKEWNESS	1.495
RANGE	3.500	MINIMUM	1.000	MAXIMUM	4.500
SUM	83.390				

VALID OBSERVATIONS - 45 MISSING OBSERVATIONS - 0

## VARIABLE LENGTH

MEAN	44.944	STD ERROR	2.496	STD DEV	16.741
VARIANCE	280.253	KURTOSIS	-0.456	SKEWNESS	0.198
RANGE	70.000	MINIMUM	10.000	MAXIMUM	80.000
SUM	2022.500				

VALID OBSERVATIONS - 45 MISSING OBSERVATIONS - 0

## VARIABLE WIDTH

MEAN	25.523	STD ERROR	1.561	STD DEV	10.475
VARIANCE	109.715	KURTOSIS	0.205	SKEWNESS	0.611
RANGE	45.000	MINIMUM	10.000	MAXIMUM	55.000
SUM	1148.500				

VALID OBSERVATIONS - 45 MISSING OBSERVATIONS - 0

V-F

## VARIABLE RATIO

MEAN	2.079	STD ERROR	0.214	STD DEV	1.194
VARIANCE	1.426	KURTOSIS	2.284	SKEWNESS	1.749
RANGE	4.600	MINIMUM	1.000	MAXIMUM	5.600
SUM	64.440				

VALID OBSERVATIONS - 31 MISSING OBSERVATIONS - 0

## VARIABLE LENGTH

MEAN	35.887	STD ERROR	2.948	STD DEV	16.413
VARIANCE	269.395	KURTOSIS	0.237	SKEWNESS	0.973
RANGE	60.000	MINIMUM	15.000	MAXIMUM	75.000
SUM	1112.500				

VALID OBSERVATIONS - 31 MISSING OBSERVATIONS - 0

## VARIABLE WIDTH

MEAN	19.177	STD ERROR	1.505	STD DEV	8.378
VARIANCE	70.192	KURTOSIS	1.703	SKEWNESS	1.074
RANGE	37.500	MINIMUM	7.500	MAXIMUM	45.000
SUM	594.500				

VALID OBSERVATIONS - 31 MISSING OBSERVATIONS - 0

V-C

## VARIABLE RATIO

MEAN	1.989	STD ERROR	0.110	STD DEV	0.924
VARIANCE	0.989	KURTOSIS	1.657	SKEWNESS	1.351
RANGE	4.500	MINIMUM	1.000	MAXIMUM	5.500
SUM	163.090				

VALID OBSERVATIONS - 82 MISSING OBSERVATIONS - 0

## VARIABLE LENGTH

MEAN	35.415	STD ERROR	1.923	STD DEV	17.417
VARIANCE	303.357	KURTOSIS	0.126	SKEWNESS	0.779
RANGE	70.000	MINIMUM	10.000	MAXIMUM	80.000
SUM	2904.000				

VALID OBSERVATIONS - 82 MISSING OBSERVATIONS - 0

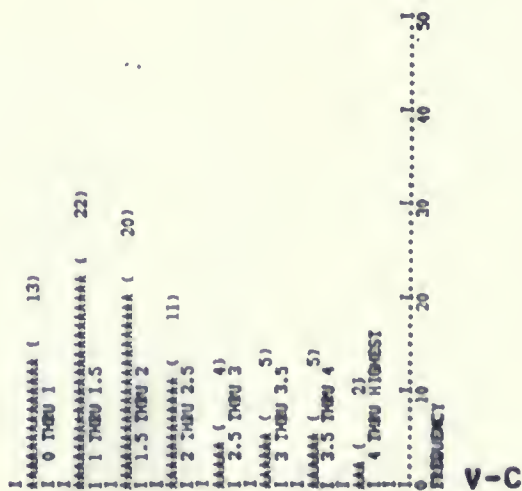
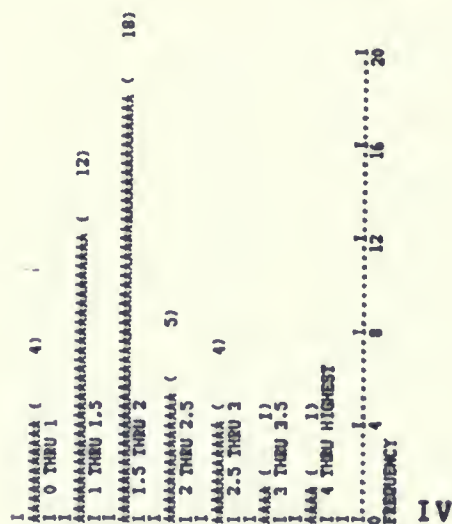
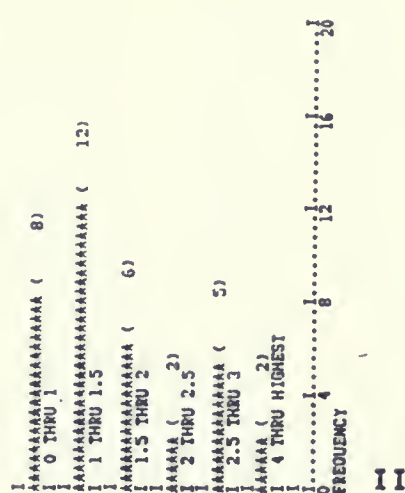
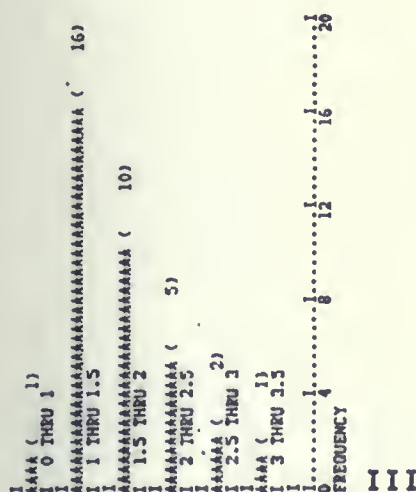
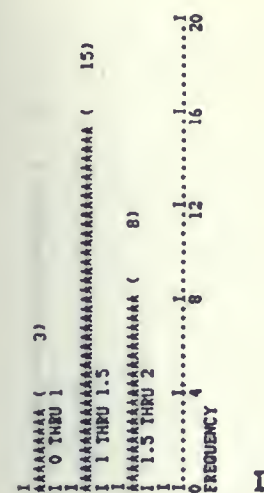
## VARIABLE WIDTH

MEAN	20.109	STD ERROR	1.533	STD DEV	13.980
VARIANCE	192.652	KURTOSIS	40.342	SKEWNESS	5.455
RANGE	117.500	MINIMUM	7.500	MAXIMUM	125.000
SUM	1655.500				

VALID OBSERVATIONS - 82 MISSING OBSERVATIONS - 0



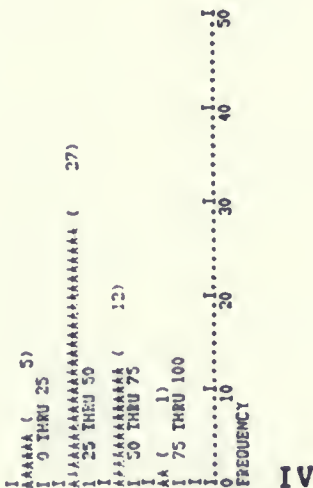
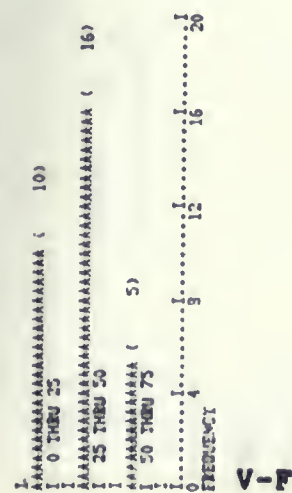
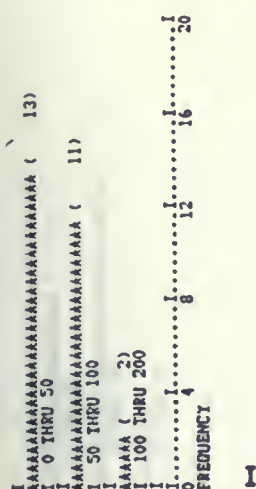
## EPIDOTE GRAINS-RATIO





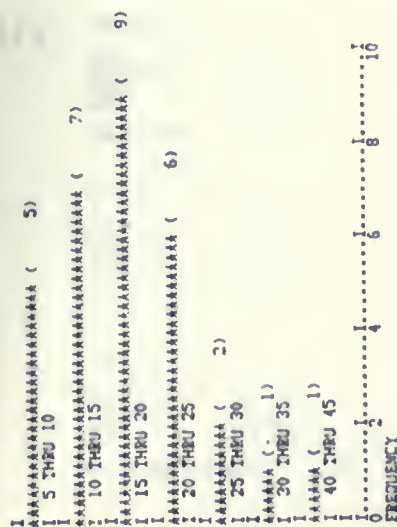


## EPIDOTE GRAINS-LENGTH





## EPIDOTE GRAINS-WIDTH





## EPIDOTE AGG.-STATISTICS

I

VARIABLE RATIO					
MEAN	3.024	STD ERROR	0.239	STD DEV	1.588
VARIANCE	7.522	KURTOSIS	1.009	SKEWNESS	1.236
RANGE	6.250	MINIMUM	1.000	MAXIMUM	7.250
SUM	133.060				
VALID OBSERVATIONS -	44	MISSING OBSERVATIONS -	0		
-----					
VARIABLE LENGTH					
MEAN	238.659	STD ERROR	27.843	STD DEV	184.688
VARIANCE	34109.579	KURTOSIS	4.402	SKEWNESS	1.991
RANGE	840.000	MINIMUM	60.000	MAXIMUM	900.000
SUM	10501.000				
VALID OBSERVATIONS -	44	MISSING OBSERVATIONS -	0		
-----					
VARIABLE WIDTH					
MEAN	78.636	STD ERROR	6.426	STD DEV	42.623
VARIANCE	1816.702	KURTOSIS	-0.484	SKEWNESS	0.589
RANGE	170.000	MINIMUM	10.000	MAXIMUM	180.000
SUM	3460.000				
VALID OBSERVATIONS -	44	MISSING OBSERVATIONS -	0		

II

VARIABLE RATIO					
MEAN	2.054	STD ERROR	0.127	STD DEV	1.013
VARIANCE	1.026	KURTOSIS	2.961	SKEWNESS	1.605
RANGE	4.710	MINIMUM	1.000	MAXIMUM	5.710
SUM	131.460				
VALID OBSERVATIONS -	64	MISSING OBSERVATIONS -	0		
-----					
VARIABLE LENGTH					
MEAN	172.656	STD ERROR	15.892	STD DEV	127.139
VARIANCE	16164.261	KURTOSIS	5.066	SKEWNESS	2.077
RANGE	640.000	MINIMUM	40.000	MAXIMUM	680.000
SUM	11050.000				
VALID OBSERVATIONS -	64	MISSING OBSERVATIONS -	0		
-----					
VARIABLE WIDTH					
MEAN	90.938	STD ERROR	8.215	STD DEV	65.719
VARIANCE	4318.948	KURTOSIS	7.154	SKEWNESS	2.314
RANGE	325.000	MINIMUM	25.000	MAXIMUM	400.000
SUM	5820.000				
VALID OBSERVATIONS -	64	MISSING OBSERVATIONS -	0		

III

VARIABLE RATIO					
MEAN	1.786	STD ERROR	0.079	STD DEV	0.683
VARIANCE	0.467	KURTOSIS	6.493	SKEWNESS	2.101
RANGE	4.000	MINIMUM	1.000	MAXIMUM	5.000
SUM	132.150				
VALID OBSERVATIONS -	74	MISSING OBSERVATIONS -	0		
-----					
VARIABLE LENGTH					
MEAN	97.770	STD ERROR	8.443	STD DEV	72.632
VARIANCE	5275.440	KURTOSIS	13.859	SKEWNESS	3.125
RANGE	475.000	MINIMUM	25.000	MAXIMUM	500.000
SUM	7235.000				
VALID OBSERVATIONS -	74	MISSING OBSERVATIONS -	0		
-----					
VARIABLE WIDTH					
MEAN	57.635	STD ERROR	4.997	STD DEV	42.982
VARIANCE	1847.413	KURTOSIS	14.947	SKEWNESS	3.314
RANGE	285.000	MINIMUM	15.000	MAXIMUM	300.000
SUM	4265.000				
VALID OBSERVATIONS -	74	MISSING OBSERVATIONS -	0		



















# LEUCOXENE-STATISTICS

163

I

VARIABLE RATIO					
MEAN	3.020	STD ERROR	0.263	STD DEV	2.258
VARIANCE	5.100	KURTOSIS	2.455	SKEWNESS	1.623
RANGE	10.000	MINIMUM	1.000	MAXIMUM	11.000
SUM	223.450				
VALID OBSERVATIONS -	74	MISSING OBSERVATIONS -	0		
-----					
VARIABLE LENGTH					
MEAN	160.595	STD ERROR	17.711	STD DEV	152.356
VARIANCE	23212.464	KURTOSIS	6.552	SKEWNESS	2.078
RANGE	826.000	MINIMUM	4.000	MAXIMUM	830.000
SUM	11884.000				
VALID OBSERVATIONS -	74	MISSING OBSERVATIONS -	0		
-----					
VARIABLE WIDTH					
MEAN	56.622	STD ERROR	5.855	STD DEV	50.370
VARIANCE	2537.088	KURTOSIS	4.162	SKEWNESS	1.902
RANGE	246.000	MINIMUM	4.000	MAXIMUM	250.000
SUM	4190.000				
VALID OBSERVATIONS -	74	MISSING OBSERVATIONS -	0		

II

VARIABLE RATIO					
MEAN	9.827	STD ERROR	1.107	STD DEV	9.904
VARIANCE	98.091	KURTOSIS	6.560	SKEWNESS	2.416
RANGE	52.340	MINIMUM	1.660	MAXIMUM	54.000
SUM	786.120				
VALID OBSERVATIONS -	80	MISSING OBSERVATIONS -	0		
-----					
VARIABLE LENGTH					
MEAN	190.506	STD ERROR	12.527	STD DEV	174.655
VARIANCE	30504.523	KURTOSIS	3.652	SKEWNESS	1.838
RANGE	875.000	MINIMUM	5.000	MAXIMUM	880.000
SUM	15240.500				
VALID OBSERVATIONS -	80	MISSING OBSERVATIONS -	0		
-----					
VARIABLE WIDTH					
MEAN	23.894	STD ERROR	2.382	STD DEV	21.302
VARIANCE	453.750	KURTOSIS	9.232	SKEWNESS	2.649
RANGE	117.500	MINIMUM	2.500	MAXIMUM	120.000
SUM	1911.500				
VALID OBSERVATIONS -	80	MISSING OBSERVATIONS -	0		

III

VARIABLE RATIO					
MEAN	11.617	STD ERROR	1.080	STD DEV	10.016
VARIANCE	100.330	KURTOSIS	3.895	SKEWNESS	1.879
RANGE	49.000	MINIMUM	1.000	MAXIMUM	50.000
SUM	999.100				
VALID OBSERVATIONS -	86	MISSING OBSERVATIONS -	0		
-----					
VARIABLE LENGTH					
MEAN	254.419	STD ERROR	26.300	STD DEV	243.898
VARIANCE	59486.129	KURTOSIS	3.945	SKEWNESS	1.246
RANGE	1280.000	MINIMUM	20.000	MAXIMUM	1300.000
SUM	21880.000				
VALID OBSERVATIONS -	86	MISSING OBSERVATIONS -	0		
-----					
VARIABLE WIDTH					
MEAN	24.605	STD ERROR	1.694	STD DEV	15.708
VARIANCE	246.736	KURTOSIS	1.631	SKEWNESS	1.351
RANGE	75.000	MINIMUM	5.000	MAXIMUM	80.000
SUM	2116.000				
VALID OBSERVATIONS -	86	MISSING OBSERVATIONS -	0		



# LEUCOXENE-STATISTICS

164

IV

VARIABLE RATIO					
MEAN	2.437	STD ERROR	0.198	STD DEV	1.066
VARIANCE	1.137	KURTOSIS	-1.256	SKEWNESS	0.101
RANGE	3.400	MINIMUM	1.000	MAXIMUM	4.400
SUM	70.670				
VALID OBSERVATIONS -	29	MISSING OBSERVATIONS -	0		
-----					
VARIABLE LENGTH					
MEAN	32.069	STD ERROR	3.828	STD DEV	20.616
VARIANCE	423.031	KURTOSIS	3.318	SKEWNESS	1.559
RANGE	95.000	MINIMUM	5.000	MAXIMUM	100.000
SUM	930.000				
VALID OBSERVATIONS -	29	MISSING OBSERVATIONS -	0		
-----					
VARIABLE WIDTH					
MEAN	13.707	STD ERROR	1.523	STD DEV	8.200
VARIANCE	67.241	KURTOSIS	1.814	SKEWNESS	1.540
RANGE	30.000	MINIMUM	5.000	MAXIMUM	35.000
SUM	397.500				
VALID OBSERVATIONS -	29	MISSING OBSERVATIONS -	0		

V-F

VARIABLE RATIO					
MEAN	8.295	STD ERROR	0.849	STD DEV	5.944
VARIANCE	35.334	KURTOSIS	-0.175	SKEWNESS	0.853
RANGE	22.080	MINIMUM	1.250	MAXIMUM	23.330
SUM	406.470				
VALID OBSERVATIONS -	49	MISSING OBSERVATIONS -	0		
-----					
VARIABLE LENGTH					
MEAN	134.541	STD ERROR	23.630	STD DEV	165.413
VARIANCE	27361.373	KURTOSIS	15.600	SKEWNESS	3.540
RANGE	987.500	MINIMUM	12.500	MAXIMUM	1000.000
SUM	6592.500				
VALID OBSERVATIONS -	49	MISSING OBSERVATIONS -	0		
-----					
VARIABLE WIDTH					
MEAN	16.071	STD ERROR	1.496	STD DEV	10.471
VARIANCE	109.635	KURTOSIS	7.121	SKEWNESS	2.261
RANGE	55.000	MINIMUM	5.000	MAXIMUM	60.000
SUM	787.500				
VALID OBSERVATIONS -	49	MISSING OBSERVATIONS -	0		

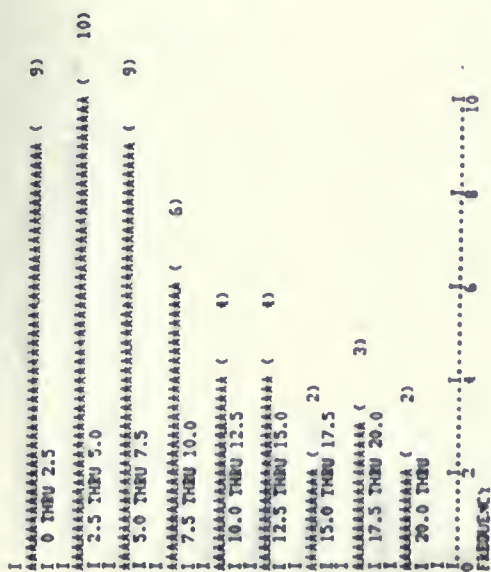
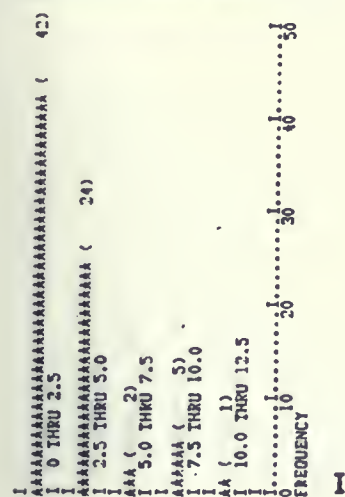
V-C

VARIABLE RATIO					
MEAN	5.235	STD ERROR	0.562	STD DEV	2.755
VARIANCE	7.588	KURTOSIS	-0.525	SKEWNESS	0.605
RANGE	10.000	MINIMUM	1.200	MAXIMUM	11.200
SUM	125.650				
VALID OBSERVATIONS -	24	MISSING OBSERVATIONS -	0		
-----					
VARIABLE LENGTH					
MEAN	98.833	STD ERROR	17.101	STD DEV	83.775
VARIANCE	7018.319	KURTOSIS	8.679	SKEWNESS	2.623
RANGE	413.000	MINIMUM	2.000	MAXIMUM	415.000
SUM	2372.000				
VALID OBSERVATIONS -	24	MISSING OBSERVATIONS -	0		
-----					
VARIABLE WIDTH					
MEAN	19.792	STD ERROR	2.355	STD DEV	11.537
VARIANCE	133.107	KURTOSIS	2.613	SKEWNESS	1.801
RANGE	40.000	MINIMUM	10.000	MAXIMUM	50.000
SUM	475.000				
VALID OBSERVATIONS -	24	MISSING OBSERVATIONS -	0		

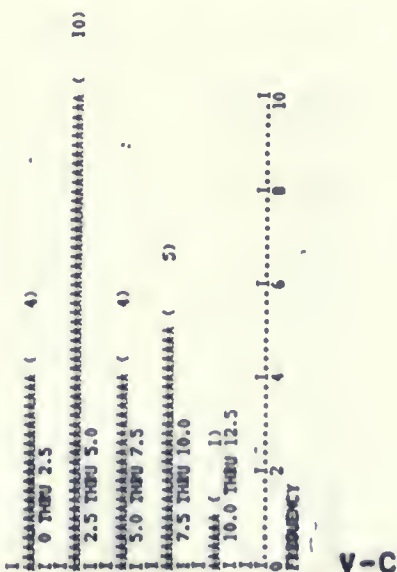
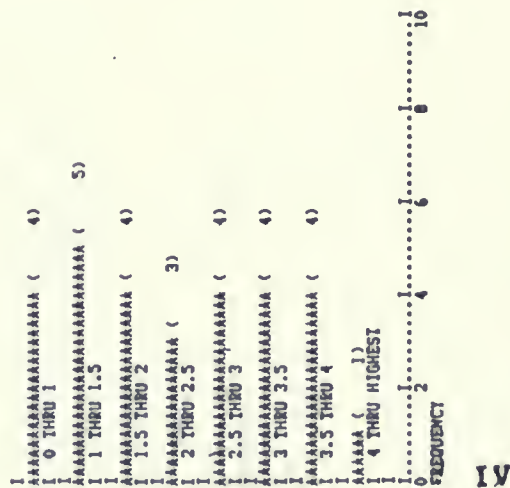
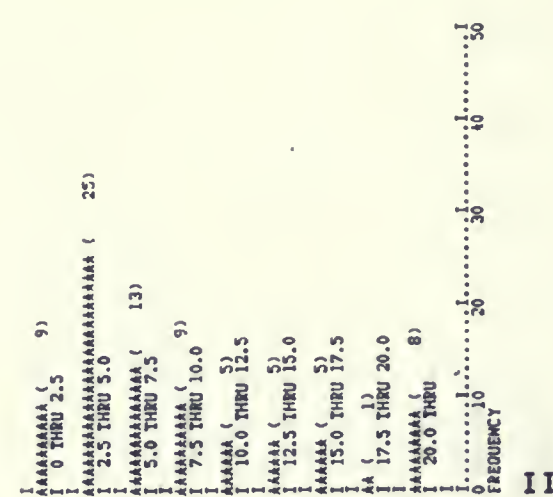




## LEUCOXENE-RATIO



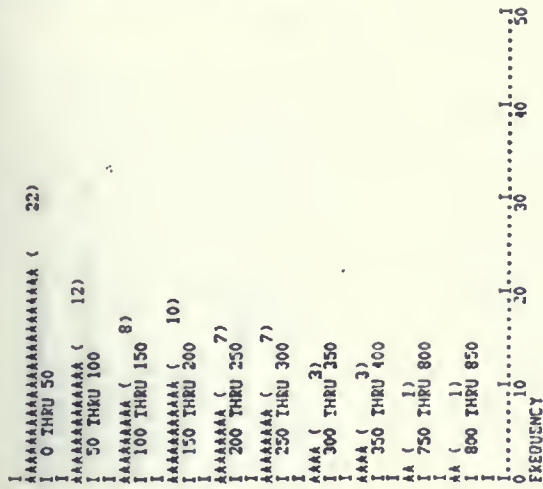
V-F



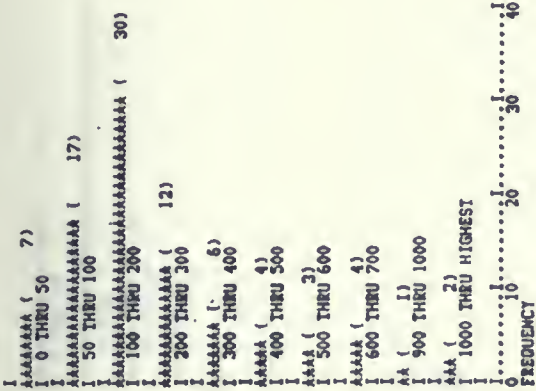
V-C



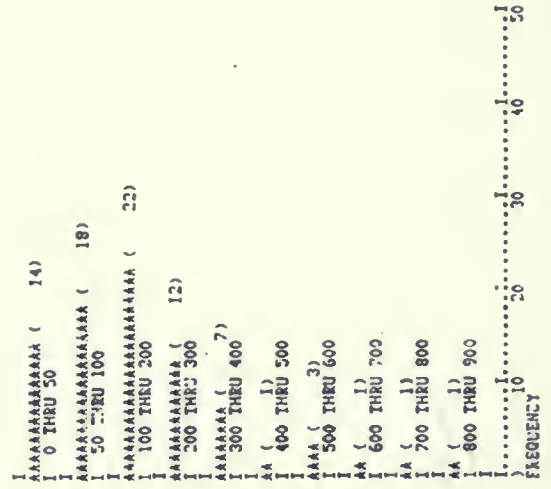
LEUCOXENE-LENGTH



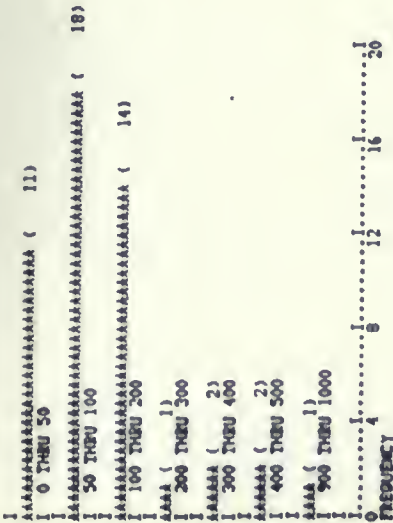
I



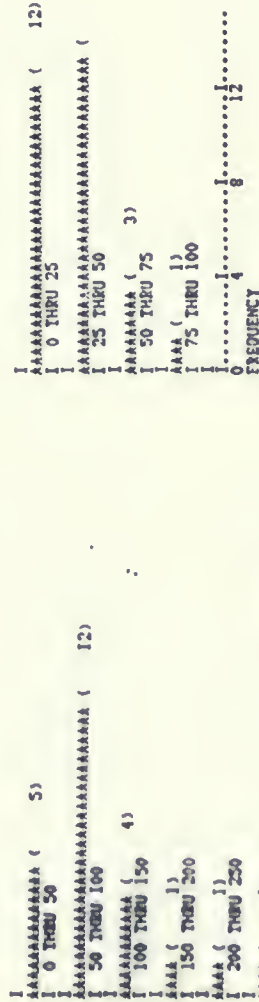
II



III



V

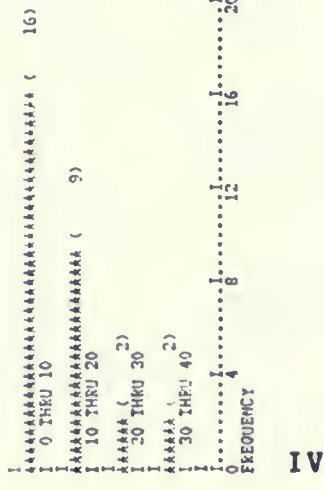
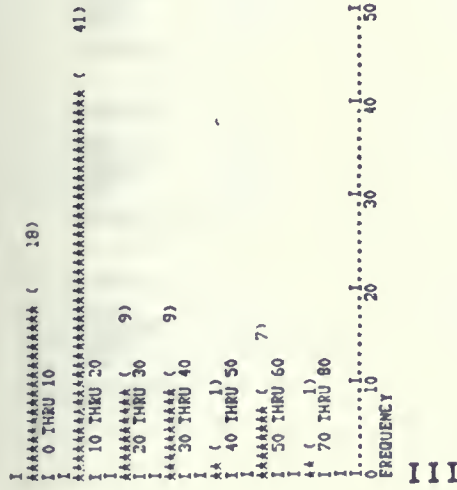
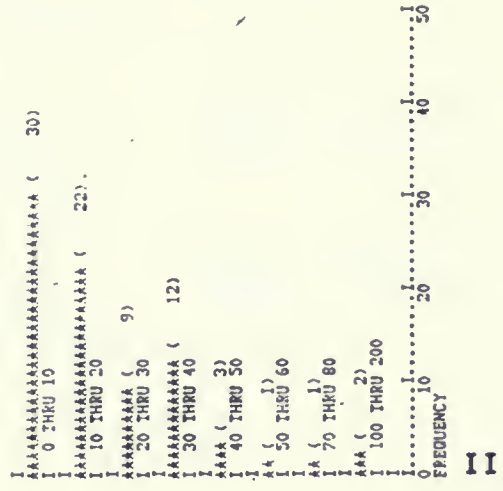


V-C





# LEUCOXENE-WIDTH



V-F



V-C



# CHLORITE-STATISTICS

168

I

VARIABLE RATIO					
MEAN	2.621	STD ERROR	0.219	STD DEV	1.847
VARIANCE	3.410	KURTOSIS	6.886	SKEWNESS	2.305
RANGE	10.300	MINIMUM	1.000	MAXIMUM	11.300
SUM	186.110				
VALID OBSERVATIONS -	71	MISSING OBSERVATIONS -	0		
-----					
VARIABLE LENGTH					
MEAN	188.225	STD ERROR	23.854	STD DEV	290.993
VARIANCE	40398.320	KURTOSIS	5.622	SKEWNESS	2.237
RANGE	1035.000	MINIMUM	25.000	MAXIMUM	1060.000
SUM	13364.000				
VALID OBSERVATIONS -	71	MISSING OBSERVATIONS -	0		
-----					
VARIABLE WIDTH					
MEAN	90.951	STD ERROR	13.356	STD DEV	112.541
VARIANCE	12665.423	KURTOSIS	20.024	SKEWNESS	3.814
RANGE	772.500	MINIMUM	7.500	MAXIMUM	780.000
SUM	6457.500				
VALID OBSERVATIONS -	71	MISSING OBSERVATIONS -	0		

II

VARIABLE RATIO					
MEAN	8.616	STD ERROR	0.674	STD DEV	5.360
VARIANCE	30.912	KURTOSIS	1.145	SKEWNESS	1.216
RANGE	23.600	MINIMUM	1.400	MAXIMUM	25.000
SUM	585.900				
VALID OBSERVATIONS -	68	MISSING OBSERVATIONS -	0		
-----					
VARIABLE LENGTH					
MEAN	173.824	STD ERROR	15.790	STD DEV	130.210
VARIANCE	16954.565	KURTOSIS	8.103	SKEWNESS	2.104
RANGE	725.000	MINIMUM	25.000	MAXIMUM	750.000
SUM	11820.000				
VALID OBSERVATIONS -	68	MISSING OBSERVATIONS -	0		
-----					
VARIABLE WIDTH					
MEAN	28.309	STD ERROR	3.700	STD DEV	30.508
VARIANCE	930.709	KURTOSIS	14.751	SKEWNESS	3.279
RANGE	197.500	MINIMUM	2.500	MAXIMUM	200.000
SUM	1925.000				
VALID OBSERVATIONS -	68	MISSING OBSERVATIONS -	0		

III

VARIABLE RATIO					
MEAN	9.607	STD ERROR	0.806	STD DEV	7.893
VARIANCE	62.398	KURTOSIS	16.668	SKEWNESS	3.152
RANGE	58.100	MINIMUM	1.900	MAXIMUM	60.000
SUM	922.290				
VALID OBSERVATIONS -	96	MISSING OBSERVATIONS -	0		
-----					
VARIABLE LENGTH					
MEAN	181.146	STD ERROR	15.799	STD DEV	154.798
VARIANCE	23962.357	KURTOSIS	8.609	SKEWNESS	2.507
RANGE	975.000	MINIMUM	25.000	MAXIMUM	1000.000
SUM	17390.000				
VALID OBSERVATIONS -	96	MISSING OBSERVATIONS -	0		
-----					
VARIABLE WIDTH					
MEAN	24.219	STD ERROR	2.100	STD DEV	20.370
VARIANCE	423.462	KURTOSIS	7.648	SKEWNESS	2.421
RANGE	122.500	MINIMUM	2.500	MAXIMUM	125.000
SUM	2325.000				
VALID OBSERVATIONS -	96	MISSING OBSERVATIONS -	0		



# CHLORITE-STATISTICS

169

IV

## VARIABLE RATIO

MEAN	10.042	STD ERROR	1.104	STD DEV	7.569
VARIANCE	57.283	KURTOSIS	1.039	SKEWNESS	1.194
RANGE	32.400	MINIMUM	1.600	MAXIMUM	34.000
SUM	471.960				

VALID OBSERVATIONS - 47 MISSING OBSERVATIONS - 0

## VARIABLE LENGTH

MEAN	93.564	STD ERROR	10.588	STD DEV	72.586
VARIANCE	5268.681	KURTOSIS	4.912	SKEWNESS	2.078
RANGE	360.000	MINIMUM	15.000	MAXIMUM	375.000
SUM	4397.500				

VALID OBSERVATIONS - 47 MISSING OBSERVATIONS - 0

## VARIABLE WIDTH

MEAN	11.645	STD ERROR	1.179	STD DEV	8.085
VARIANCE	65.360	KURTOSIS	1.206	SKEWNESS	1.260
RANGE	35.000	MINIMUM	2.500	MAXIMUM	37.500
SUM	547.500				

VALID OBSERVATIONS - 47 MISSING OBSERVATIONS - 0

V-F

## VARIABLE RATIO

MEAN	6.345	STD ERROR	0.837	STD DEV	5.617
VARIANCE	31.555	KURTOSIS	6.842	SKEWNESS	2.384
RANGE	29.000	MINIMUM	1.000	MAXIMUM	30.000
SUM	285.520				

VALID OBSERVATIONS - 45 MISSING OBSERVATIONS - 0

## VARIABLE LENGTH

MEAN	102.333	STD ERROR	10.152	STD DEV	68.104
VARIANCE	4638.182	KURTOSIS	2.495	SKEWNESS	1.341
RANGE	315.000	MINIMUM	10.000	MAXIMUM	325.000
SUM	4605.000				

VALID OBSERVATIONS - 45 MISSING OBSERVATIONS - 0

## VARIABLE WIDTH

MEAN	22.944	STD ERROR	2.582	STD DEV	17.323
VARIANCE	300.082	KURTOSIS	2.623	SKEWNESS	1.414
RANGE	82.500	MINIMUM	2.500	MAXIMUM	85.000
SUM	1032.500				

VALID OBSERVATIONS - 45 MISSING OBSERVATIONS - 0

V-C

## VARIABLE RATIO

MEAN	5.678	STD ERROR	0.374	STD DEV	3.348
VARIANCE	11.211	KURTOSIS	2.039	SKEWNESS	1.323
RANGE	13.900	MINIMUM	1.430	MAXIMUM	15.330
SUM	193.060				

VALID OBSERVATIONS - 34 MISSING OBSERVATIONS - 0

## VARIABLE LENGTH

MEAN	79.559	STD ERROR	6.589	STD DEV	38.423
VARIANCE	1476.315	KURTOSIS	-0.370	SKEWNESS	0.687
RANGE	155.000	MINIMUM	20.000	MAXIMUM	175.000
SUM	2705.000				

VALID OBSERVATIONS - 34 MISSING OBSERVATIONS - 0

## VARIABLE WIDTH

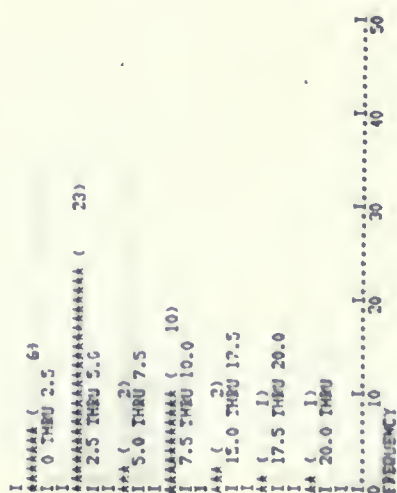
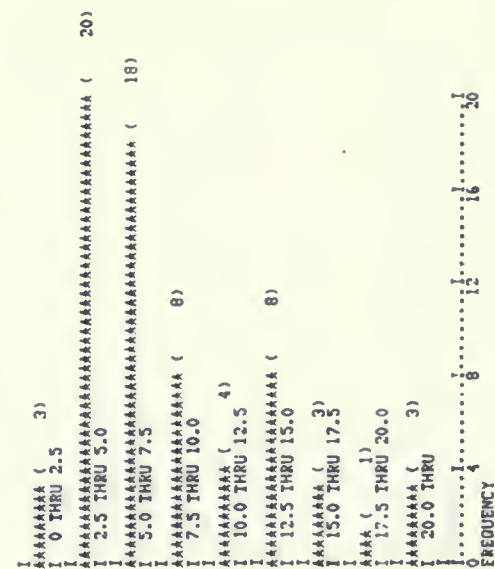
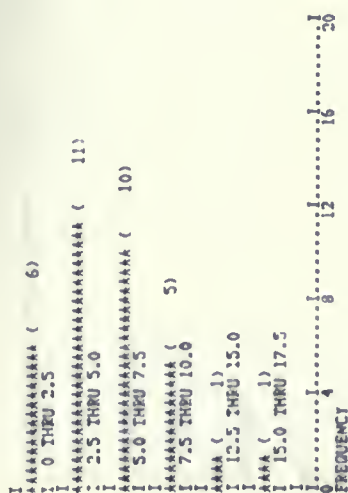
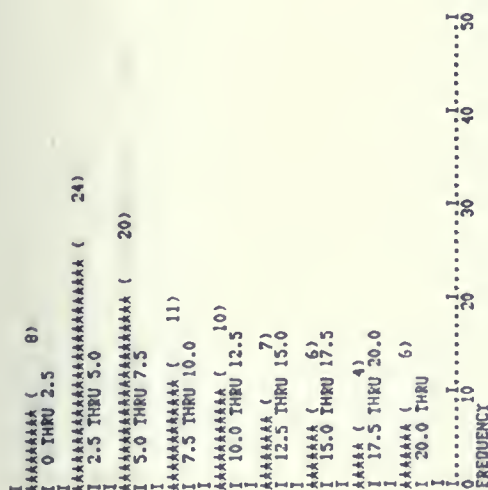
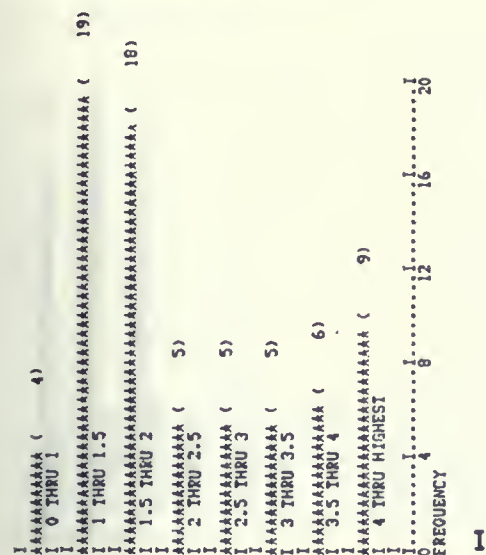
MEAN	17.500	STD ERROR	1.760	STD DEV	10.263
VARIANCE	105.303	KURTOSIS	-0.830	SKEWNESS	0.573
RANGE	35.000	MINIMUM	5.000	MAXIMUM	40.000
SUM	595.000				

VALID OBSERVATIONS - 34 MISSING OBSERVATIONS - 0



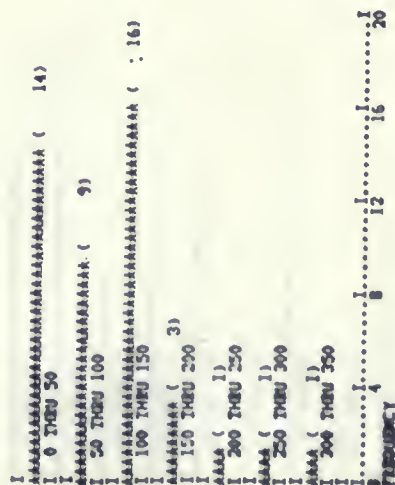
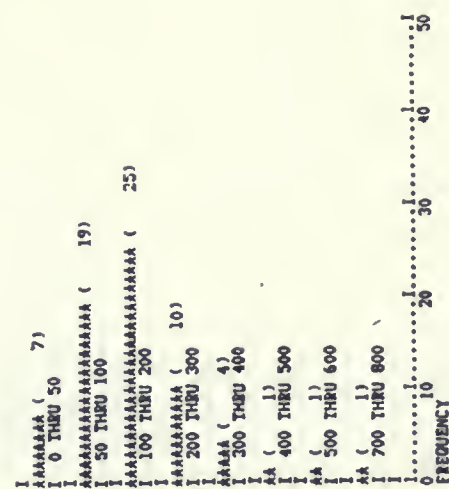
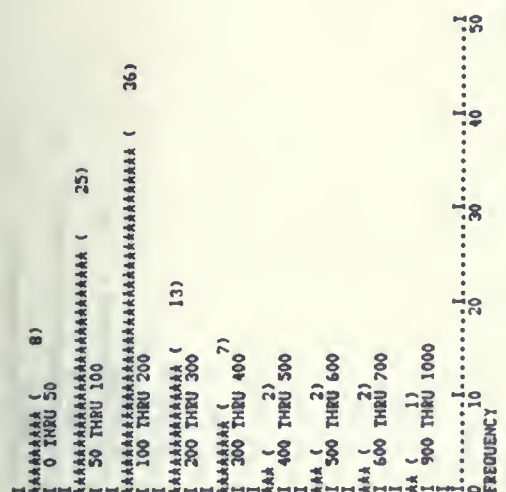
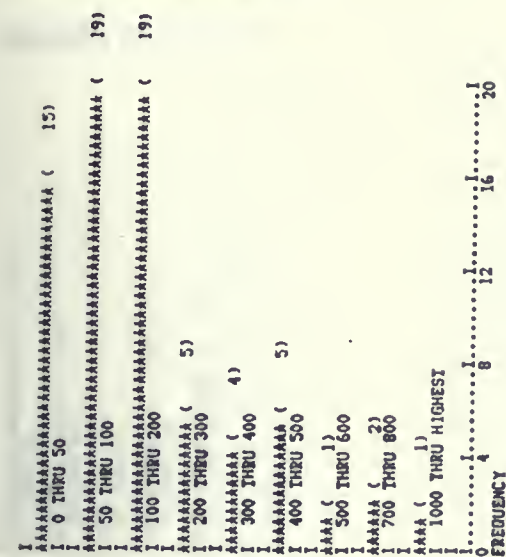


## CHLORITE-RATIO





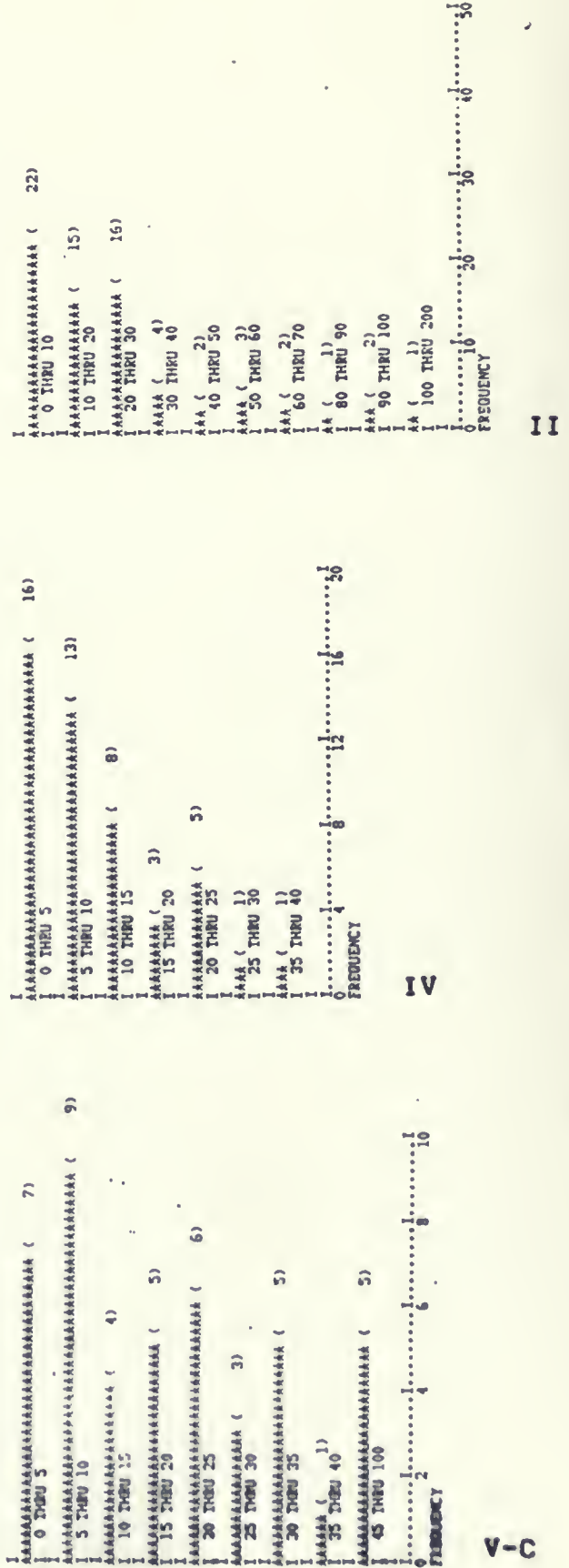
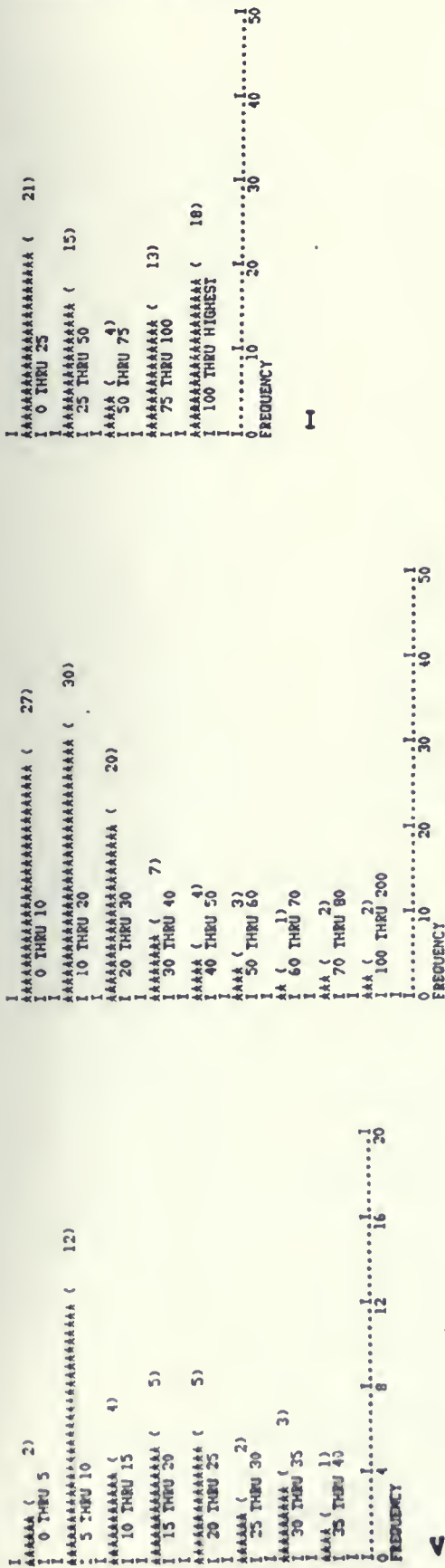
## CHLORITE-LENGTH







## CHLORITE-WIDTH







5





